UNIVERSITY OF SOUTHAMPTON

SCHOOL OF OCEAN AND EARTH SCIENCE

Variability and control of the surface ocean carbonate system observed from ships of opportunity

by

Zong-Pei Jiang

Thesis for the degree of Doctor of Philosophy

January 2014

Abstract

UNIVERSITY OF SOUTHAMPTON

ABSTRACT

SCHOOL OF OCEAN AND EARTH SCIENCE

Oceanography

Thesis for the degree of Doctor of Philosophy

VARIABILITY AND CONTROL OF THE SURFACE OCEAN CARBONATE SYSTEM OBSERVED FROM SHIPS OF OPPORTUNITY

Zong-Pei Jiang

The surface ocean plays an important role in the marine carbon cycle linking the atmosphere and the deep ocean. There are substantial variations in the surface ocean carbonate system in different environments and on various time scales, resulting from the interactions of various physical and biogeochemical processes. In this study, the use of Ships of Opportunity (SOO, as carriers of automatic underway measuring systems and platforms for sample collections) was promoted to enhance the surface ocean observing capacity to provide in-situ observations with better temporal resolution and spatial coverage in a cost-effective way (Chapter 2). The functionality, reliability and accuracy of an automatic pCO_2 sensor were assessed extensively under various field and laboratory conditions (Chapter 3). The sensor proved to be suitable for long-term onboard and in-situ measurements, while its uncertainty is largely determined by the reference used for calibration. Observations made from two SOOs were examined to better understand the variability and control of the surface ocean carbonate system (Chapter 4, 5).

The spatial variability of alkalinity in different marine environmental settings were investigated focusing on the influences of physical and biogeochemical processes on the alkalinity-salinity relationship (Chapter 4). By using salinity-normalized alkalinity as an indicator, the TA addition or removal processes were examined in the open ocean regime in the Atlantic, Pacific and Indian Ocean (mainly controlled by precipitation and evaporation), in the western North Atlantic margin, eastern North Pacific and Mediterranean Sea (additional alkalinity inputs from rivers, currents or the Black Sea), and in the Red Sea (alkalinity removal by $CaCO_3$ precipitation). In coastal regions, a regional-specific term for zero salinity end member should be considered in salinity normalization practice, and care should be taken when use the

intercept of alkalinity-salinity regression to estimate the river water end member (only works reliably in river-dominated systems).

The temporal variations of the surface carbonate system and air-sea CO_2 flux in the Northeast Atlantic (Bay of Biscay) were examined on seasonal to interannual time scales (Chapter 5). The seasonal variability of DIC (single annual peak in winter, shaped by the winter increase due to deep convection followed by the spring biological drawdown) is different to the seasonal cycle of pCO_2 (double annual peaks in winter and summer, determined by the competing effects of temperature and non-thermal processes on pCO_2). A comparative study shows a latitudinal transition of pCO_2 seasonality in the North Atlantic: from the temperature-dominated oligotrophic subtropical gyre to the subpolar region where pCO_2 is dominated by changing concentrations of DIC. Located in the transition zone, pCO_2 in the mid-latitude Bay of Biscay shows a double-peak distribution in its annual cycle: the summer peak is dominated by temperature increase while the winter peak results from the dominant convection effect. The interannual biogeochemical changes in the Bay of Biscay were found to be closely related to the varying intensity of winter mixing, with higher seasonal amplitudes of DIC and nutrients observed in cold years in response to negative phases of the North Atlantic Oscillation. An increase in annual mean seawater pCO_2 was observed from 2002 to 2010 associated with decreased rates of oceanic CO_2 uptake.

Contents

List of tables

List of figures

List of accompanying materials

1. Corresponding to the study of the "Application and assessment of the membrane-based ProOceanus CO_2-Pro™ sensor for pCO_2 under field and laboratory conditions" (Chapter 3), the manufacturer's response by the Pro-Oceanus Instruments is attached in the Appendix.

2. Some data reported in this thesis have been submitted to the Carbon Dioxide Information Analysis Center (CDIAC). They are available from the CDIAC website:

   - The SNOMS data (Chapter 4):

   http://cdiac.ornl.gov/oceans/VOS_Program/bilbao.html

   - The POB data (Chapter 5):

   http://cdiac.ornl.gov/oceans/VOS_Program/celebes.html

DECLARATION OF AUTHORSHIP

I, **Zong-Pei Jiang**, declare that the thesis entitled **'Variability and control of the surface ocean carbonate system observed from ship of opportunity"** and the work presented in the thesis are both my own, and have been generated by me as the result of my own original research. I confirm that:

this work was done wholly or mainly while in candidature for a research degree at this University;

where any part of this thesis has previously been submitted for a degree or any other qualification at this University or any other institution, this has been clearly stated;

where I have consulted the published work of others, this is always clearly attributed;

where I have quoted from the work of others, the source is always given. With the exception of such quotations, this thesis is entirely my own work;

I have acknowledged all main sources of help;

where the thesis is based on work done by myself jointly with others, I have made clear exactly what was done by others and what I have contributed myself;

parts of this work have been published as:

Jiang, Z.-P., D. J. Hydes, T. Tyrrell, S. E. Hartman, M. C. Hartman, C. Dumousseaud, X. A. Padin, I. Skjelvan, and C. González-Pola (2013), Key controls on the seasonal and interannual variations of the carbonate system and air-sea CO_2 flux in the Northeast Atlantic (Bay of Biscay), *J. Geophys. Res.*, *118*, 1-16.

Signed: ……..

Date:…….

Acknowledgements

Time flies. I can barely believe that four years have passed by since I started my PhD study at the National Oceanography Centre, Southampton (NOCS). It has been a long journey for completing my PhD and many things have happened and changed. I still remember how excited I was when I got my first publication after numerous revisions. It has been a great privilege to spend the past four years in the seaside NOCS building although it looked like a maze to me when I first come in. During my PhD study, I have learned a lot and got myself well prepared for the future career development. However, I could not have succeeded without the invaluable support from many people throughout my PhD project.

First and foremost, I would like to acknowledge my supervisors David Hydes, Toby Tyrrell and Minhan Dai for their distinguished advice, support, encouragement and supervision despite their busy schedules. I appreciate the great efforts and time that David has put into helping me as well as his care for my life. I will always remember that he drove a long way to the Heathrow airport to pick me up and accommodated me at his home when I first arrived in UK. Special thanks to Toby who took over as my main supervisor after David's retirement. He has provided insightful discussion on my research and helped a lot during the preparation of my viva. Minhan is the one who guided me into the marine science when I started my master study at Xiamen University. As my best role model for a scientist and mentor, he has provided consistent support to me since then. I am also grateful to other members in my supervision panel: Boris Kelly-Gerreyn and Peter Statham. I also thank Shuh-Ji Kao for his constant support on my study both as a mentor and a friend.

The Swire Education Trust is gratefully acknowledged for funding the scholarship for my PhD study. My PhD project included several related programs and received help from many colleagues and collaborators at NOCS and other universities and research institutes. Many thanks to Sue Hartman, Mark Hartman and Jon Campbell who worked closely with me in various programs. The Swire Charitable Trust, the Swire Group Company China Navigation and the crews on the *MV Pacific Celebes* are to be thanked for funding and supporting the operation of the Swire NOCS Ocean Monitoring System (SNOMS) program. Dave Childs provided invaluable analysis of the salinity samples at the NOCS. At the Institute of Ocean Science in Canada, Marty

Davelaar, Jim Christian and Kyle Davidson helped with sample pickups and joined in the SNOMS sample processing exercise. I am grateful for the assistance of the P&O Ferries Ltd. and the captain and crews of *Mv Pride of Bilbao*. My thanks also go to the technicians and students who contributed to the sampling and measurement on the *Mv Pride of Bilbao*. For the sensor evaluation program, Richard Lampitt, Kate Larkin, Maureen Pagnani, Thanos Gkritzalis at the NOCS; Daniela Turk, Douglas Wallace, William Burt, Helmuth Thomas, Jim Eddington, Emily Chua, Claire Normandeau, Trina Whitsitt and Douglas Schillinger at Dalhousie University; Bruce Johnson, Bryan Schofield at the ProOceanus Systems Inc; Cathy Cosca and Richard Feely at Pacific Marine Environmental Lab are to be acknowledged.

I would like to thank all my friends who made my life colorful and cheered me up when the time was tough, especially Suyu Xu, Tingting Shi, Tongchen Han, Chuanpin Zou, Yolanda Mao, Pin-ru Huang, Casey Nixon, Laura Hepburn, Leigh Marsh in Southampton and friends at Xiamen University.

Above all, I dedicate this dissertation to my family for their constant support and unconditional love.

Abbreviations

ACT: Alliance for Coastal Technologies

ALOHA: A Long-Term Oligotrophic Habitat Assessment

BATS: Bermuda Atlantic Time-Series

CARINA: CARbon dioxide IN the Atlantic Ocean

CDIAC: Carbon Dioxide Information Analysis Center

Chl-a: chlorophyll-a

CO_2: carbon dioxide

CRM: Certified Reference Material

DIC: dissolved inorganic carbon

DO: dissolved oxygen

EA: Eastern Atlantic pattern

ENSO: El Nino Southern Oscillation

ESTOC: European Station for Time Series in the ocean

GLODAP: GLobal Ocean Data Analysis Project

HOT: Hawaii Ocean Time-series

MLD: mixed layer depth

NAO: North Atlantic Oscillation

NCP: net community production

NDIR: non-dispersive infrared

Abbreviations

NOAA: National Oceanic and Atmospheric Administration

NOCS: National Oceanography Centre, Southampton

NTA: salinity-normalized alkalinity

PACIFICA: PACIFic ocean Interior Carbon

PAP: Porcupine Abyssal Plain

pCO_2: partial pressure of carbon dioxide

PDO: Pacific Decadal Oscillation

POB: Mv Pride of Bilbao

POM: particulate organic matter

SD: standard deviation

SDC: Simple Dilution or Concentration

SNOMS: Swire NOCS Ocean Monitoring System

SOO: ship of opportunity

SST: sea surface temperature

TA: total alkalinity

VOS: Volunteer Observing Ship

ZPC: zero point calibration

Ω: saturation state of $CaCO_3$

Chapter 1: Introduction

This chapter begins with a brief introduction to the research background of the present carbon cycle study, which is followed by a general review of the variability of the marine carbonate system and air-sea CO_2 flux, as well as the predicted future changes in the seawater CO_2 system response to the oceanic uptake of anthropogenic CO_2. The objectives of this PhD project and the structure of this dissertation were described at the end of this chapter.

1.1 Research Background

Carbon dioxide (CO_2) is one of the most important greenhouse gases and it plays a critical role in modulating the climate of the planet. Since the beginning of the industrial revolution, large quantities of CO_2 have been emitted into the atmosphere by human activities, which has resulted in a rapid increase in the concentration of atmospheric CO_2 (see the Keeling Curve at http://keelingcurve.ucsd.edu/). As shown in Figure 1.1, the accumulation of anthropogenic CO_2 very likely has a significant impact on the warming of the Earth's climate [IPCC, 2007, 2013].

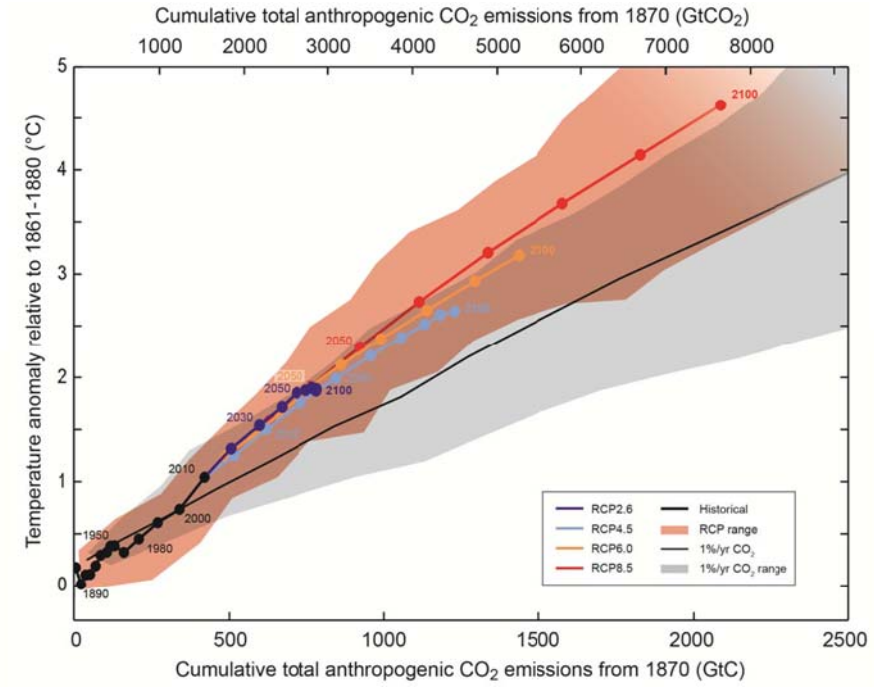

Figure 1.1 Observations and models suggest that the cumulative emissions of anthropogenic CO_2 largely determine the global mean surface warming. Figure from IPCC [2013].

The world's ocean is the largest non-geological carbon reservoir and the inorganic carbon dissolved in the ocean is about 50 times more than the CO_2 in the atmosphere [Field and Raupach, 2004; Zeebe and Wolf-Gladrow, 2001]. The ocean rapidly exchanges CO_2 with the atmosphere and takes up about 25% of anthropogenic CO_2 annually, thereby decreasing the atmospheric CO_2 level [Le Quere et al., 2009, 2010; McKinley et al., 2011; Sabine et al., 2004; Takahashi et al., 2002]. Once CO_2 is taken up and transported from the upper layer (~100 m) into the ocean interior, it is isolated from the atmosphere on time scales of hundreds and thousands of years. This

carbon transportation is mainly carried out through the solubility and biological pumps relating to the deep water formation and the marine biological production, respectively [Emerson and Hedges, 2008]. On the time scale of several thousands of years, it is estimated that ~90% of anthropogenic CO_2 will end up in the ocean [Sabine et al., 2004].

On one hand, the oceanic carbon uptake slows the buildup of atmospheric CO_2 and mitigates human-driven climate change. On the other hand, the invasion of anthropogenic CO_2 is acidifying the ocean and altering the seawater carbonate chemistry (Figure 1.2), which results in ocean acidification as 'the other CO_2 problem' [Doney et al., 2009a]. This could have a variety of deleterious impacts on marine ecosystems especially for the calcifying organisms such as corals and coccolithophores [Andersson and Gledhill, 2013; Doney, 2009; Gattuso and Hansson, 2011; Orr et al., 2005].

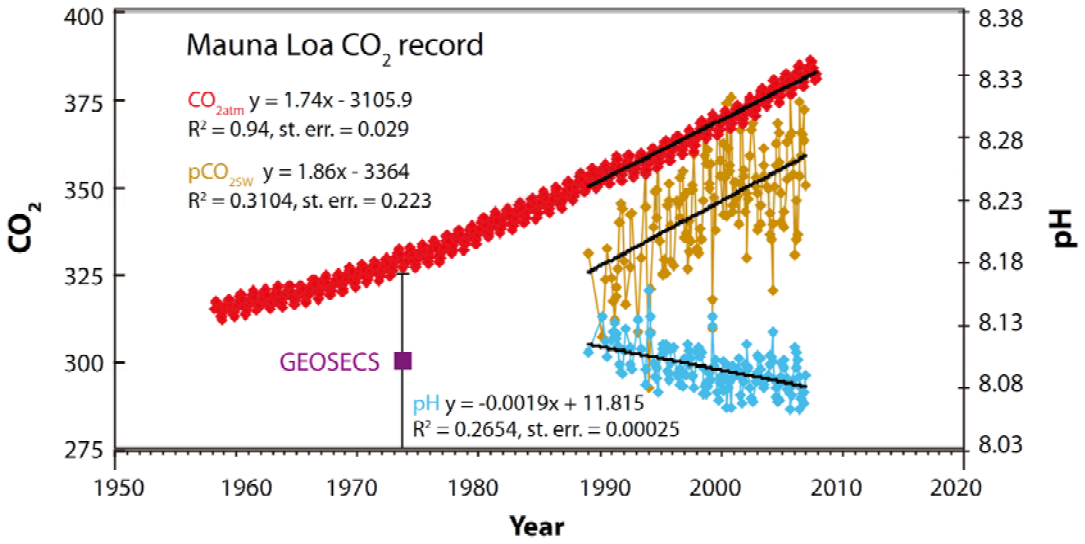

Figure 1.2 The increasing atmospheric CO_2 concentration at Mauna Loa in ppm (red), and the increasing seawater pCO_2 in µatm (tan) and decreasing pH (cyan) in the surface water in the subtropical North Pacific. Figure adapted from Doney et al. [2009a].

1.2 The marine carbonate system

The marine carbonate system can be characterized from any two of the four key parameters: dissolved inorganic carbon (DIC), total alkalinity (TA), pH and partial

pressure of CO_2 (pCO_2), together with the knowledge of relevant dissociation constants and auxiliary environmental variables such as temperature, salinity and nutrients [Zeebe and Wolf-Gladrow, 2001].

The solution chemistry of CO_2 is different to most other gases due to the fact that CO_2 not only dissolves in seawater, but also reacts with water as a proton donor:

$$CO_2 + H_2O \overset{K_0}{\Leftrightarrow} H_2CO_3^* \overset{K_1}{\Leftrightarrow} H^+ + HCO_3^- \overset{K_2}{\Leftrightarrow} 2H^+ + CO_3^{2-} \qquad (1.1)$$

$$CO_2 + CO_3^{2-} + H_2O \Leftrightarrow 2HCO_3^- \qquad (1.2)$$

where K_0 is the solubility coefficient of CO_2, K_1 and K_2 are the first and second dissociation constants of carbonic acid, respectively. DIC is the sum of concentrations of the three different inorganic forms of CO_2: aqueous CO_2 plus carbonic acid ($H_2CO_3^*$), bicarbonate (HCO_3^-) and carbonate ions (CO_3^{2-}):

$$DIC = H_2CO_3^* + [HCO_3^-] + [CO_3^{2-}] \qquad (1.3)$$

At typical seawater conditions, HCO_3^- is the dominant species followed by CO_3^{2-}, while $H_2CO_3^*$ only accounts for ~1% of DIC (Figure 1.3). The chemical equilibrium among these components happens on time scales of a few minutes [Emerson and Hedges, 2008].

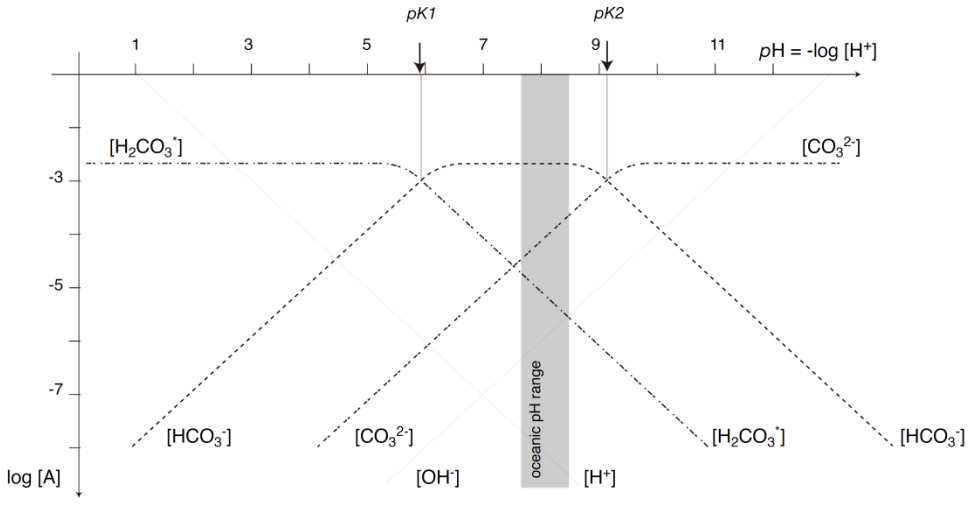

Figure 1.3 The concentrations of different components of DIC as a function of pH. Note that it is the relative proportions of these components that controls the pH and not vice versa. Figure from Sarmiento and Gruber [2006].

TA is defined as the numbers of moles of hydrogen ion equivalent to the excess of proton acceptors (bases formed form weak acids with a dissociation constant pK > 4.5 at 25°C, standard pressure and at zero ionic strength) over proton donators (acids with pK < 4.5) in one kilogram of seawater [Dickson, 1981, 1992; Dickson et al., 2007]. Based on this definition Dickson derived the following expression for TA in seawater:

$$TA = [HCO_3^-] + 2[CO_3^{2-}] + [B(OH)_4^-] + [OH^-] + [HPO_4^{2-}] + 2[PO_4^{3-}] + [H_3SiO_4^-] + [NH_3] + [HS^-] + \cdots - [H^+] - [HSO_4^-] - [HF] - [H_3PO_4] - [HNO_2] - \cdots \quad (1.4)$$

where the ellipses refer to other minor acid-base pairs including those that have not yet been fully identified (e.g. organic alkalinity) which contribute to TA [Dickson, 1981, 1992; Dickson et al., 2007]. At the global mean surface seawater condition, the most abundant components of TA are $[HCO_3^-]$ (76.8%), $2[CO_3^{2-}]$ (18.8%) and $[B(OH)_4^-]$ (4.2%) [Sarmiento and Gruber, 2006].

TA is closely related to the charge balance in seawater. By combining Dickson's definition of TA with the fact of electroneutrality of aqueous solutions, Wolf-Gladrow et al. [2007] derived an alternative 'explicit conservative' expression for TA:

$$TA_{ec} = [Na^+] + 2[Mg^{2+}] + 2[Ca^{2+}] + [K^+] + 2[Sr^{2+}] + \ldots - [Cl^-] - [Br^-] - [NO_3^-] - \ldots + TNH_3 - TPO_4 - 2TSO_4 - THF - THNO_2 \quad (1.5)$$

where the ellipses refer to the additional ions with minor or even negligible concentrations, and TPO_4, TNH_3, TSO_4, THF and $THNO_2$ are the total concentrations of phosphate, ammonia, sulphate, fluoride and nitrite respectively. The expression TA_{ec} is especially well suited to derive alkalinity changes due to biogeochemical processes such as precipitation and dissolution of carbonates or uptake of various nutrients by microalgae (for details see Wolf-Gladrow et al. [2007]). A comprehensive discussion on the variability of TA and the TA-salinity relationship is presented in Chapter 4.

pH ($pH = -\log_{10} [H^+]$) reflects the thermodynamic state of the acid-base systems in the seawater. The ocean can be seen as a natural buffer system and the pH of

seawater (normal range: 7.5 to 8.4) is mainly regulated by the carbonate buffering system ($CO_2-HCO_3^- -CO_3^{2-}$) [Zeebe, 2012].

pCO_2 assigned to a seawater sample refers to the partial pressure of CO_2 in the gas phase that is in equilibrium with the seawater. By recasting the equations of the dissociation constants of K_0, K_1 and K_2 [Sarmiento and Gruber, 2006], pCO_2 can be expressed as:

$$pCO_2 = \frac{K_2}{K_0 K_1}\frac{[HCO_3^-]^2}{[CO_3^{2-}]} \qquad (1.6)$$

We can approximate DIC as the sum of bicarbonate and carbonate ions and approximate TA as the carbonate alkalinity respectively:

$$TA \approx [HCO_3^-] + 2[CO_3^{2-}] \qquad (1.7)$$

$$DIC \approx [HCO_3^-] + [CO_3^{2-}] \qquad (1.8)$$

Combining Equations of 1.7 and 1.8, we can express $[HCO_3^-]$ and $[CO_3^{2-}]$ in terms of DIC and TA (usually good to within 10%) [Sarmiento and Gruber, 2006].

$$[HCO_3^-] \approx 2DIC - TA \qquad (1.9)$$

$$[CO_3^{2-}] \approx TA - DIC \qquad (1.10)$$

Accordingly, we can rewrite Equation 1.6 as:

$$pCO_2 = \frac{K_2}{K_0 K_1}\frac{[HCO_3^-]^2}{[CO_3^{2-}]} \approx \frac{K_2}{K_0 K_1}\frac{(2DIC-TA)^2}{(TA-DIC)} \qquad (1.11)$$

As indicated by Equation 1.11, pCO_2 is affected by the ratio of dissociation constants ($\frac{K_2}{K_0 K_1}$, which is a function of seawater temperature and salinity), and the concentrations of DIC and TA.

1.3 Control of the marine carbonate system

In the ocean, physical transport redistributes materials within the water column, while biological and chemical processes transform carbon between inorganic and organic matters forms, as well as between dissolved and particulate phases. The oceanic distributions of the carbonate variables are thus mainly controlled by the

interplay of physical and biogeochemical processes. Meanwhile, external sources may also play an important role in certain marine environments (e.g. riverine inputs in coastal regions). The following subsections describe the influences of some important controlling factors on the marine carbonate system.

1.3.1 Physical mixing

Mixing processes (e.g. currents, tides, advection, upwelling) result in changes in seawater biogeochemistry because different water parcels have different properties. DIC and TA (in gravimetric units) are both conservative quantities with respect to mixing. This means, given that there is no biogeochemical alteration when water parcels are mixed together, the amount of DIC (or TA) in the mixture is equal to the sum of those in the individual initial parcels:

$$X_m * \sum_i M_i = \sum_i X_i M_i \qquad (1.12)$$

where X_m is the concentration in the mixture, X_i and M_i refer to the concentrations and masses of different water parcels, respectively. However, pH and pCO_2 are not conservative during mixing and do not follow this linear mixing relationship.

Precipitation over the ocean can be considered as a mixing between seawater and freshwater, while evaporation is a special mixing theme with a negative mixing fraction of the freshwater component. Typical biogeochemical changes in DIC and TA are generally much smaller than their mean values, while freshwater addition and removal have an important impact on the concentrations of DIC and TA. Therefore, DIC and TA measured at different salinities are usually normalized to a constant salinity in order to remove the effect of freshwater fluxes:

$$nX = X_{obs} * S_{ref} / S_{obs} \qquad (1.13)$$

where X_{obs} refers to the measured variable (e.g. DIC, TA), S_{obs} is the measured salinity, and S_{ref} is a constant salinity value (35 or the mean salinity from observation). In coastal regions, a salinity adjustment using the region specific zero-salinity end-member (X_{S0}) is suggested [Friis et al., 2003]:

$$nX = (X_{obs} - X_{S0}) * S_{ref} / S_{obs} + X_{S0} \qquad (1.14)$$

where the non-zero freshwater end member X_{S0} represents the influences of local river run off, upwelling, sediment flux, calcification etc. (see the discussion in Chapter 4).

1.3.2 Air-sea CO_2 exchange

The developments in techniques quantifying air-sea gas exchange and gas transfer velocity were extensively reviewed by Wanninkhof et al. [2009]. The gas exchange of CO_2 at the air-sea interface is driven by the difference of pCO_2 between the lower atmosphere ($pCO_{2,air}$) and the surface ocean ($pCO_{2,sea}$). The ocean takes up CO_2 from the atmosphere if $pCO_{2,sea}$ is lower than $pCO_{2,air}$ (ocean as a CO_2 sink). In the opposite case when $pCO_{2,sea} > pCO_{2,air}$, there would be a net CO_2 efflux from the ocean (ocean as a CO_2 source). Since $pCO_{2,air}$ is relatively uniform over the globe, the variability of the air-sea pCO_2 difference is mainly determined by variations in $pCO_{2,sea}$ [Sarmiento and Gruber, 2006].

It is obvious that oceanic CO_2 uptake results in increases in $pCO_{2,sea}$ and the concentrations of DIC. However, the changes in the components of DIC are not the same: the CO_2 invasion results in increases in concentrations of $H_2CO_3^*$ and HCO_3^-, but decreases in that of CO_3^{2-} (Equations 1.1 and 1.2). The part dissociations of $H_2CO_3^*$ and HCO_3^- increase the concentration of H^+ and decrease the seawater pH. On the contrary, the release of CO_2 from the ocean has the opposite effect. It is noted that TA remains constant during the CO_2 gas transfer because the charge balance is not affected (Figure 1.4) [Wolf-Gladrow et al., 2007].

1.3.3 Biological production

The variability of the marine carbonate system is related to several important biological processes in the ocean carbon cycle, e.g. production and decomposition of organic carbon matter, precipitation and dissolution of $CaCO_3$. The relative changes in the carbonate variables associated with these processes are demonstrated in Figure 1.4 [Falkowski et al., 1998; Gattuso et al., 1998; Zeebe and Wolf-Gladrow, 2001].

As shown in Equation 1.15 and Figure 1.4, precipitation of $CaCO_3$ decreases DIC and TA in a ratio of 1:2. Meanwhile, this process releases dissolved CO_2 to the

surrounding water resulting in an increase in pCO_2 and a decrease in pH respectively [Ware et al., 1992; Zeebe and Wolf-Gladrow, 2001]. In contrast, dissolution of $CaCO_3$ has the opposite effects.

$$\begin{aligned} &Ca^{2+} + 2HCO_3^- \underset{\text{CaCO}_3\text{ dissolution}}{\overset{\text{CaCO}_3\text{ precipiation}}{\rightleftharpoons}} CaCO_3 + CO_2 + H_2O; \\ &\Delta DIC / \Delta TA = 1:2 \end{aligned} \tag{1.15}$$

Particulate organic matter (POM) produced by biological production in the surface ocean has a rather constant elemental composition. The traditional stoichiometric formula for the production and decomposition of the marine POM is written as:

$$\begin{aligned} &106CO_2 + 16HNO_3 + H_3PO_4 + 122H_2O \underset{\text{Remineralization}}{\overset{\text{Photosynthesis}}{\rightleftharpoons}} (CH_2O)_{106}(NO_3)_{16}H_3PO_4 + 138O_2 \\ &\Delta DIC / \Delta TA = -106:17 \text{ (only consider N, P)} \\ &\Delta DIC / \Delta TA = -106:21.8 \text{ (assuming a S:P ratio of 2.4)} \end{aligned} \tag{1.16}$$

The 'Redfield Ratios' (C:N:P:O_2 = 106:16:1:-138 in Equation 1.16) are named after the oceanographer A. C. Redfield who was among the first to quantify them [Redfield et al., 1934, 1963; Sarmiento and Gruber, 2006]. These ratios are very useful to quantitatively relate the fluxes of carbon and nutrients in marine biogeochemistry research. However, this stoichiometry has been challenged by studies that suggested lower contents of hydrogen and oxygen of the POM [Anderson, 1995; Anderson and Sarmiento, 1994; Hedges et al., 2002], and studies that observed variable carbon to nitrogen ratios in the surface ocean [Koeve, 2006; Quigg et al., 2003; Sambrotto et al., 1993] (also see the discussion in Chapter 5).

As shown in Equation 1.16 and Figure 1.4, photosynthesis of marine plankton utilizes CO_2 and nutrients to produce organic matter and oxygen. This process decreases the values of DIC and pCO_2 while pH is elevated. Meanwhile, it results in a slight increase in TA because of the co-transportation of nutrients and H^+ (or OH^-) by the phytoplankton. Estimated from the classical Redfield Ratios of C:N:P and the nutrient-H^+-compensation principle [Wolf-Gladrow et al., 2007], the relative ratio of the changes in DIC and TA for photosynthesis is -106:17. If sulphur is also considered and a S:P ratio of 2.4 is assumed, the ratio of the changes in DIC and TA for photosynthesis is -106:21.8 [Wolf-Gladrow et al., 2007]. Conversely, remineralization of organic matter leads to increases in DIC and pCO_2 coupled with decreases in pH and TA.

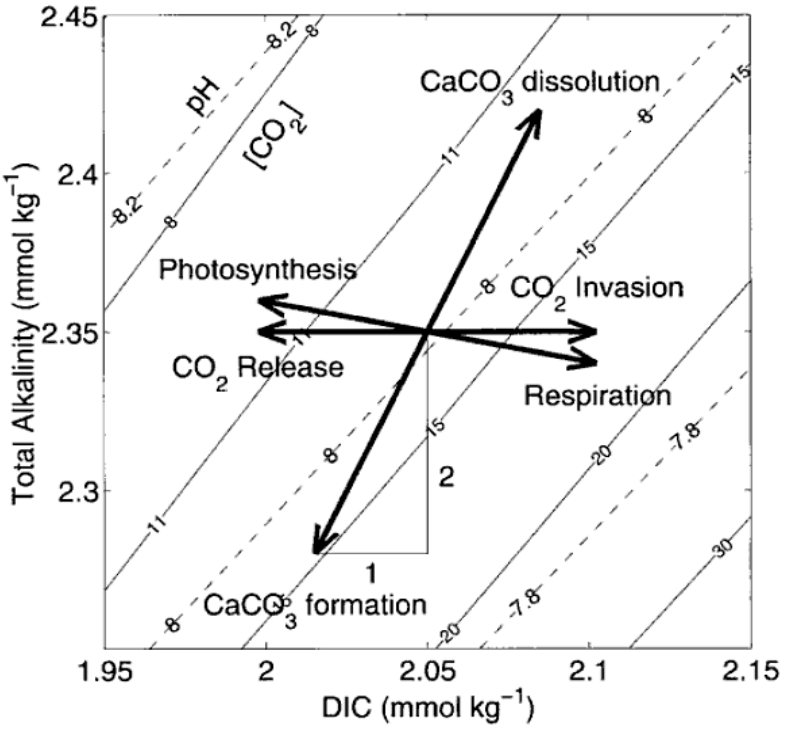

Figure 1.4 The vector diagram showing the influences of various processes on the marine carbonate system. Air-sea CO_2 exchange alters DIC without changing TA; the formation and dissolution of $CaCO_3$ result in changes in DIC and TA in a ratio of 1:2; the photosynthesis and respiration change DIC and TA in a ratio of -106:17 (-106:21.8 if assuming a S:P ratio of 2.4). See the text for detail. Figure from Zeebe and Wolf-Gladrow [2001].

Aside from the production/dissolution of $CaCO_3$ and photosynthesis/respiration as discussed above, changes in TA could result from other biogeochemical processes, such as assimilation of other nutrients (e.g. N_2 fixation, NH_3, silicate), anaerobic oxidation of organic matter. The physical and biogeochemical processes affecting TA are summarized in Table 1.1.

Table 1.1 Changes in seawater TA caused by various physical and biogeochemical processes, after Wolf-Gladrow et al. [2007] and Chen [2002].

(The table is shown on the next page)

Processes	Changes of TA in seawater
Addition or removal of freshwater with zero TA concentration	$TA_{S1} = TA_{S0} * S_1/S_0$, where TA_{S0} and TA_{S1} are the TA corresponding to salinity S_0 and S_1 respectively
Mixing of water masses with different alkalinity contents	$TA_m = \sum_i TA_i M_i / \sum_i M_i$, where TA_m is the TA in the mixture, TA_i and M_i refer to the TA and masses of different water masses
Air-sea CO_2 exchange	No changes in TA
Precipitation and dissolution of $CaCO_3$: $Ca^{2+} + CO_3^{2-} \Leftrightarrow CaCO_3$; $Ca^{2+} + 2HCO_3^- \Leftrightarrow CaCO_3 + CO_2 + H_2O$	Production/dissolution of 1 mole of $CaCO_3$: decreases/increases TA by 2 moles
Photosynthesis and respiration: $106CO_2 + 122H_2O + 16HNO_3 + H_3PO_4 \Leftrightarrow (CH_2O)_{106}(NH_3)_{16}H_3PO_4 + 138O_2$	Production/decomposition of 1 mole of $(CH_2O)_{106}(NH_3)_{16}H_3PO_4$ assuming a S:P ratio of 2.4: increases/decreases TA by 21.8 moles
Uptake and release of nutrients by algae: the column on the right shows the changes in TA caused by uptake of nutrients, which has the opposite effects to that of release of nutrients	For 1 mole of nutrient uptake: NO_3^-, NO_2^-, HNO_2: increases TA by 1 mole NH_3, NH_4^+: decreases TA by 1 mole $H_3PO_4, H_2PO_4^-$, HPO_4^{2-}, PO_4^{3-}: increases TA by 1 mole HSO_4^-, SO_4^{2-}: increases TA by 2 moles N_2 (nitrogen fixation): no change in TA unless combined with nitrification $H_4SiO_4, H_3SiO_4^-$: no change in TA
Nitrification: $NH_4^+ + 1.5\ O_2 \Rightarrow NO_2^- + 2H_2O + 2H^+$ (step 1) $NO_2^- + 0.5\ O_2 \Rightarrow NO_3^-$ (step 2)	For 1 mole of NH_4^+: step 1: decreases TA by 2 moles; step 2: no change in TA
Denitrification (anaerobic): $5CH_2O + 4H^+ + 4NO_3^- \Rightarrow 2N_2 + 5CO_2 + 7H_2O$	For 1 mole of NO_3^- : increases TA by 1 mole
Oxidation of organic matters (anaerobic): $(CH_2O)_{106}(NH_3)_{16}H_3PO_4 + 236MnO_2 + 472H^+ \Rightarrow 106CO_2 + 366H_2O + 236Mn^{2+} + 8N_2 + H_3PO_4$ $+424FeOOH + 848H^+ \Rightarrow 106CO_2 + 742H_2O + 424Fe^{2+} + 16NH_3 + H_3PO_4$ $+53SO_4^{2-} + 106H^+ \Rightarrow 106CO_2 + 106H_2O + 53H_2S + 16NH_3 + H_3PO_4$	For 1 mole of $(CH_2O)_{106}(NH_3)_{16}H_3PO_4$: manganese reduction: increase TA by 471 moles iron reduction: increase TA by 863 moles sulfate reduction: increase TA by 121 moles
Methane oxidation (anaerobic): $CH_4 + SO_4^{2-} \Rightarrow HCO_3^- + HS^- + H_2O$	For 1 mole of CH_4: increase TA by 2 moles
Changes in organic bases	Not fully quantified

1.3.4 Temperature and salinity effects on pCO_2

The aqueous pCO_2 can be expressed as a function of the ratio of dissociation constants, DIC and TA (Equation 1.11). As a result, all processes affecting DIC and TA would result in corresponding changes in pCO_2. Moreover, seawater pCO_2 varies with temperature and salinity under an isochemical condition (DIC and TA keep constant). The sensitivity of pCO_2 with respect to temperature and salinity is a result of temperature and salinity dependency of the dissociations constants [Sarmiento and Gruber, 2006].

It was shown that pCO_2 increases with temperature in a closed system when the seawater chemical composition remains constant [Takahashi et al., 1993]. In order to distinguish the thermal and non-thermal forcing of pCO_2, a simplistic but instructive temperature normalization was proposed [Takahashi et al., 1993]:

$$pCO_{2,NT} = pCO_{2,Tobs} * e^{0.0423(T_{mean} - T_{obs})} \qquad (1.17)$$

where the $pCO_{2,Tobs}$ and T_{obs} stand for the observed temperature and pCO_2, and $pCO_{2,NT}$ is the value being normalized to the mean temperature (T_{mean}). The variability of the temperature-normalized $pCO_{2,NT}$ reflects the pCO_2 changes caused by non-thermal processes such as biological activity, mixing and air-sea CO_2 transfer. On the other hand, the thermally forced pCO_2 variation ($pCO_{2,Temp}$) can be estimated to assess the potential temperature influence on seawater pCO_2 under isochemical conditions:

$$pCO_{2,Temp} = pCO_{2,mean} * e^{0.0423(T_{obs} - T_{mean})} \qquad (1.18)$$

The salinity dependence of pCO_2 (γS) can be expressed as [Sarmiento and Gruber, 2006]:

$$\gamma S = \frac{S}{pCO_2}\frac{\partial pCO_2}{\partial S} = \frac{\partial \ln pCO_2}{\partial S} \approx 1 \qquad (1.19)$$

The changes in salinity at the surface are mainly driven by precipitation and evaporation which also change DIC and TA. When the salinity-related changes in DIC and TA are taken into account, the net effect of freshwater changes on the pCO_2

sensitivity increases by 60% compared to that shown in the Equation 1.19 [Sarmiento and Gruber, 2006].

1.4 Variability of the marine carbonate system

1.4.1 Spatial variability

The vertical distribution of the carbonate variables in the water column is mainly controlled by physical mixing coupled with the biological pump [Emerson and Hedges, 2008; Sarmiento and Gruber, 2006]. The surface concentrations of DIC and TA are lower than those in the deep ocean (Figure 1.5). The vertical gradients of DIC and TA are mainly generated by the biological production of POM and $CaCO_3$ in the upper ocean (decrease DIC and TA) and their decomposition during the sinking process (increase DIC and TA). As the downward transport of $CaCO_3$ is about 10 times smaller than that of organic matter, the vertical difference of TA is much smaller than that of DIC [Sarmiento and Gruber, 2006]. Because of the CO_2 released from the remineralization of the export POM, pCO_2 generally increases with depth which is similar to DIC (pH decreases with depth). In the open ocean, the distribution and movements of major water masses also have a significant impact on the vertical distribution of the carbonate variables. In shallow waters, re-suspension and the processes at the water-sediment interface could play an important role in affecting the properties of bottom waters.

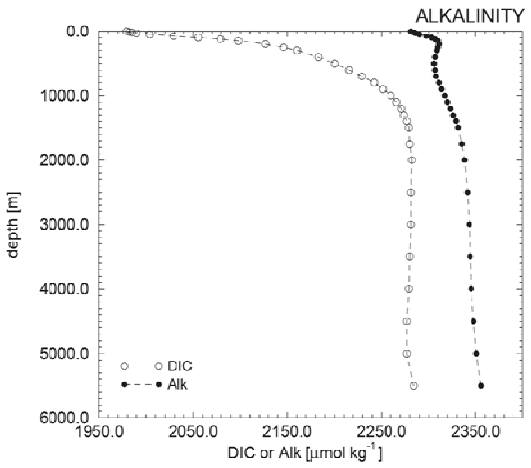

Figure 1.5 The global mean profiles of DIC and TA. Figure from Sarmiento and Gruber [2006].

In the surface ocean, the carbonate system varies regionally with contrasting environmental settings relating to various physical and biogeochemical processes. Generally, the spatial variability in coastal regions is more intense in comparison to that in the open ocean. This is due to the fact that the coastal regions are more dynamic in physical processes; more biologically productive because of the nutrient inputs from rivers and coastal upwelling; and more vulnerable to anthropogenic influences [Cao et al., 2011; Chen and Borges, 2009; Chen et al., 2003; Gattuso et al., 1998]. Spatial differences need to be taken into consideration when generalizing observations to larger scales. Take the CO_2 flux estimation for example, the US South Atlantic Bight was estimated to be a strong CO_2 source to the atmosphere based on one single linear transect (2.5 mol C m^{-2} yr^{-1}) [Cai et al., 2003], while an entire-basin survey reveals that it is a CO_2 sink at a rate of 0.5 mol C m^{-2} yr^{-1} [Jiang et al., 2008]. Adequate spatial coverage and resolution is thus important to produce a robust upscale estimation especially in dynamic regions.

1.4.2 Diurnal to intra-seasonal variability

The dominating controlling factor of the surface ocean carbonate system on short-term time scales is mainly associated with local physical and biological conditions. In the oligotrophic open ocean, the daily changes in DIC and TA are generally insignificant while the diurnal pCO_2 cycle is mainly regulated by temperature effects [Bates et al., 1996; Dai et al., 2009]. In highly productive areas, diurnal variations of oxygen and carbonate variables tend to be dominated by biological cycles [Dai et al., 2009; Yates et al., 2007]. In hydro-dynamic regions such as estuaries and coastal shallow water, tidal advection and currents may be the dominant factor controlling the variability of the CO_2 system [Dai et al., 2009; de la Paz et al., 2008a; Jiang et al., 2011]. Coccolithophore blooms [Harlay et al., 2010, 2011] and meteorological forcing such as tropical cyclones and typhoons [Bates et al., 1998; Nemoto et al., 2009] also can be important controls resulting in significant short-term changes in the carbonate system.

However, variability of the seawater carbonate system is often modulated by the bio-physical interactions rather than by one single dominant factor. In the English Channel, Borges and Frankignoulle [1999] found that the daily variations in pCO_2

mainly depended on the tidal motions but were modulated by the biological activities. In a shallow tidal creek in the Bay of Cadiz, the daily variability of the carbonate system was mainly controlled by tidal mixing and modulated by the residence time of the water relating to the spring-neap tidal cycle [de la Paz et al., 2008b]. The diurnal to weekly dynamics of carbon and oxygen in two productive nearshore shallow systems off Taiwan was found to be controlled by the interactions of biological production of local benthic ecosystems and the varying intensities of tidal mixing and coastal upwelling during the spring-neap tidal cycle [Jiang et al., 2011]. DeGrandpre et al. [1998] attributed the short-term biogeochemical dynamics in California coastal waters to the thermocline movement and the advection of distinct water types. The one-month mooring observations of pCO_2 and O_2 in Cape Hateras indicated that the gas variability was dominated by biological and advective processes [DeGrandpre et al., 1997].

1.4.3 Seasonal variability

In the temperate and subpolar regions, the seasonal biogeochemical variations have been well constrained by the long-term measurements at marine time-series stations such as ALOHA (A Long-Term Oligotrophic Habitat Assessment, also referred to as Hawaii Ocean Time-series (HOT)) in the North Pacific subtropical gyre [Keeling et al., 2004], BATS (Bermuda Atlantic Time-Series) in the western North Atlantic subtropical gyre [Bates, 2001, 2007; Bates et al., 1996], ESTOC (European Station for Time Series in the ocean) in the eastern part of the North Atlantic subtropical gyre [González-Dávila et al., 2003, 2007a; Santana-Casiano et al., 2007], and OWSM (Ocean Weather Station M) in the high-latitude Norwegian Sea [Skjelvan et al., 2008].

As shown in Figure 1.6b and Figure 1.7c, the seasonal variations of salinity-normalized DIC in the subtropical gyre and high-latitude region are both characterized by winter-spring maxima (associated primarily with the entrainment of subsurface water) and summer-autumn minima (generated from biological uptake), while the changes in the salinity-normalized TA are negligible (Figure 1.6d). On the other hand, the seasonal variability of pCO_2 generally shows a latitudinal difference from temperate to subpolar regions. In the oligotrophic subtropical gyre with

relatively low biological production rate, seawater pCO_2 is dominated by temperature with a single summer maximum and a single winter minimum (Figure 1.6e) which is opposite to that of DIC (Figure 1.6b) [Bates et al., 1996; González-Dávila et al., 2003; Keeling et al., 2004]. In contrast, pCO_2 in the high latitude North Atlantic generally varies in parallel to that of DIC characterized by an annual cycle with a winter peak (Figure 1.7b) [Körtzinger et al., 2008; Olsen et al., 2008; Takahashi et al., 1993]. Also see the discussion in Chapter 5.7.

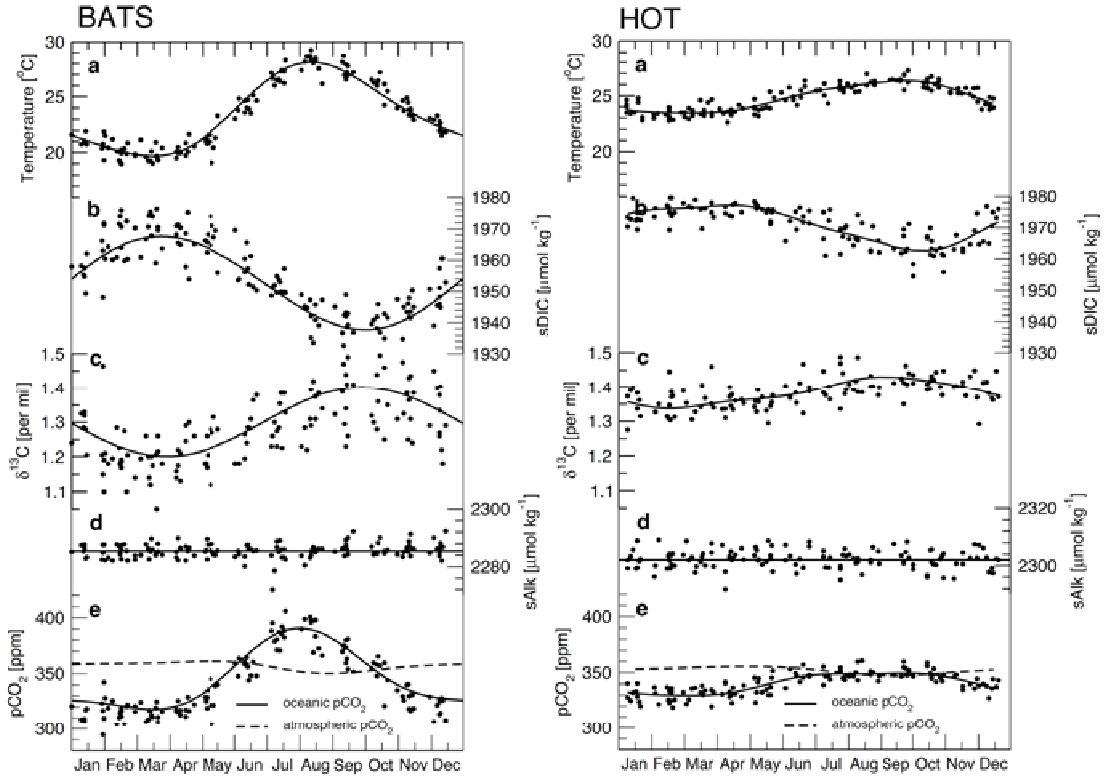

Figure 1.6 Seasonal variations of (a) temperature, (b) salinity-normalized DIC, (c) the reduced isotopic ratio ($\delta^{13}C$) of DIC, (d) salinity-normalized TA, and (e) computed pCO_2 in the surface waters at BTAS and HOT in the subtropical gyre. Figure from Sarmiento and Gruber [2006] based on data reported by Gruber et al. [2002] and Keeling et al. [2004].

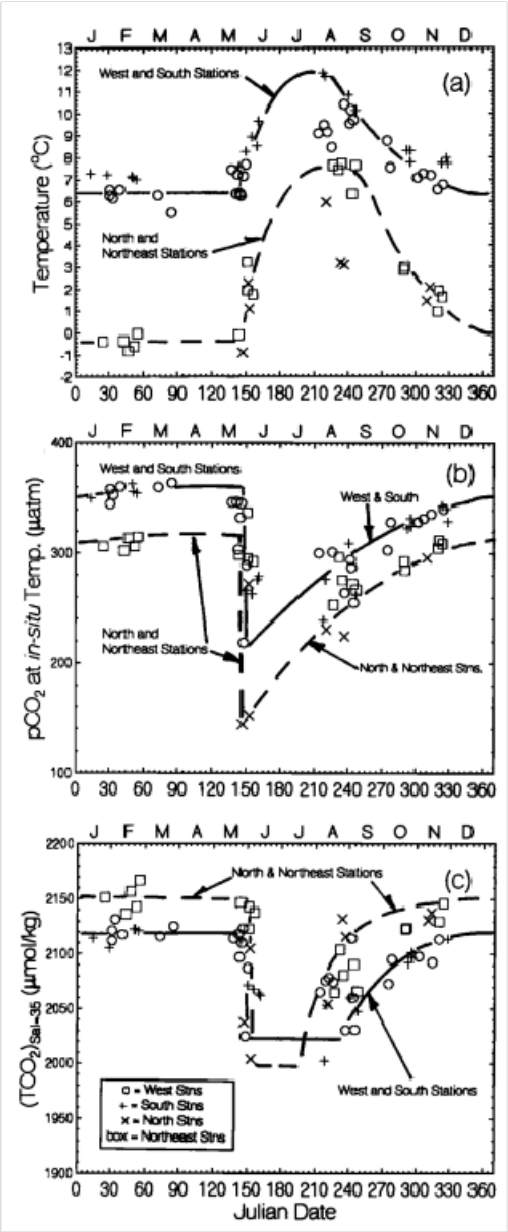

Figure 1.7 Seasonal variations of (a) temperature, (b) seawater pCO_2, and (c) salinity-normalized DIC in the surface water at high-latitude stations around Iceland. Figure adapted from Takahashi et al. [1993].

In biologically active regions, the seasonal variability may result from changes in biological mechanisms and community structure [Bates, 2002]. In coastal regions, the seasonality of the carbonate system can also be related to variations of river input [Borges and Frankignoulle, 1999] and aquaculture discharge [de la Paz et al., 2008b]. In the northern South China Sea, a modeling study suggested that the cumulative effect of air-sea CO_2 exchange is a primary process that modulates the surface pCO_2 on the seasonal time scale [Lu et al., 2012].

1.4.4 Inter-annual to decadal variability

On regional and basin scales, changes in large-scale ocean-atmosphere patterns such as El Nino Southern Oscillation (ENSO), the Pacific Decadal Oscillation (PDO), Eastern Atlantic pattern (EA), and the North Atlantic Oscillation (NAO) appear to drive much of the inter-annual variability of the carbonate system in the ocean [Bates, 2007; Keeling et al., 2004; Takahashi et al., 2009]. For example, the interannual variations of sea surface temperature, mixed-layer depth and DIC in the western North Atlantic subtropical gyre appear to be correlated with the variability of NAO [Bates, 2001, 2007; Gruber et al., 2002]. Studies at ESTOC suggested that the oceanic response in the eastern North Atlantic subtropical gyre is apparently delayed by 3 years relative to the shifts in the NAO and was instead more directly related to the EA [González-Dávila et al., 2003, 2007a; Santana-Casiano et al., 2007]. In a given region, the inter-annual variability can also be caused by the changes in local processes such as the monsoon, river discharge, winter mixing and biological blooms.

Decadal trends of CO_2 variability in surface seawater can only be considered in several well-studied areas that have accumulated enough historical data (e.g. Figure 1.2). Data from BATS give a two-decadal mean rate of surface pCO_2 increase as 1.67 ± 0.28 μatm yr^{-1}, which is similar to the rate of increase in atmospheric pCO_2 (1.78 ± 0.02 μatm yr^{-1}) [Bates, 2007]. At ALOHA in the Pacific, the oceanic pCO_2 increase (2.5 ± 0.02 μatm yr^{-1}) substantially exceeds the 1.5 ± 0.0 μatm yr^{-1} increasing rate of atmospheric pCO_2 [Keeling et al., 2004]. Corresponding increases in surface DIC concentration and decreases in pH were also observed at these stations, as evidence of anthropogenic CO_2 uptake and ocean acidification. Synthesis studies suggested that the mean rate of pCO_2 increase in the surface ocean is 1.8 μatm yr^{-1} in the North Atlantic from 1982 to 1998 [Lefevre et al., 2004], and 0.5 to 2 μatm yr^{-1} in the Equatorial Pacific from a 35-year data collection [Takahashi et al., 2006]. By using a time-trend analysis of deseasonalized surface seawater pCO_2 data, Takahashi et al. [2009] suggested that pCO_2 in the North Atlantic, North and South Pacific and Southern Oceans has increased at an average rate of 1.5 μatm yr^{-1} with basin-specific rates ranging from 1.2 to 2.1 μatm yr^{-1}. For three-decade average (1970-2006), the rate of pCO_2 increase in the surface ocean appears to be similar to that in atmosphere [Takahashi et al., 2009].

1.5 Global synthesis of air-sea CO_2 flux

With the observations of pCO_2 and wind speed, air-sea CO_2 flux (F) can be estimated as:

$$F = k * \alpha * (pCO_{2,sea} - pCO_{2,air}) \qquad (1.20)$$

where α is the CO_2 solubility in seawater as a function of temperature and salinity [Weiss, 1974a], and k is the gas transfer velocity which can be estimated from wind speed [Liss and Merlivat, 1986; McGillis et al., 2001; Nightingale et al., 2000; Sweeney et al., 2007b; Wanninkhof, 1992]. A negative F value corresponds to a net flux direction from the atmosphere to the ocean, while a positive flux indicates a net CO_2 emission from the ocean.

1.5.1 CO_2 flux in the global open ocean

During the past several decades, oceanographic cruises have accumulated large amounts of pCO_2 data which enables the generation of climatological atlases of seawater pCO_2 and air-sea CO_2 flux in the global ocean [Takahashi et al., 1997, 2002, 2009]. Based on millions of pCO_2 measurements obtained since 1970, the climatology pCO_2 was estimated month-by-month with spatial resolution of 4^o latitude by 5^o longitude in the reference year of 2000 (Figure 1.8a) [Takahashi et al., 2009].

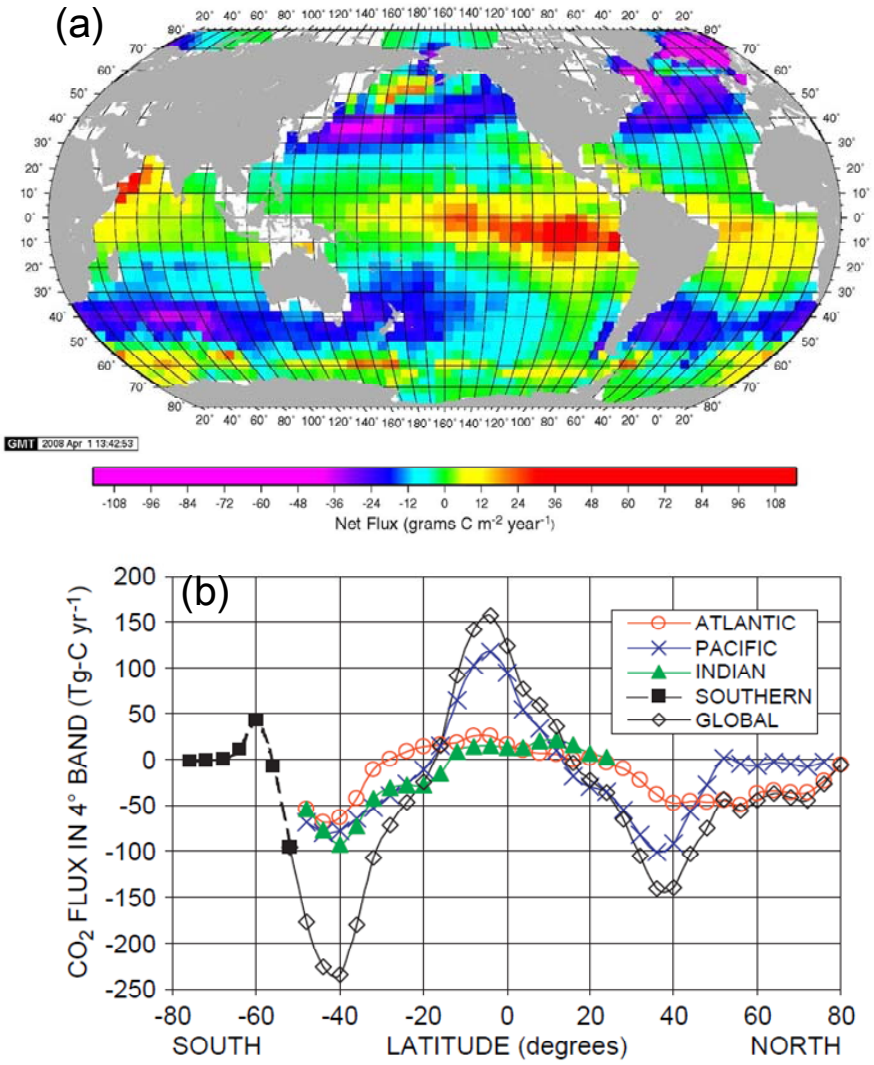

Figure 1.8 (a) Climatological mean annual air-sea CO_2 flux (g C m^{-2} yr^{-1}) and (b) the latitudinal distribution of the air-sea CO_2 flux (Tg C yr^{-1}, Tg = 10^{12} g) for the reference non-El Nino year 2000 [Takahashi et al., 2009].

It is well established that the CO_2 flux shows a latitudinal distribution (Figure 1.8b): the ocean takes up CO_2 mostly in temperate and high latitudes while the outgassing of CO_2 generally occurs in the tropics [Takahashi et al., 2009]. The equatorial ocean is the most prominent CO_2 source to the atmosphere especially in the eastern upwelling region. The Arabian Sea is also an intense source of atmospheric CO_2 due to the high monsoon winds coupled with a high seawater pCO_2 caused by the upwelled deepwater in the northwestern Arabian Sea. When the warm surface water is transported by ocean currents from tropics to higher latitudes, the solubility effect of the cooling seawater creates CO_2 uptake in the subtropical regions. Due to the

combination of the strong winds and the low pCO_2 in the subtropical convergence zone, the temperate mid-latitude oceans in both hemispheres are major sinks absorbing CO_2 from the atmosphere. The Atlantic takes up 41% of the annual global ocean flux although it only covers 23% of the global ocean area. The high-latitude North Atlantic is the most intense CO_2 sink because of the strong phytoplankton bloom in spring and cooling effect in winter. The net flux in the Southern Ocean is small for several reasons: 1) ice cover reduces the gas transfer in winter; 2) the cancellation of summer uptake of CO_2 and winter CO_2 release from the deepwater upwelling; 3) the low biological production probably due to the iron limitation.

The latest global synthesis lead to an estimate of the annual CO_2 sea-air flux in open oceans at -1.4 ± 0.7 Pg yr^{-1}, while the value is -1.6 ± 0.9 Pg yr^{-1} if corrected for under-sampling [Takahashi et al., 2009]. Considering the pre-industrial steady-state ocean as a CO_2 source of 0.4 ± 0.2 Pg yr^{-1}, the total ocean uptake flux was estimated to be -2.0 ± 1.0 Pg yr^{-1} [Takahashi et al., 2009]. This was similar to the results from other independent studies which suggested that the global ocean is presently taking up CO_2 at a rate of 1.5 to 2.0 Pg yr^{-1} [Bender et al., 2005; Fletcher et al., 2006; Gloor et al., 2003; Jacobson et al., 2007a, b; Sarmiento et al., 2000].

1.5.2 CO_2 flux in the global continental margins

Despite the moderate surface area (7% of the sea surface), continental margins are among the most biologically and geochemically active areas of the biosphere and play a significant role in the global biogeochemical cycles [Chen and Borges, 2009; Chen and Swaney, 2012; Gattuso et al., 1998; Muller-Karger et al., 2005]. These regions are characterized by highly dynamic mixing processes such as river input, tides, currents, upwelling. Moreover, nutrient supply from riverine input and coastal upwelling supports a disproportionally high biological production. The high spatiotemporal variability in coastal environments thus makes assessing the carbon fluxes a challenging task in these regions. There were long-lived arguments on whether the continental margins are net sources [Mackenzie et al., 2000; Smith and Mackenzie, 1987; Smith and Hollibaugh, 1993] or sinks [Borges et al., 2005; Chen, 2004; Gattuso et al., 1998] for atmospheric CO_2.

The opposing views seem to be reconciled by the conclusion that continental shelves act as sinks and near-shore ecosystems as sources of atmospheric CO_2 [Chen and Borges, 2009]. pCO_2 data from 60 continental shelves indicate that most open shelves in the temperate and high-latitude regions are indeed CO_2 sinks during all seasons, while the low latitude shelves seem to be over-saturated in CO_2 [Chen and Borges, 2009]. Such latitudinal variability of air-sea flux is related to biological activity and the background pCO_2 level of the oceanic water circulating over these shelves. In order to answer why are some marginal seas sources of atmospheric CO_2, Dai et al. [2013] proposed the concept of Ocean-dominated Margin in contrast to previously recognized River-dominated Ocean Margin. The case studies in the South China Sea and the Caribbean Sea showed that the open ocean could provide external CO_2 sources to continental margins thereby modulating the CO_2 fluxes in the Ocean-dominated Margin [Dai et al., 2013]. In total, Chen and Borges [2009] estimated that the continental shelves absorbed CO_2 with the rates as 0.33-0.36 Pg yr^{-1}, which corresponds to an additional sink of 27-30% of the CO_2 absorbed by the open ocean. This assessment agreed with the corrected air-sea CO_2 flux estimated by other researchers [Cai et al., 2006; Mackenzie et al., 2000; Ver et al., 1999a, b].

On the other hand, Chen et al. [2012] suggested a transit from strong sources of CO_2 in the upper estuaries to sinks of CO_2 in large river plums. Most inner estuaries act as source of CO_2 to the atmosphere due to their heterotrophic metabolism status sustained by the terrestrial input of organic carbon and waste water in populated areas [Chen et al., 2012; Chen and Swaney, 2012]. Based on data from 106 estuaries, Chen et al. [2012] estimated that the global estuaries release 0.26 Pg C yr^{-1} to the atmosphere. By summarizing data from 118 world's rivers, the global riverine transport of dissolved organic carbon was estimated to be 0.20 Pg C yr^{-1} with a 0.05 Pg C yr^{-1} removal in the estuaries (net input into the ocean = 0.15 Pg C yr^{-1}) [Dai et al., 2012]. Fuelled by the degradation of terrestrial organic matter [Borges et al., 2005], the near-shore aquatic systems are estimated to release CO_2 to the atmosphere at a rate of 0.50 Pg yr^{-1} [Chen and Borges, 2009]. It should be noted that the although the aquatic compartments are CO_2 sources, the whole systems of salt marshes and mangroves act as sinks for atmospheric CO_2 because of their above-ground high primary production [Hopkinson, 1988; Wang and Cai, 2004]. However, the magnitude of carbon burial in coastal vegetated habitats was estimated to have been

decreasing rapidly over the past century due to the anthropogenic influences [Hopkinson et al., 2012].

1.6 Predicted future changes in the marine carbonate system

The impacts of anthropogenic CO_2 have already been observed in the ocean, e.g. the decadal variations of the carbonate system in the surface water (Chapter 1.4.4). The surface ocean pH is estimated to have decreased by 0.1 unit from 8.2 to 8.1 since the industrial revolution [Royal Society, 2005]. Direct measurements at several long-term time-series stations clearly show the decreasing pH and saturation state of $CaCO_3$ (Ω) in the surface ocean [Bates, 2007; González-Dávila et al., 2007b]. The concentration of atmospheric CO_2 is expected to continue to increase in years to come [IPCC, 2007]. However, assessing future changes in the ocean-carbon-climate system is complex due to interactions of the potential negative/positive feedbacks of ocean physics and biology [Doney et al., 2009b; Gruber et al., 2004]. The major vulnerabilities in the prediction include ocean warming, enhanced ocean stratification, changes in wind pattern and the biological pump [Doney et al., 2009b].

From the chemical aspect, the changes in the marine carbonate system due to the anthropogenic CO_2 invasion can be well constrained. In response to the increasing atmospheric CO_2 level, the concentrations of $H_2CO_3^*$, HCO_3^- and DIC in the seawater will increase, which are accompanied by decreases in the concentration of CO_3^{2-}, pH and Ω (Figure 1.9). The surface ocean pH is predicted to decrease by 0.3 to 0.4 unit at the end of this century under the business-as-usual scenario if CO_2 emissions continue to increase [Orr et al., 2005]. Depending on the influences of temperature, buffering capacity and circulation, the undersaturation of $CaCO_3$ ($\Omega < 1$) is expected to be first observed in the Arctic and the Southern Ocean [Feely et al., 2009; Orr et al., 2005; Steinacher et al., 2009].

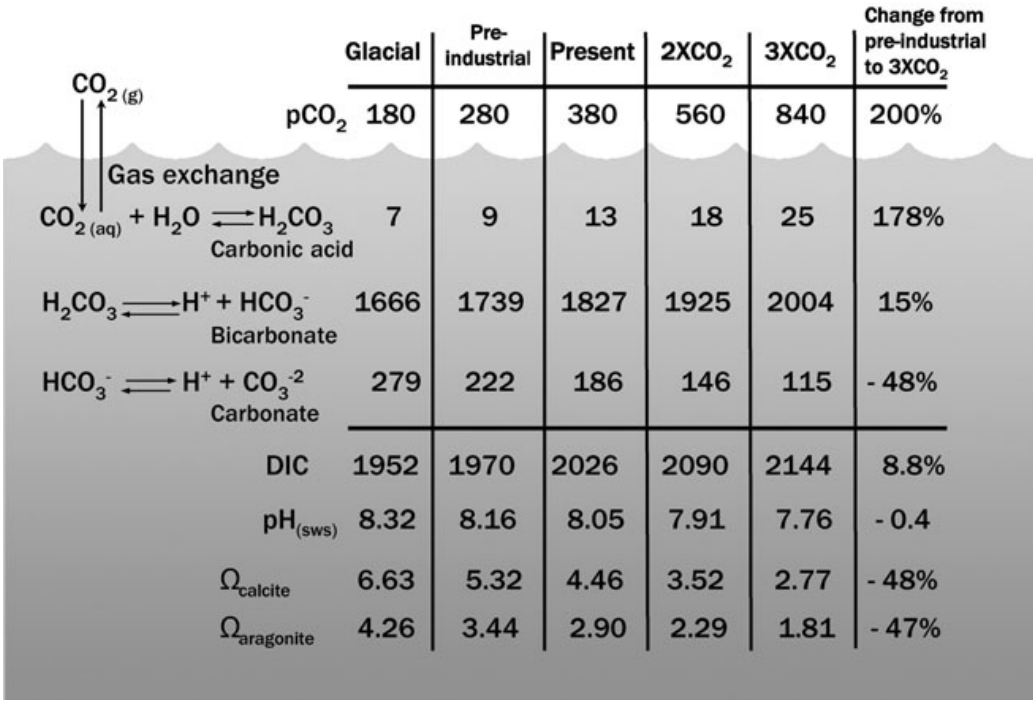

	Glacial	Pre-industrial	Present	$2XCO_2$	$3XCO_2$	Change from pre-industrial to $3XCO_2$
pCO_2	180	280	380	560	840	200%
	7	9	13	18	25	178%
	1666	1739	1827	1925	2004	15%
	279	222	186	146	115	- 48%
DIC	1952	1970	2026	2090	2144	8.8%
$pH_{(sws)}$	8.32	8.16	8.05	7.91	7.76	- 0.4
$\Omega_{calcite}$	6.63	5.32	4.46	3.52	2.77	- 48%
$\Omega_{aragonite}$	4.26	3.44	2.90	2.29	1.81	- 47%

Figure 1.9 Changes in the concentrations of carbon species (μmol kg^{-1}), pH, and aragonite and calcite saturation states (Ω) of the average surface seawater for pCO_2 concentrations (ppm) during glacial, preindustrial, present day, two times pre-industrial CO_2, and three times pre-industrial CO_2. Figure from Fabry et al. [2008].

1.7 Objectives of this study

The surface ocean exchanges material and energy directly with the atmosphere and is more vulnerable to anthropogenic influences. Most of the marine primary production occurs in the euphotic zone in the upper ocean because of the availability of light and nutrients. Therefore, the surface ocean is an important component in the marine carbon cycle linking the atmosphere and the deep ocean. A key factor for understanding critical processes modulating the ocean carbon cycle is a sound knowledge of the surface ocean carbonate chemistry (Chapter 1.3). Although we have learnt a lot on this subject (Chapter 1.4 and 1.5), there are still knowledge gaps which limit our ability to accurately understand the current marine carbon cycle as well as its future changes responding to climate change:

- Although observations of the surface ocean CO_2 system have been significantly improved during the past few decades, there are still large areas of the globe with no or few data available [Doney et al., 2009b]. The knowledge of the marine

biogeochemical dynamics is still limited by our observing capacity of the ocean [Watson et al., 2011].

- It is evident from Figure 1.10 that oceanic processes occur on various spatial and temporal scales, which results in substantial variability in the marine carbonate system (Chapter 1.4). Addressing this problem requires not only observations with appropriate spatial coverage and temporal resolution, but also the mechanistic understanding of the variability of the surface ocean CO_2 system in different marine environments and on different time scales.

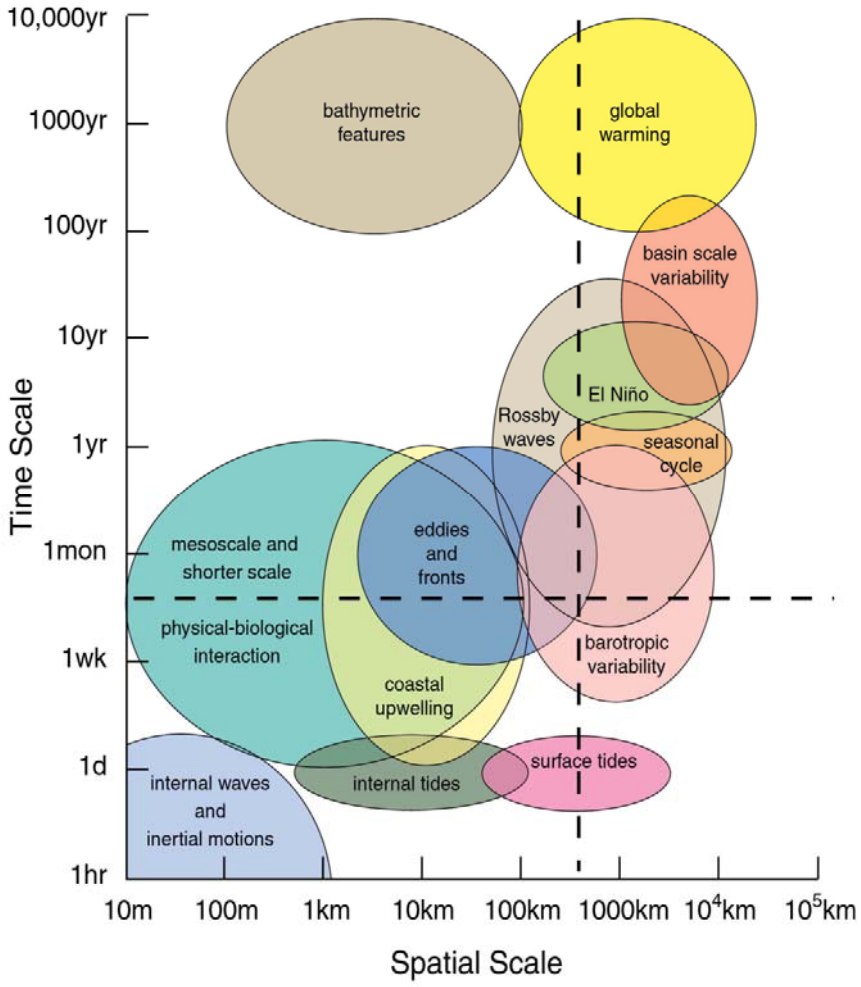

Figure 1.10 Schematic diagram of the spatial and temporal scales of various oceanic phenomena. Figure from Chelton [2001].

Existing gaps in the ocean CO_2 study motivated this PhD project which aims to use the observations made from Ships of Opportunity (SOO, or VOS: Volunteer Observing Ship) to examine the spatial and temporal variability and the underlying

controlling mechanisms of the surface ocean carbonate system. The major objectives of this dissertation are:

- To enhance our capacity for surface ocean observation by testing and assessing the performance of low-maintenance SOO systems for CO_2-related measurements (Chapter 2) and an automatic pCO_2 sensor (Chapter 3).
- To understand the **spatial variability** and control of the surface ocean carbonate system by taking advantage of the wide spatial coverage of the SOO *Mv Pacific Celebes*, particularly on the variability of TA and the TA-salinity relationship in a range of different oceanic environmental settings including open oceans, continental margins and inland seas (Chapter 4).
- To examine the **temporal variability** and control of the surface ocean carbonate system in the mid-latitude Northeast Atlantic (Bay of Biscay) by the repeat measurements along the regular route of the SOO *Mv Pride of Bilbao* (Chapter 5). This includes 1) to identify the key controlling factors of the seasonal variability of the carbonate system by distinguishing the contributions of mixing processes, biological activities and gas transfer to the monthly changes in DIC and pCO_2; 2) to compare the seasonality of DIC and pCO_2 in different latitudinal regions in the Atlantic; 3) to examine the link between the inter-annual variations of the CO_2 system and large-scale climate variability.

1.8 Dissertation structure

Chapter 2: Methodology

This chapter describes the methodology that was used in this dissertation, which includes the underway shipboard measurements, collection of discrete samples, laboratory analysis and thermodynamic calculation of the carbonate system. Low-maintenance SOO-based automatic measuring systems were highlighted as a cost-effective approach for surface ocean observation.

Chapter 3: Application and assessment of the membrane-based pCO_2 sensor (ProOceanus CO_2-Pro^{TM}) under field and laboratory conditions

This chapter introduces the principal of an automatic pCO_2 sensor (ProOceanus CO_2-Pro^{TM}) which can potentially be deployed on various platforms where very limited

maintenance is available. The sensor performance was assessed under various field and laboratory conditions based on comparisons of the sensor outputs against two pCO_2 references: 1) direct measurement using the calibrated traditional water-gas equilibrator system and 2) thermodynamic calculation from measurements of other carbonate variables. Recommendations were provided to the manufacturer for future improvement and to the users for a better use of the sensor.

Chapter 4: Variability of alkalinity and alkalinity-salinity relationship in the tropical and subtropical surface ocean

This chapter investigates the distribution and variability of surface ocean TA and TA-salinity relationship in various oceanographic regions including the open ocean, marginal seas and inland seas. The measured concentrations of TA were compared with those predicted from salinity and temperature. The salinity-normalized alkalinity was used as an indicator to identify processes which add or remove TA in coastal regions and inland seas (e.g. riverine inputs, currents, biological calcification). The TA-salinity relationships under different mixing schemes were also discussed focusing on the intercept of the TA-salinity relationship.

Chapter 5: Key controls on the seasonal and interannual variations of the carbonate system and air-sea CO_2 flux in the Northeast Atlantic (Bay of Biscay)

This chapter examines the biogeochemical variations of the surface water in the Northeast Atlantic (Bay of Biscay) using repeated SOO-based underway measurements combined with monthly sampling of carbon-related variables. The mechanisms controlling seasonal CO_2 variability were investigated by breaking down the monthly changes in DIC and pCO_2 into the contribution of various physical and biological processes. The seasonal CO_2 variability in the Bay of Biscay was compared to other time series data at different latitudes to examine the regional differences in seasonal patterns of the carbonate system in the North Atlantic. The interannual variability (2002 to 2010) was investigated focusing on the role of winter mixing and its link with large-scale climate variability.

Chapter 6: Conclusion and Discussion

This chapter discusses the implications of the major findings of this PhD project, as well as the pending questions and the recommendations for future research.

Chapter 2: Methodology

This chapter describes the methodology that was used in this dissertation, which includes the underway shipboard measurements, collection of discrete samples, laboratory analysis and thermodynamic calculation of the carbonate system. Low-maintenance SOO-based automatic measuring systems were highlighted as a cost-effective approach for surface ocean observation.

2.1 Introduction

Understanding of the marine physical and biogeochemical dynamics and their underlying controlling mechanisms needs to be built based on comprehensive observations. Considering the strong spatial heterogeneity and temporal variability in the ocean (as discussed in Chapter 1.4), it is critical that appropriate observing systems are in place to monitor the marine environment with sufficient spatial coverage and temporal resolution. Historically, most observational data in marine science came from dedicated scientific expeditions and time series operations at certain stations. However, research surveys only present a snapshot of the ocean dynamics and fixed station observations provide little information on spatial variability. The inherent limitations of these traditional observation methods make it difficult to meet the fast-growing demands for widespread, long-term and sustained in-situ data. These gaps in the data are major hindrances limiting our ability to accurately assess the climate- and human-induced changes in the marine environment [Petersen et al., 2011].

In order to enhance our capacity of ocean monitoring, the use of SOOs as platforms for marine research has been promoted [Ainsworth, 2008; Goni, 2010; Rossby et al., 1995; SCOR/IAPSO, 2011]. Merchant vessel routes provide a much wider spatial coverage than research ships, and repeated measurements can be obtained on regularly operated routes [Ainsworth, 2008; Kaluza et al., 2010]. Recent developments in sensor technology and instrumentation provide the possibility to use SOO to collect high quality scientific data in a cost-effective way. The emerging measurement systems on SOOs are proving to be useful tools to address the paucity of in-situ observations. The observations made from SOOs have included a range of parameters: upper ocean thermal structure [Beggs et al., 2012; Donlon et al., 2008; Goni, 2010], marine phytoplankton [Reid et al., 1998; Schneider et al., 2006; Seppälä et al., 2007], anthropogenic pollutants [Kelly-Gerreyn et al., 2007], and biogeochemical variables such as nutrients, dissolved oxygen (DO), and pCO_2 [de la Paz et al., 2010; Hydes et al., 2009; Luger et al., 2006; Petersen et al., 2011; Schneider et al., 2006]. In this study, two SOO-based systems were used and their details are described below.

2.2 SNOMS on the *MV Pacific Celebes*

2.2.1 System design

In 2006 the Swire Group offered the National Oceanography Centre, Southampton (NOCS) the use of one of their cargo ships to support the study of marine science and climate change. The working route of the *MV Pacific Celebes* set a constraint on the design of the onboard measuring system as the service intervals would be four to six months apart. Set against this was the major practical advantage that this ship has a very clear chain of management and responsibility. It was therefore possible to work with the ship's crew and have them involved in maintaining the system and collecting calibration samples. A low-maintenance system named Swire NOCS Ocean Monitoring System (SNOMS) was assembled by NOCS and was operated on the *MV Pacific Celebes* from June 2007 to March 2012 [Hydes and Campbell, 2007; Hydes et al., 2013]. The SNOMS measured seawater properties including pCO_2, sea surface temperature (SST), conductivity, DO, total gas tension, as well as atmospheric temperature, pressure, humidity, and CO_2 concentration. Discrete samples were also collected by the trained crew on a daily basis when the system was in operation. The details of the system are described below and the measured variables are summarized in Table 2.1.

As shown in Figure 2.1, the SNOMS consisted of two instrument packages: one for atmospheric measurements and satellite communication (Figure 2.1b) and the other for seawater measurements (Figure 2.1d). On the bridge top, the atmospheric instrumentations were installed in a Stevenson Screen box at a height of 34 m above sea level. The box contains a Vaisala GMP343 CO_2 probe measuring atmospheric CO_2 concentrations alongside a Vaisala PTU300 sensor for barometric pressure, air temperature and humidity. In the ship's machinery space adjacent to the engine room, the hydrographic sensors were mounted in a specially designed flow-through pressure tank (Figure 2.1d). The tank housed a ProOceanus CO_2-Pro^{TM} sensor measuring seawater pCO_2 and a ProOceanus GTD sensor measuring total dissolved gas pressure (Figure 2.1f). Triplicate sensors for temperature (Aanderaa 4050), conductivity (Aanderaa 3919), and DO (Aanderaa Optode 3835) were fitted integral

to the lid of the tank (Figure 2.1e). An insulated Seabird 48 hull temperature sensor was mounted to the hull close to the tank to monitor the SST [Beggs et al., 2012].

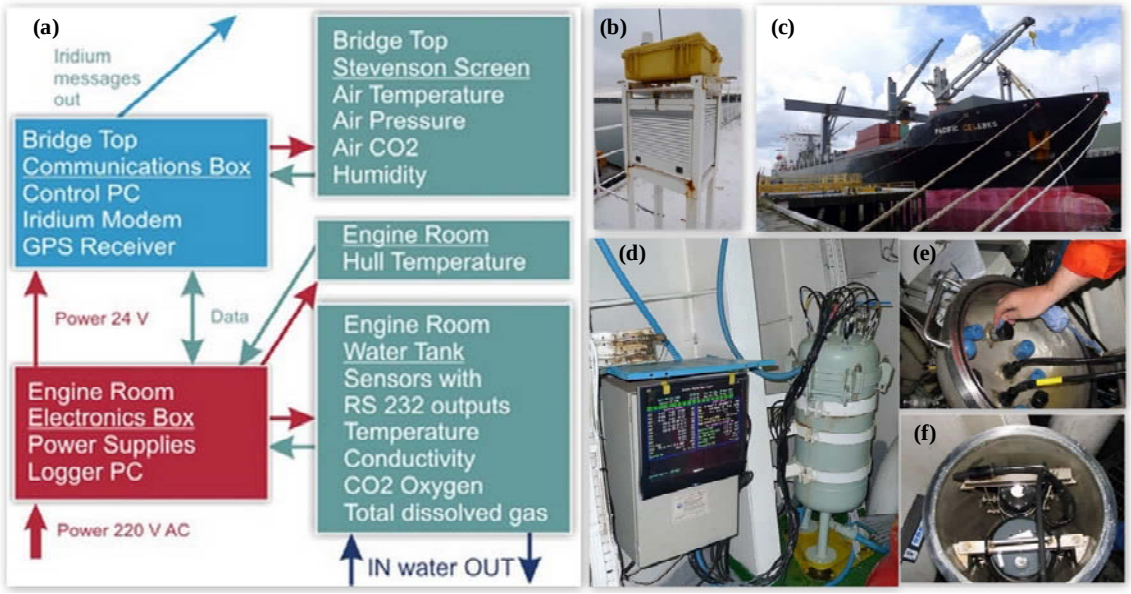

Figure 2.1 (a) The schematic of the SNOMS, see the text for detail; (b) the Stevenson Screen box (bottom) for atmospheric measurements and the electronic cabinet (top) containing the Iridium satellite modem on the bridge top; (c) the *MV Pacific Celebes*; (d) the instrument package in the engine room including the flow-through pressure tank and controlling computer; (e) the triplicate sensors for temperature, conductivity, and DO fitted to the lid of the tank; (f) the ProOceanus CO_2-Pro^{TM} and GTD sensor in the tank.

The design of a flow-through tank was chosen for several reasons: (1) it allows all the sensors to operate in an approximately isothermal environment; (2) it provides a simple and rapid method of access for cleaning and exchange of sensors; (3) the water remains under pressure inhibiting degassing and bubbling which preserves the integrity of the water for pCO_2 measurement. The free volume of the SNOMS tank was approximately 45 litres with the sensors in place. It was fed at a flow rate of 28 ± 2 litres minute^{-1} by a branch of the non-toxic seawater being pumped to the ship's fresh water generator. The water supply was routinely turned off (the SNOMS system was also shut down) in shallow and potentially turbid water to avoid contamination of the ship's water purification system. In turn this prevented sedimentation in the tank and protected the membrane of the ProOceanus CO_2-Pro^{TM} from contaminants such as oil in harbour waters.

Table 2.1 Methodology and accuracy of the measured variables of the SNOMS operation

Variables	**Sensor/Measurement**	**Precision/Resolution; Stability**	**Accuracy**
		Underway Atmospheric Measurement	
Air Temperature	Vaisala PTU300	0.01°C	± 0.2°C
Barometric pressure	Vaisala PTU300	± 0.03 hPa, stability: ± 0.1 hPa $year^{-1}$	± 0.15 hPa
Humidity	Vaisala PTU300	0.1%RH ,stability: < 1%RH $year^{-1}$	± 1.7 %RH
Atmospheric CO_2	Vaisala GMP343 CO_2 sensor	± 1 ppm for xCO2	± (3 ppm+1% of reading) in 0 to1000 ppm
		Underway Seawater Measurement	
SST	SBE 48 Hull Temperature Sensor	0.0001°C, stability: < 0.002°C $year^{-1}$	± 0.1°C
Water temperature	Triplicate Aanderaa Temperature 4050	0.001°C	± 0.03°C
Salinity	Triplicate Aanderaa Conductivity 3919	0.002	< 0.1 after correction with discrete samples
DO	Triplicate Oxygen Optode 3835	< 1 μmol L^{-1}	< 8 μmol L^{-1} or 5%
pCO_2	ProOceanus CO_2-ProTM	0.01 uatm	± 6.5 μatm after correction
Total gas tension	ProOceanus GTD	0.002 mb, stability: < 0.02 mb $year^{-1}$	0.02 mb
		Discrete Samples	
Salinity	Guildline Autosal Salinometer 8400B	< 0.0002	< ± 0.002
DIC	Marianda VINDTA 3C	± 2 μmol kg^{-1}	± 2 μmol kg^{-1}
TA	Marianda VINDTA 3C	± 1.5 μmol kg^{-1}	± 2 μmol kg^{-1}

The full high resolution data from all sensors were logged to a NOCS-built control and logging system, together with the ship's position identified by a Global Positioning System unit and ancillary variables such as the ship's speed and flow rate of water supply. The data were averaged and binned into 5-minute time intervals and transmitted to NOCS every 6 hours via an Iridium satellite modem. The near real-time data were then displayed on the public access webpage (http://www.noc.soton.ac.uk/snoms/).

When the ship was at sea, the system was supervised by the ship's engineers who were trained by NOCS staff. When the ship called at ports, the SNOMS tank was opened and cleaned by wiping the surface of sensors and hosing down all units with fresh water. The technician at NOCS serviced the system every 4 to 5 months when the ship arrived in ports adjacent to Europe to replace and calibrate the sensors and download the full data.

2.2.2 Collection of discrete samples

When the SNOMS system was in operation, two discrete samples were collected on a daily basis by the trained crew: one for the determination of salinity and one for both DIC and TA. Salinity samples were collected into 100 mL high-density glass bottles. Samples for DIC and TA were collected into 250 mL borosilicate glass bottles (Schott Duran) and poisoned with 50 μL saturated $HgCl_2$ solution to prevent biological alteration during storage [Dickson et al., 2007]. A head-space of 2.5 mL was left to allow for water expansion and the bottles were sealed using a greased ground glass stoppers to ensure they remained gas-tight [Dickson et al., 2007]. These samples were shipped to NOCS about every four months and measured there (Chapter 2.4).

2.2.3 Underway measurements

The use of triplicate sensors for temperature, conductivity and DO enables the identification of malfunction or drift of any single sensor (should it occur). By comparing the triplicate readings, a single output was generated based on the averages of the two better functioning instruments showing more consistent results.

Temperature and salinity: For the measurement of seawater temperature in the SNOMS tank, the precision of the Aanderaa 4050 temperature sensors is 0.001°C and the results from the two better functioning instruments agreed within ± 0.03°C. As no temperature sensor was installed in the water intake, the SST was measured by a thermally isolated SeaBird 48 hull-contact temperature sensor. Based on experience of similar systems, the likely uncertainty of the true SST from the hull measurement is considered to be ~0.1°C [Beggs et al., 2012; Hydes et al., 2008, 2009]. The readings of the Aanderaa 4050 sensor were 0.08°C on average higher than those of the Seabird 48 hull sensor, which suggests that the water reaching the tank was slightly warmed above its in-situ temperature during the pumping process. Salinity was calculated from the temperature, conductivity, and pressure measured in the tank [Fofonoff and Millard, 1983]. The derived salinity was then corrected against the bottle salinity measurements under stable laboratory conditions (accuracy of ± 0.002) with uncertainty of ± 0.05.

DO: The Aanderaa oxygen optode has been evaluated to be a relatively accurate and stable sensor suitable for long-term oxygen monitoring in aquatic systems [Körtzinger et al., 2005; Tengberg et al., 2006].The precision of the sensor is 1 μmol L^{-1} and it was demonstrated that the accuracy in practice was likely to be better than the manufacturers specifications which is < 8 μmol L^{-1} or 5% of the saturation [Hydes et al., 2009]. During the SNOMS operation, the outputs from the two better functioning optodes generally agreed within ± 3.5 μmol L^{-1}.

Seawater pCO_2: As the key variable for the SNOMS operation, a detailed description and evaluation of the pCO_2 sensor are given in Chapter 3. It is shown that, when corrected against pCO_2 references, the overall uncertainties of the corrected sensor results are similar to those of the references (± 2 and ± 8 μatm for direct measurements and calculated pCO_2 respectively).

2.3 Ferry-Box on the *MV Pride of Bilbao*

From April 2002, a low-maintenance underway measuring system (Ferry-Box) was installed on the P&O European Ferries Ltd. ship *MV Pride of Bilbao* to measure temperature, conductivity, chlorophyll fluorescence, and DO (since February 2005) along the ferry's route: http://www.noc.soton.ac.uk/ops/ferrybox_index.php [Hydes

et al., 2003]. This ferry ran twice weekly along the 1000 km route between Portsmouth, UK (50.8°N, 1.1°W) and Bilbao, Spain (43.4°N, 3.0°W). The ship's route covered a suite of different oceanographic regions from the shallow English Channel to the deep oceanic Bay of Biscay [Bargeron et al., 2006]. The Ferry-Box system operated successfully until September 2010 when this ferry service was withdrawn. During the operation period, the Ferry-Box operated year round except for January when the ship was in dry dock for its annual refit.

This Ferry-Box was located in the engine room with a similar flow-through chamber system design compared to that of SNOMS. The non-toxic seawater was supplied at a flow rate of 12 to 20 L minute^{-1} by the ship's pumping system from an intake depth of 5 m below the sea surface. Measurements were made of temperature, conductivity and chlorophyll fluorescence (Chelsea Technologies Group MINIpack CTD-F, UK). In addition to the temperature measurement in the sensor chamber, a SeaBird SBE48 hull temperature sensor was used to monitor the SST. From February 2005, an optode sensor (Aanderaa 3835) was added into the instrument pack to take measurements of DO [Hydes et al., 2009]. All underway data were logged on a home-built control system while sub-data were transferred to NOCS by the Orbcom satellite unit on the bridge deck.

In addition to the underway measurements, researcher-occupied calibration crossings were carried out on a monthly basis since 2005 when possible. Discrete samples were collected during these crossings, which included salinity, nutrients, DIC and TA, DO, and coccolithophore abundance. Discrete samples for DO were determined onboard by Winkler titration in order to calibrate the optode output [Hydes et al., 2009] while others were taken back to NOCS for laboratory measurements (Chapter 2.4). The measured variables and their accuracy are summarized in Table 2.2.

Table 2.2 Methodology and accuracy of the measured variables of the Ferry-Box operation

Variables	Type	Methodology	Accuracy
SST	underway	Chelsea MINIpack CTD-F temperature sensor SeaBird SBE48 hull temperature sensor	± 0.1°C
salinity	underway	Calculated from temperature and conductivity (Chelsea MINIpack CTD-F), calibrated by discrete sample measurements	± 0.03
chlorophyll fluorescence	underway	Chelsea MINIpack CTD-F	
DO	underway	Aanaderaa 3835 sensor, calibrated by discrete samples measured by onboard Winkler titration	± 1 μmol L^{-1}
DIC	discrete	Coulometric titration by Marianda VINDTA 3C, corrected by Certified Reference Materials from Scripps Institution of Oceanography	± 2 μmol kg^{-1}
TA	discrete	HCl titration by Marianda VINDTA 3C, corrected by Certified Reference Materials from Scripps Institution of Oceanography	± 1.5 μmol kg^{-1}
salinity	discrete	Guildline Autosal Salinometer 8400B	± 0.002
nutrients	discrete	SEAL AutoAnalyzer	± 0.1 μmol kg^{-1} for nitrate and nitrite; ± 0.1 μmol kg^{-1} for silicate; ± 0.02 μmol kg^{-1} for phosphate
coccolithophore abundance	discrete	Scanning Electron Microscope (Carl Zeiss Leo 1450VP) counts	

2.4 Laboratory measurements

The discrete samples for salinity, DIC and TA, nutrients and coccolithophore abundance collected on SOOs (Chapter 2.2 and 2.3) were analyzed at NOCS under stable laboratory conditions. Salinity was measured using a high precision Guildline 8400 B Autosal salinometer in a temperature controlled laboratory with an accuracy of ± 0.002. DIC and TA were analyzed in batches (6 to 12 samples) using a VINDTA 3C (Marianda, Germany). DIC was measured by a coulometric titration (coulometer 5011, UIC, USA) following the extraction of CO_2 from ~20 mL sample. TA was determined by HCl titration of ~100 mL sample with a pH half cell electrode (Orion, Ross, USA) and Ag/AgCl reference electrode (Metrohm, Switzerland). Repeat measurements on 'pooled' samples were undertaken before sample analysis each day ($n > 3$), which suggested a precision better than ± 2 μmol kg^{-1} for DIC and ± 1.5 μmol kg^{-1} for TA respectively. Certified Reference Materials from Dr. Andrew Dickson (Scripps Institution of Oceanography) were used for calibration to assure the accuracy of the measurements (Millero et al. 1998). Nutrient samples were analyzed by a SEAL AutoAnalyzer using standard methods [Hansen and Koroleff, 2007]. The precision and accuracy were ± 0.1 μmol L^{-1} for nitrate and silicate and ± 0.02 μmol L^{-1} for phosphate. Coccolithophore abundances were counted using scanning electron microscopy [Smith et al., 2012].

2.5 The carbonate calculation

The marine carbonate system can be characterized from any two of the four parameters: DIC, TA, pCO_2 and pH [Zeebe and Wolf-Gladrow, 2001]. In this study, the Excel program 'CO2SYS' [Pierrot et al., 2006] was used for the carbonate calculations. The dissociation constants of carbonic acid (pK_1 and pK_2) determined in real seawater by Millero et al. [2006] are in good agreement with previous measurements [Mehrbach et al., 1973; Mojica Prieto and Millero, 2002], and are more reliable than those measured in artificial seawater [Millero et al., 2006]. Therefore, the constants of Millero et al. [2006] were used in the CO2SYS calculation. The sulphuric dissociation was chosen as Dickson [1990] and the total boron fomualtion was selected as Lee et al. [2010].

Chapter 3: Application and assessment of the membrane-based ProOceanus CO_2-Pro^{TM} sensor for pCO_2 under field and laboratory conditions

This chapter is adapted from a manuscript submitted to Limnology and Oceanography: Method by Jiang, Z.-P., D. J. Hydes, S. E. Hartman, M. C. Hartman, J. M. Campbell, B. D. Johnson, B. Schofield, D. Turk, D. Wallace, W. Burt, H. Thomas, C. Cosca, and R. Feely (in press): 'Application and assessment of a membrane-based pCO_2 sensor under field and laboratory conditions'.

3.1 Abstract

The principle, application and assessment of the membrane-based ProOceanus CO_2-Pro^{TM} sensor for pCO_2 are presented. The performance of the sensor was evaluated extensively under field and laboratory conditions by comparing the sensor outputs with reference to direct pCO_2 measurements from calibrated water-gas equilibrator systems and the thermodynamic carbonate calculation from discrete samples for other carbonate variables (dissolved inorganic carbon, total alkalinity, or pH). Under stable laboratory condition, the sensor agreed with a calibrated water-air equilibrator system at -3.0 ± 4.4 µatm during a two-month intercomparison experiment. When applied in field deployments, the larger differences between measurements and the calculated pCO_2 references (6.4 ± 12.3 µatm on a ship of opportunity and 8.7 ± 14.1 µatm on a mooring) are related not only to the sensor error, but also to the uncertainties of the reference pCO_2 and the comparison process, as well as the changes in working environments of the sensor. When corrected against the references, the overall uncertainties of the corrected sensor results are similar to those of the references (± 2 and ± 8 µatm for direct measurements and calculated pCO_2 respectively). This study suggests that inaccuracy of the sensor can result from calibration error and temperature fluctuations of the detector optical cell. Recommendations were provided for manufacturer for future improvement and for users to better use the sensor. Another interesting result in the laboratory test is the abnormal changes in alkalinity in the harbour water, which results in significant underestimation in the pCO_2 calculation in compared to the direct measurement (up to 90 µatm).

3.2 Introduction

The knowledge of surface ocean CO_2 variability is important for us to understand the marine carbon cycle and its future response to the absorption of anthropogenic CO_2 [Doney et al., 2009b]. In the past few decades, high-accuracy seawater pCO_2 measuring systems [Dickson et al., 2007; Pierrot et al., 2009] have been widely used on research vessels providing high quality pCO_2 data, which leads to the generation of a global atlas of the surface ocean pCO_2 and CO_2 flux (Chapter 1.5.1) [Takahashi et al., 2009]. However, there is still a lack of data from large areas of the globe,

especially in the shelf seas, Southern Ocean, and southern-hemisphere subtropical gyres [Doney et al., 2009b]. Moreover, changes in seawater pCO_2 can occur on time scales from daily [Dai et al., 2009; DeGrandpre et al., 1998; Turk et al., 2013; Yates et al., 2007] to seasonal and interannual [Bates, 2002, 2007; Jiang et al., 2013; Watson et al., 2009], especially in the dynamic coastal environments [de la Paz et al., 2008a; Jiang et al., 2011; Turk et al., 2010], also see Chapter 1.4. Observations with sufficient temporal and spatial resolution are thus needed for a better understanding of the controlling mechanism of pCO_2 variability in different regions and a more reliable CO_2 flux estimation.

In addition to the traditional shipboard measuring system, there are emerging techniques to develop autonomous pCO_2 sensors. As summarized in Table 3.1, these sensors generally follow the same basic concept based on the measurement of a gas or indicator solution that is in equilibrium with the seawater to be determined. The equilibrium state can be reached by using water-gas equilibrators where the gas is directly in contact with the seawater, or via gas permeable interface such as silicone, PTFE or Teflon AF^{TM} membrane. The equilibrated gas can be measured by a non-dispersive infrared (NDIR) method, while the equilibrated indicator solution can be determined by electrode, fluorescence or spectrophotometric methods (Table 3.1). For these reagent-based fiber optic chemical sensors [DeGrandpre, 1993; DeGrandpre et al., 1995; Goyet et al., 1992; Lefévre et al., 1993], improvements have been made by using multi-wavelength detection and long pathlength liquid-core waveguide for a better precision and accuracy [DeGrandpre et al., 1999; Lu et al., 2008; Nakano et al., 2006; Wang et al., 2002, 2003]. The devolving sensor technology enables cost-effective pCO_2 measurements to be made on various platforms such as SOO, buoy and mooring, glider, profiling float and autonomous underwater vehicle [DeGrandpre et al., 1998; Fiedler et al., 2012; Nakano et al., 2006, 2009; Saderne et al., 2013; Willcox et al., 2009].

Table 3.1 The various designs of pCO_2 sensors

Equilibrator	Measured phase	Determination	References
direct contact of water-gas	gas	NDIR	ACT [2009a]; Nemoto et al. [2009]
gas permeable interface	gas	NDIR	Kayanne et al. [2002]; Fiedler et al. [2012]; Saderne et al. [2013], this study
gas permeable interface	indicator solution	electrode	Shitashima 2010
gas permeable interface	indicator solution	fluorescence	Goyet et al. [1992]; Tabacco et al. [1999]; Rubin and Ping Wu [2000]
gas permeable interface	indicator solution	spectrophotometry	Degrandpre [1993]; Lefévre et al. [1993]; Degrandpre et al. [1995; 1999]; Wang et al. [2002; 2003]; Nakano et al. [2006]; Lu et al. [2008]

Table 3.2 The estimated uncertainties of pCO_2 (μatm) calculated from various inputs (pH and TA, or DIC and TA) in this study

	Measured pCO_2	Sources of uncertainty in pCO_2 calculation				Uncertainty of the calculated pCO_2
		pK_1, pK_2	TA	DIC	pH	
ACT	280 to 840	4 to 12	0.5		6.8	7.5
SNOMS	300 to 500	7 to 10	2.3	3.8		8.1
Aquatron	280 to 860	6 to 15	4.4	6.6		9.9

In this chapter, the principle and design of a membrane-based NDIR pCO_2 sensor (ProOceanus CO_2-Pro^{TM}, hereafter referred to as CO_2-Pro) were described. The sensor's functionality, reliability and accuracy were evaluated under various situations including: a 16-day coastal mooring deployment test in coral reef water in Hawaii (October to November 2009), shipboard underway mapping on a SOO (October 2009 to March 2012), intercomparison with a calibrated water-gas equilibrator system in the Aquatron Laboratory at Dalhousie University (May to September 2012) and long-term open-ocean mooring deployment in the Northeast Atlantic (June 2010 to July 2012). The performance of CO_2-Pro was assessed by comparing the sensor outputs against two kinds of reference: (1) the thermodynamic carbonate calculation of pCO_2 from the determinations of DIC, TA, and pH from discrete samples; (2) direct measurements by the traditional water-gas equilibrator NDIR systems which were regularly calibrated against standard gases. Based on the experiences gained from these operations, the advantages and limitations of the CO_2-Pro were summarized and recommendations were provided for the manufacturer and users.

3.3 Materials and Procedures

3.3.1 Principle of the CO_2-Pro

The CO_2-Pro is designed as a light-weight, compact, plug and play, versatile instrument for pCO_2 measurements on moorings, drifters and profilers, in underway mode and in the laboratory. As shown in Figure 3.1, the sensor is fitted with an equilibrator made of gas permeable silicone membrane and an internal detection loop with a NDIR detector of PPSystems SBA-4 CO_2 analyzer. The patented gas transfer interface of the equilibrator features a tubular design, through which the equilibration between the surrounding water and the internal gas stream can be achieved. Copper wire is wound round the tube to inhibit the potential for bio-film formation and the equilibrator is protected from physical damage by an end-cap. An associated SBE 5M submersible pump drives water past the outer surface of the equilibrator membrane to accelerate the equilibration. The response time, i.e. the time for the membrane to reduce the perturbation in pCO_2 by a factor of 1/e, is typically 2 minutes depending on the pumping rate. NDIR measurement on the equilibrated

internal gas is taken at a wavelength of 4.26 μm at a controlled optical cell temperature (40 or 60°C). In addition, temperature, pressure and humidity of the internal gas are determined to correct the CO_2 measurement. Further detailed specifications of the CO_2-Pro can be found at the company's website http://www.pro-oceanus.com/co2-pro.php.

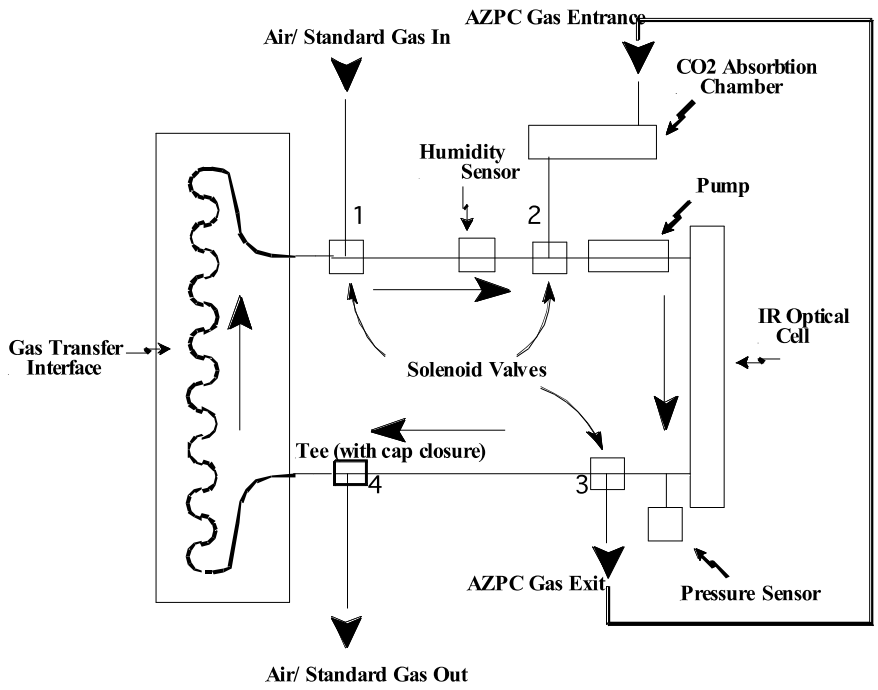

Figure 3.1 Schematic of the flow paths of the ProOceanus CO_2-Pro^{TM} sensor. See the text for detail.

When the sensor is turned on, the optical cell of the detector is warmed up and stabilized at the set value. A zero point calibration (ZPC) is then carried out to provide a zero-CO_2 baseline (C_{zero}) for the subsequent NDIR absorption measurement. This is done by circulating the internal gas through a CO_2 absorption chamber containing soda lime or Ascarite (flow path: valve 2 - circulation pump - optical cell - valve 3 - absorption chamber - valve 2, Figure 3.1). When the ZPC finishes, the solenoid valves 2 and 3 are activated to circulate the internal gas around a closed circuit connecting the equilibrator and detector (flow path: valve 2 - circulation pump - optical cell - valve 3 - valve 4 - equilibrator - valve 1- valve 2, Figure 3.1). The inferred signal of the internal gas (C_{meas}) is measured for the calculation of absorbance ($\varepsilon = C_{meas}/ C_{zero}$) and CO_2 concentration. Once the internal gas is equilibrated with the water surrounding the equilibrator (typically 10 to 15

minutes after the ZPC), the seawater CO_2 concentration can be determined. The CO_2-Pro features a programmable regular automatic ZPC function to correct the detector drift which can be caused by contamination of optical cell, optical source ageing and changes in detector sensitivity.

Each CO_2-Pro is factory calibrated at known optical cell temperature and pressure against 5 standard gasses with xCO_2 spanning from 0 to 600 ppm (mole fraction of CO_2 in dry air). The calibration equation is obtained by a three-segment least-squares fitting to a quadratic equation between ε and xCO_2, and this equation is subsequently tested by measuring a further three known mixtures of CO_2. While the calibration equation provides a raw xCO_2 from the inferred measurement, empirical corrections are applied to account for the differences of conditions between calibration and measurement (temperature, pressure, water vapour). As the actual measurement is made on gas which is nearly saturated with water vapour, the output of CO_2-Pro is the mole fraction of CO_2 in wet air (wCO_2, ppm) and pCO_2 in the measured water is obtained by: $pCO_2 = wCO_2 * P_{wet}$, where P_{wet} is the measured total pressure of the internal gas which includes water vapour pressure.

3.3.2 ACT coastal mooring test

The application of CO_2-Pro in coastal mooring measurement was previously tested in a demonstration project organized by Alliance for Coastal Technologies (ACT) (http://www.act-us.info/evaluations.php#pco2). During October to November 2009, a CO_2-Pro was mounted on a surface mooring and deployed at a fixed depth of 1 m in a shallow sub-tropical coral reef in Kaneohe Bay, Hawaii. Continuous measurements were made by the CO_2-Pro on a hourly basis and the results were compared with the reference pCO_2 calculated from discrete samples. pH and TA of these samples were measured spectrophotometically using meta-cresol purple and bromo-cresol green as indicator respectively [Dickson et al., 2007]. Both measurements were calibrated against the CRM from Scripps Institution of Oceanography. The accuracy of the pH measurement was estimated to be 0.005 and the standard deviation (SD) of repeated TA measurements was 1.9 μmol kg^{-1} [ACT, 2009b]. The assessment was carried out by the ACT staff, and the sensor data were provided by the ProOceanus company.

Details of the deployment, measurements, calculation and quality control were documented by ACT [2009a, b].

3.3.3 SNOMS underway measurements

From June 2007 to March 2012, CO_2-Pro was used for continuous shipboard underway measurement in the operation of the SOO-based measuring system SNOMS on the *MV Pacific Celebes* (Chapter 2.2) [Hydes et al., 2013]. The CO_2-Pro was mounted in a 45-litres flow-through pressure tank, together with other sensors for temperature, conductivity, dissolved oxygen and total dissolved gas pressure. Adapted to the SNOMS tank, the protecting end-cap and the associated pump of CO_2-Pro were removed. The gas transfer interface was thus directly exposed to the seawater for pCO_2 measurement, which also enables a direct cleaning of the membrane surface. The SNOMS tank was fed at a flow rate of 28 ± 2 litres $minute^{-1}$ by a branch of the non-toxic seawater being pumped to the ship's fresh water generator. This water supply was routinely turned off in shallow and potentially turbid water, which prevents sedimentation in the tank and contamination of the membrane of the CO_2-Pro. At each port, the tank was opened and the membrane of CO_2-Pro was cleaned by hosing down with fresh water.

The CO_2-Pro was continuously working when the SNOMS system was in operation. The frequency of the automatic ZPC was set to be 6 hours, and the 15-minute data after each ZPC (when the gas was re-equilibrating with the water) were discarded. In order to account for the difference between the water temperature in the tank (T_{tank}) and that in the surface ocean, an insulated Seabird 48 hull-contact temperature sensor was used to monitor the SST. By considering the temperature effect on pCO_2 [Takahashi et al., 1993], the tank water pCO_2 measured by CO_2-Pro ($pCO_{2,Pro}$) was corrected to the sea surface condition: $pCO_{2,SST} = pCO_{2,Pro} * \exp[0.0423* (SST-T_{tank})]$. The likely accuracy of SST from the hull measurement is 0.1°C [Beggs et al., 2012], which results in an uncertainty of ~1.5 µatm in converting $pCO_{2,Pro}$ to $pCO_{2,SST}$. In addition to the underway measurements, discrete samples were collected by the ship's engineers for the determination of DIC and TA at NOCS (Chapter 2.4).

3.3.4 The Aquatron laboratory test

After the operation on the *MV Pacific Celebes*, a controlled test of the CO_2-Pro as a part of the SNOMS tank was carried out in the Aquatron Laboratory at Dalhousie University during May to September 2012. To carry out this test, a two cubic metre open tank (referred to as the Aquatron tank) was set up beside the SNOMS tank. The two tanks were filled with sand-bed filtered seawater pumped from an adjacent harbour (estuary) on 23 May. The water was continuously pumped in a circuit between the two tanks with a turnover time of about 2 hours. The pCO_2 of the tank water was minored by the CO_2-Pro in the SNOMS system which operated in a similar way as on the *MV Pacific Celebes*. After a stabilization period of ~50 days when the pCO_2 reached a relative constant range, another pCO_2 measuring system (referred to as the NOIZ system) was set up in the Aquatron tank for a side-by-side comparison with CO_2-Pro. In order to control pCO_2 to ocean values during the two-month intercomparison excise (13 July to 11 September), a simple system was developed to bubble CO_2-free gas (laboratory air passing through a cartridge filled with soda lime) into the Aquatron tank on three occasions (started on 10 July, 2 August and 31 August).

The NOIZ system consisted of a bubble type water-gas equilibrator, a drier unit and a Licor 7000 NDIR detector [Körtzinger et al., 1996]. The equilibrator was mounted on the Aquatron tank and its lower part was submerged in the water to minimize the temperature difference between the tank water and that in the equilibrator. The detector was calibrated every a few days with zero CO_2 concentration nitrogen gas and an air mixture calibrated with National Oceanic and Atmospheric Administration (NOAA) standard gas before 27 August 2012. After that, the calibration directly used a NOAA-supplied standard gas with an uncertainty of ± 1 ppm. No shift could be identified in the calibration when calibration gasses were changed. The output of the detector is xCO_2 in the dry air in units ppm, and the pCO_2 was calculated following Pierrot et al. [2009]: $pCO_2 = xCO_2 * (P_{equ} - pH_2O) * \exp[0.0423*(T_{insitu}-T_{equ})]$, where P_{equ} is the pressure in the equilibrator, T_{insitu} and T_{equ} are temperatures in the Aquatron tank and in the equilibrator, and pH_2O is the water vapour pressure calculated based on the T_{insitu} and salinity (Weiss and Price 1980). The accuracy of the pCO_2 measured by the NOIZ system was estimated to be within 2 µatm.

In additional to the pCO_2 measurements, discrete samples for DIC and TA were collected throughout the test on a daily basis. Nutrient samples were collected from 5 June onwards for determinations of nitrate, silicate, phosphate and ammonia [Whitledge et al., 1981]. The measurements of these discrete samples were carried out at Dalhousie University using the same methods described in Chapter 2.4. To compensate for water lose due to sampling and evaporation, the Aquatron tank was topped up every 4-7 days with newly pumped water. Although these waters were pumped from the same location, they may have different properties compared to the original tank water due to the temporal variability at the sampling site. However, these top up events had minor influences on the chemical concentrations of the tank water because of the relative small volumes been added (0.2 to 3% of the total volume of the Aquatron tank). One exception was a substantial top up on 7 August (35% of the total volume) because of a large drainage from the sampling tube, which significantly changed the properties of the tank water (see the results section below).

3.3.5 Long-term in-situ operation on the PAP mooring

Since June 2010, CO_2-Pro was used for long-term in-situ deployment at the Porcupine Abyssal Plain (PAP, 49°N 16.5°W, 4800 m) which is the longest running multidisciplinary observatory in the Northeast Atlantic [Hartman et al., 2012]. It was deployed on a sensor frame at a fixed depth (~30 m) together with other autonomous sensors for temperature, salinity, chlorophyll-a fluorescence and nitrate. All these sensors were controlled by a hub controller which communicated with NOCS via satellite in a near real-time way. The CO_2-Pro was powered by the solar panels on the mooring and its measurement frequency and the time length for each measurement can be changed remotely.

3.3.6 The carbonate calculation

The Excel program ‘CO2SYS’ [Pierrot et al., 2006] was used for the carbonate calculations (Chapter 2.5). In this study, pCO_2 was calculated eithe from the combination of pH and TA (ACT test) or DIC and TA (SNOMS and Aquatron test). The uncertainty of pCO_2 calculation comes from the inaccuracies of the thermodynamic dissociation constants (mainly pK_1 and pK_2) and the experimental

measurements of the variables used for calculation [Millero et al., 2006]. Considering the various sources of uncertainties associated with the carbonate calculation in the measured pCO_2 ranges (Table 3.2), the uncertainty of the calculated pCO_2 was estimated to be ± 7.5 µatm for the ACT test [ACT 2009a, b], ± 8.1 µatm for the SNOMS operation and ± 9.9 µatm for the Aquatron test, respectively.

3.4 Assessment

3.4.1 Results of the ACT coastal mooring test

The results of the ACT mooring test have been reported by ACT [2009a] and are briefly summarized here. During the 16-day continuous measurement in Kaneohe Bay, nearly 100% of the data were retrieved except for the data gaps during calibration cycles. The hourly time series data from the CO_2-Pro ($pCO_{2,Pro}$ in Figure 3.2a, 280 to 840 µatm) shows a significantly greater dynamic range compared to the values calculated from pH and TA ($pCO_{2,pHTA}$, 314 to 608 µatm). The higher measuring frequency of the CO_2-Pro thus better characterized the short-term variability of pCO_2 which was mainly caused by the strong biological activities of local coral reef system.

The 5-minute averages of the sensor outputs bracketing the time of discrete sample collection were compared to the calculated $pCO_{2,pHTA}$ in Figure 3.2. The mean and SD of the differences between the paired $pCO_{2,pHTA}$ and $pCO_{2,Pro}$ ($\Delta pCO_2 = pCO_{2,Pro} - pCO_{2,pHTA,}$ Figure 3.2c) are 8.7 ± 14.1 µatm. $pCO_{2,Pro}$ shows a tight correlation with $pCO_{2,pHTA}$ ($R^2 = 0.99$, n = 29, not shown), and the positive correlation between ΔpCO_2 and $pCO_{2,Pro}$ suggests an increasing offset under high pCO_2 conditions (Figure 3.2b). This indicates that the ΔpCO_2 may be due to a linear calibration error. When $pCO_{2,Pro}$ is corrected against $pCO_{2,pHTA}$, the SD of the corrected sensor output ($pCO_{2,ProCorr}$) and $pCO_{2,pHTA}$ is ± 7.4 µatm (Figure 3.2d), which is similar to the uncertainty of $pCO_{2,pHTA}$ calculation (± 7.5 µatm). There are no systematic changes in $\Delta pCO_{2,corr}$ (Figure 3.2d), which suggests no other significant sources of error (i.e. biofouling, instrument drift) during the measurement. However, the error in sensor measurement resulted from the temperature fluctuation of the optical cell (see the

PAP result section below) is not considered in the performance report by ACT [2009a].

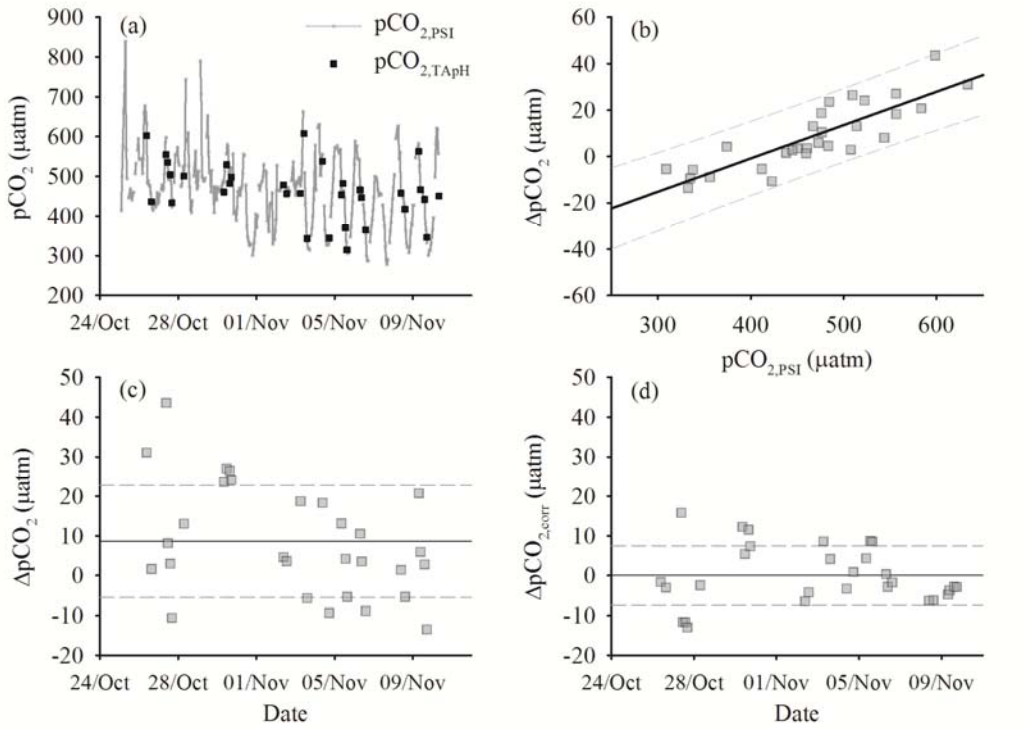

Figure 3.2 The results of the ACT test in Kaneohe Bay: (a) the continuously hourly $pCO_{2,PSI}$ from the CO_2-Pro and the $pCO_{2,pHTA}$ calculated from discrete pH and TA; (b) the correlation between the ΔpCO_2 ($\Delta pCO_2 = pCO_{2,Pro} - pCO_{2,pHTA}$) and $pCO_{2,PSI}$, the linear fit and the 95% prediction bands are shown; (c) ΔpCO_2 (8.4 ± 14.1 µatm) vs. time; (d) $\Delta pCO_{2,corr} = pCO_{2,ProCorr} - pCO_{2,pHTA}$, where $pCO_{2,ProCorr}$ is the sensor output corrected by $pCO_{2,pHTA}$ using the regression shown in panel b, and the standard deviation of $\Delta pCO_{2,corr}$ is ± 7.4 µatm. Figure adapted from ACT [2009a].

3.4.2 Results of the SNOMS underway measurement

The CO_2-Pro units used in the SNOMS operation were only factory calibrated on a yearly basis. For the evaluation purpose, $pCO_{2,Pro}$ is compared to the $pCO_{2,DICTA}$ calculated from the daily DIC and TA samples, as well as to direct measurements from other pCO_2 measuring systems in the same region. As the pCO_2 measurements were intermittent at the beginning of the SNOMS project during the circumnavigation of the *MV Pacific Celebes* (2007-2009), the assessment presented

below is based on the continuous measurements along the repeated transects in the Pacific (2009 onwards). From October 2009 to February 2012, the cargo ship in total made 18 transects between the western US coast, New Zealand and Australia and two CO_2-Pro units were used for measurement in turn (Table 3.3). Among the 14 transects with successful measurement (vs. 2 failed transects with sensor malfunction), there are 12 transects with DIC and TA data.

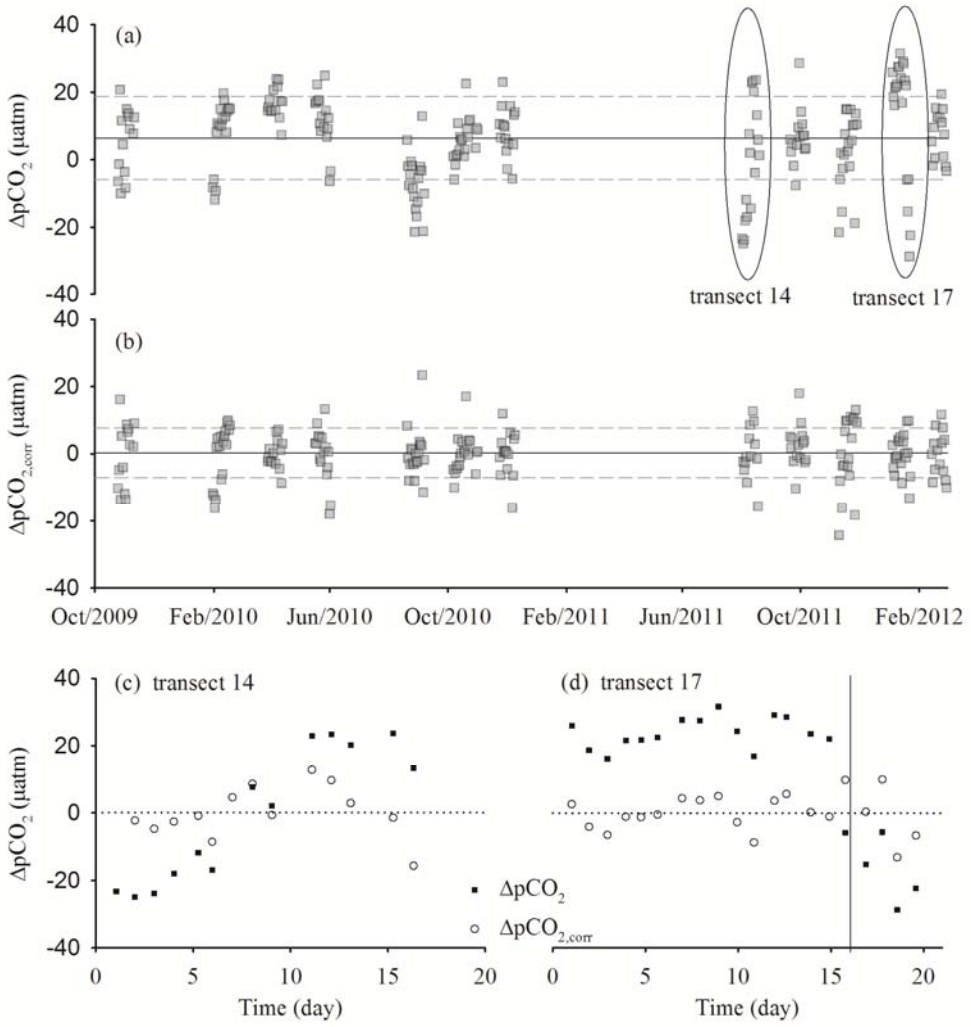

Figure 3.3 For the 12 Pacific transects during the SNOMS operation, (a) ΔpCO_2 = $pCO_{2,Pro}$ - $pCO_{2,DICTA}$, where $pCO_{2,Pro}$ is the raw sensor output and $pCO_{2,DICTA}$ is calculated from DIC and TA, the mean and SD of ΔpCO_2 are 6.4 ± 12.3 µatm; (b) $\Delta pCO_{2,corr}$ = $pCO_{2,ProCorr}$ - $pCO_{2,DICTA}$, where $pCO_{2,ProCorr}$ is the $pCO_{2,Pro}$ corrected by $pCO_{2,pHTA}$ for individual transects, the mean and SD of $\Delta pCO_{2,corr}$ are 0.2 ± 7.8 µatm. The increasing ΔpCO_2 in transect 14 and the sudden changes in ΔpCO_2 in transect 17 are shown in panel (c) and (d), together with the $\Delta pCO_{2,corr}$.

The difference between the raw sensor output $pCO_{2,Pro}$ (5-minute average corresponding to the sampling time) and $pCO_{2,DICTA}$ is shown in Figure 3.3a. The overall offset ($\Delta pCO_2 = pCO_{2,Pro} - pCO_{2,DICTA}$) for the 12 transects is 6.4 ± 12.3 µatm (n = 200). No correlation between ΔpCO_2 and the absolute concentration of pCO_2 (300-500 µatm) is identified (not shown). It is noted that the mean and SD of the ΔpCO_2 vary from transect to transect (Table 3.3). Aside from the error and potential drift of the senor, the difference in ΔpCO_2 among transects may be caused by several other reasons: 1) uncertainty in the $pCO_{2,DICTA}$ calculation; 2) the different responses of the two CO_2-Pro units and the changing response of each unit before/after the recalibration in June 2010; 3) the influence of water patchiness, i.e. taking a discrete sample from a different water patch from that measured by the CO_2-Pro as the ship travelled at a relatively high speed (~15 knots).

On the other hand, the values of ΔpCO_2 in the successive transects using the same sensor generally doesn't differ much (e.g. transects 2, 3, 4 for sensor 47 and transects 7, 8 ,9 for sensor 48, see Table 3.3). The changes in ΔpCO_2 among these successive transects may be mainly related to the changes in the condition of the gas transfer membranes (biofouling, contamination etc.) and the SNOMS tank (sedimentation). The values of ΔpCO_2 show a random distribution around the mean value for each transect except for transect 14 and 17. The ΔpCO_2 in transect 14 show a consistent increasing trend with time (Figure 3.3c). Moreover, the first 15 days of transect 17 (24.1 µatm) is significantly higher than those of the adjacent transects using the same sensor (2.6 and 7.4 µatm for transect 16 and 18 respectively), which is followed by a sudden decrease of ~40 µatm in ΔpCO_2 in the last 5 days (Figure 3.3d). The causes of these changes in ΔpCO_2 during this particular transect were not well identified.

As the calculated $pCO_{2,DICTA}$ provides a consistent reference throughout the SNOMS operation for the two CO_2-Pro units before and after recalibration, $pCO_{2,Pro}$ were calibrated against $pCO_{2,DICTA}$ for each transect individually. A time-dependent correction was applied to the transect 14, and the data in transect 17 are corrected in two sections as described above (Figure 3.3c, d). As shown in Figure 3.3b, the SD of the differences between the corrected sensor outputs and $pCO_{2,DICTA}$ is ± 7.8 µatm (Figure 3.3b), which is similar to the uncertainty of the calculation of $pCO_{2,DICTA}$ (± 8.1 µatm).

Table 3.3 The mean and standard deviation (SD) of the differences in the CO_2-Pro outputs ($pCO_{2,Pro}$) and those calculated from DIC and TA ($pCO_{2,DICTA}$) during the SNOMS operation in the Pacific. R^2 refer to the correlation coefficients and n is the number of the pairs of pCO_2.

No.	Start port	End port	Start date	End date	Sensor	$pCO_{2,Pro}$ - $pCO_{2,DICTA}$	SD	R^2	n
1	Taranga	Vancouver	23-Oct-09	11-Nov-09	48	5.7	9.8	0.91	14
2	Vancouver	Brisbane	02-Dec-09	25-Dec-09	48	failed measurement			
3	Taranga	Los Angeles	29-Jan-10	18-Feb-10	47	8.3	9.9	0.92	18
4	Los Angeles	Wellington	27-Mar-10	13-Apr-10	47	16.9	4.5	0.98	14
5	Taranga	Los Angeles	14-May-10	02-Jun-10	47	12.0	8.2	0.94	16
6	Vancouver	Auckland	25-Jun-10	14-Jul-10	48	failed measurement			
7	Taranga	Los Angeles	18-Aug-10	07-Sep-10	48	-6.6	8.6	0.97	19
8	Los Angeles	Brisbane	05-Oct-10	25-Oct-10	48	5.9	6.1	0.98	20
9	Taranga	Los Angeles	21-Nov-10	12-Dec-10	48	8.7	7.5	0.98	15
10	Los Angeles	Brisbane	18-Jan-11	12-Feb-11	none	no measurement; system removed for calibration			
11	Taranga	Los Angeles	16-Mar-11	10-Apr-11	none	no measurement; system removed for calibration			
12	Los Angeles	Brisbane	05-May-11	25-May-11	recalibrated 47	successful measurement; no DIC and TA data			
13	Taranga	Los Angeles	15-Jun-11	06-Jul-11	recalibrated 47	successful measurement; no DIC and TA data			
14	Los Angeles	Brisbane	30-Jul-11	20-Aug-11	recalibrated 47	0.3	18.0	0.85	18
15	Taranga	Los Angeles	20-Sep-11	09-Oct-11	recalibrated 47	6.6	8.3	0.94	15
16	Los Angeles	Brisbane	09-Nov-11	29-Nov-11	recalibrated 48	2.6	11.3	0.92	19
17	Taranga	Los Angeles	03-Jan-12	17-Jan-12	recalibrated 48	24.1	5.1	0.99	14
			18-Jan-12	23-Jan-12	recalibrated 48	-15.57 (sudden drop)	10.1		5
18	Los Angeles	Taranga	11-Feb-12	29-Feb-12	recalibrated 48	7.4	7.4	0.94	14

During the same period of the SNOMS transect 9, another SOO *MV Natalie Schulte* took pCO_2 measurement along the same route to that of the *MV Pacific Celebes*, but in a different direction (Figure 3.4a). The pCO_2 measuring system was operated by Pacific Marine Environmental Laboratory (PMEL), which features a showerhead design of equilibrator and NDIR detection of dried gas [Pierrot et al., 2009]. The regularly calibrated PMEL measurements (accuracy within 2 μatm) thus serves as a good case for an intercomparison to evaluate the corrected SNOMS pCO_2 data. As shown in Figure 3.4, the temperature, salinity and pCO_2 measured by the two systems generally display the same latitudinal distributions. The elevated pCO_2 observed around the equator suggests the influence of westward advected CO_2-rich water originating from the equatorial upwelling (Figure 3.4d). However, the difference in measuring time at the same location for the two ships (ΔTime in Figure 3.4) ranges 0-16 days. Therefore, the difference of the two pCO_2 measurements (Figure 3.4f) includes not only the errors of the two measurements but also the natural spatial and temporal variability of pCO_2. The latter is related to water movement and warming/cooling of the surface water, which is indicated by the temperature and salinity differences between the two datasets (Figure 3.4e).

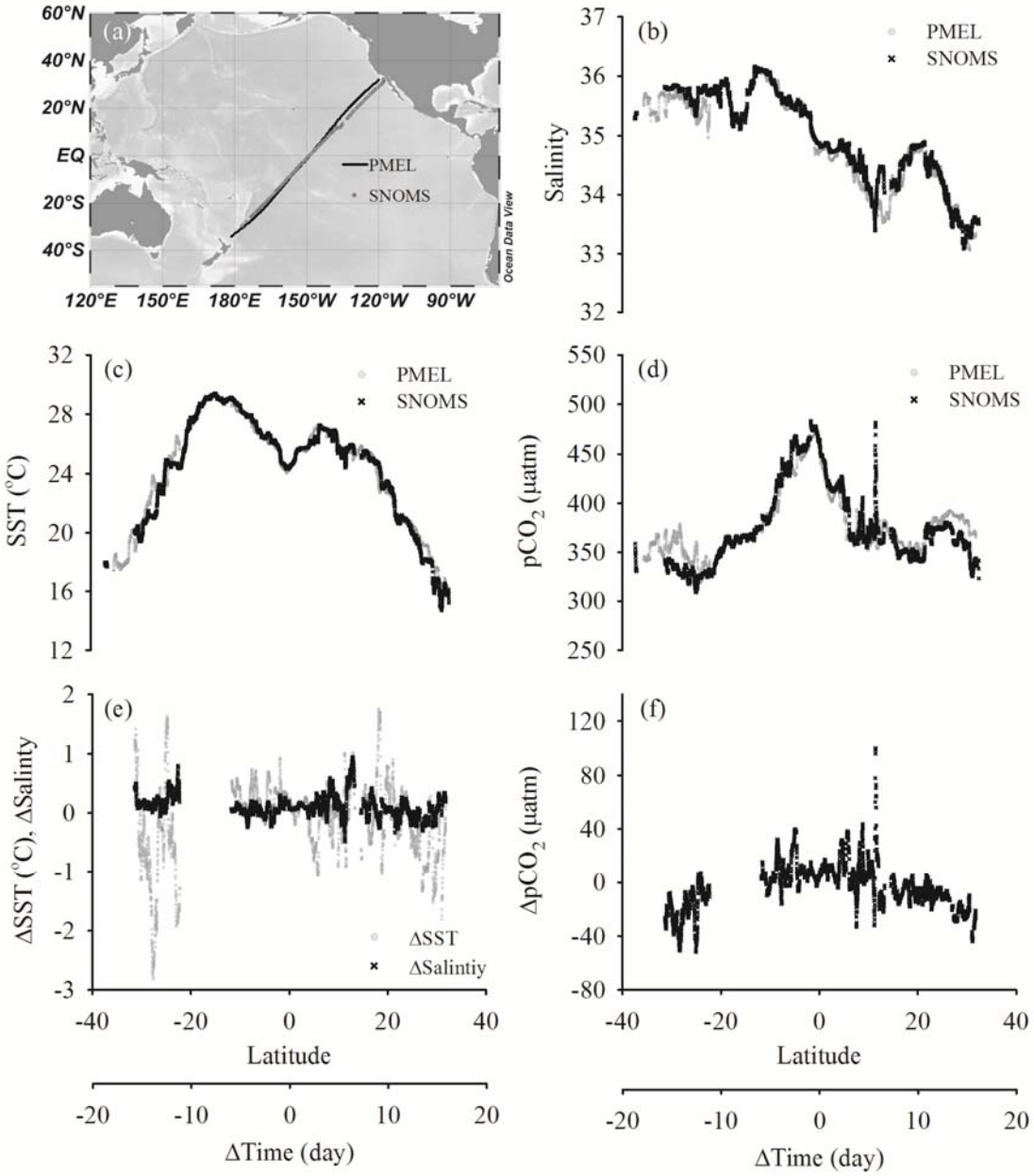

Figure 3.4 (a) The overlapping route of the two ships; the latitudinal distributions of (b) salinity, (c) SST, (d) pCO_2 measured by the PMEL and SNOMS systems; and their differences in (e) SST, salinity and (f) pCO_2. ΔTime is the difference in measuring time at the same location for the two ships.

In order to minimize the influence of natural pCO_2 variability on the comparison, the simultaneous measurements by the two systems were highlighted in Figure 3.5. These measurements, with a time difference less than 0.5 day, were made in the equatorial region when the distance of the two ships within 250 km. The results measured by the two ships generally agreed in salinity (0.14 ± 0.05) and temperature

(0.28 ± 0.09°C, Figure 3.5a). Previous time-series and Lagrangian observations in the equatorial Pacific show a diurnal pCO_2 variability of 2-8 μatm, which is mainly controlled by the temperature fluctuation [DeGrandpre et al., 2004; Goyet and Peltzer, 1997]. In order to remove the temperature effect on the pCO_2 comparison, the $pCO_{2,Pro}$ was normalized to the temperature measured by the PEML system. When the temperature effect is removed, the SNOMS pCO_2 agree well with the PMEL measurement at -0.3 ± 3.9 μatm (ΔpCO_2 in Figure 3.5b). This indicates a reasonable good accuracy of the corrected SNOMS pCO_2 data (note that the raw CO_2-Pro outputs have been corrected against the carbonate calculation by 8.7 μatm, see Table 3.3).

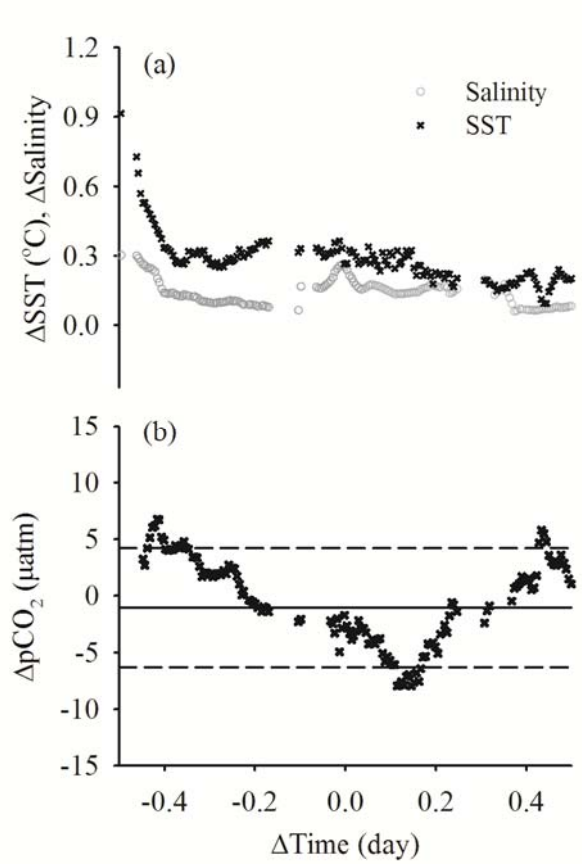

Figure 3.5 The differences of the simultaneous measurements (time difference less than 0.5 day and distance within 250 km) by the SNOMS and PMEL systems: (a) SST and salinity; (b) pCO_2

3.4.3 Results of the Aquatron laboratory test

As shown in Figure 3.6a, the water temperature during the Aquatron test generally showed a diurnal variability of 1-3°C and it varied within 15.5-17.5°C during the intercomparison period. The evaporation-induced increase in salinity was clearly observed and a sharp salinity drop on 7 August indicates the substantial addition of the fresher harbour water after a drainage from the sampling tube (Figure 3.6b). In order to account for the changes in chemical properties due to evaporation, DIC and TA are normalized to the mean salinity 32.3: nX = (X / Salinity) *32.3, where X is the measured concentration of DIC or TA, and nX is the salinity normalized concentration (Figure 3.6d). During the stabilization period, pCO_2 decreased from the initial value (up to 900 µatm) to a relative constant range within 640-690 µatm (Figure 3.6c). At the same time, DIC and TA both showed an increasing trend (Figure 3.6b) while the concentrations of nutrients remained at low levels with little variability (Figure 3.6e, f). The relatively constant nDIC (~2150 µmol kg^{-1}, Figure 3.6d) suggests that the increase in DIC (Figure 3.6b) mainly resulted from evaporation. In contrast, the salinity-normalized nTA significantly increased from 2240 to 2290 µmol kg^{-1} (Figure 3.6d). During the intercomparison period, the pCO_2 levels were adjusted to be in the 'natural' open ocean range of 300 to 550 µatm by bubbling of CO_2-free air (started on 10 July, 2 August and 31 August). Corresponding decreases in pCO_2 and DIC (Figure 3.6b, c) were observed when the CO_2-free air was purged, which were followed by progressive increases after the bubbling stopped. On 7 August, the dramatic changes in all measured variables were caused by the substantial addition of newly pumped water as described above. This induced sudden decreases in salinity, TA and DIC (Figure 3.7a, b) which were associated with increases in pCO_2 and nutrients (Figure 3.7c, e, f).

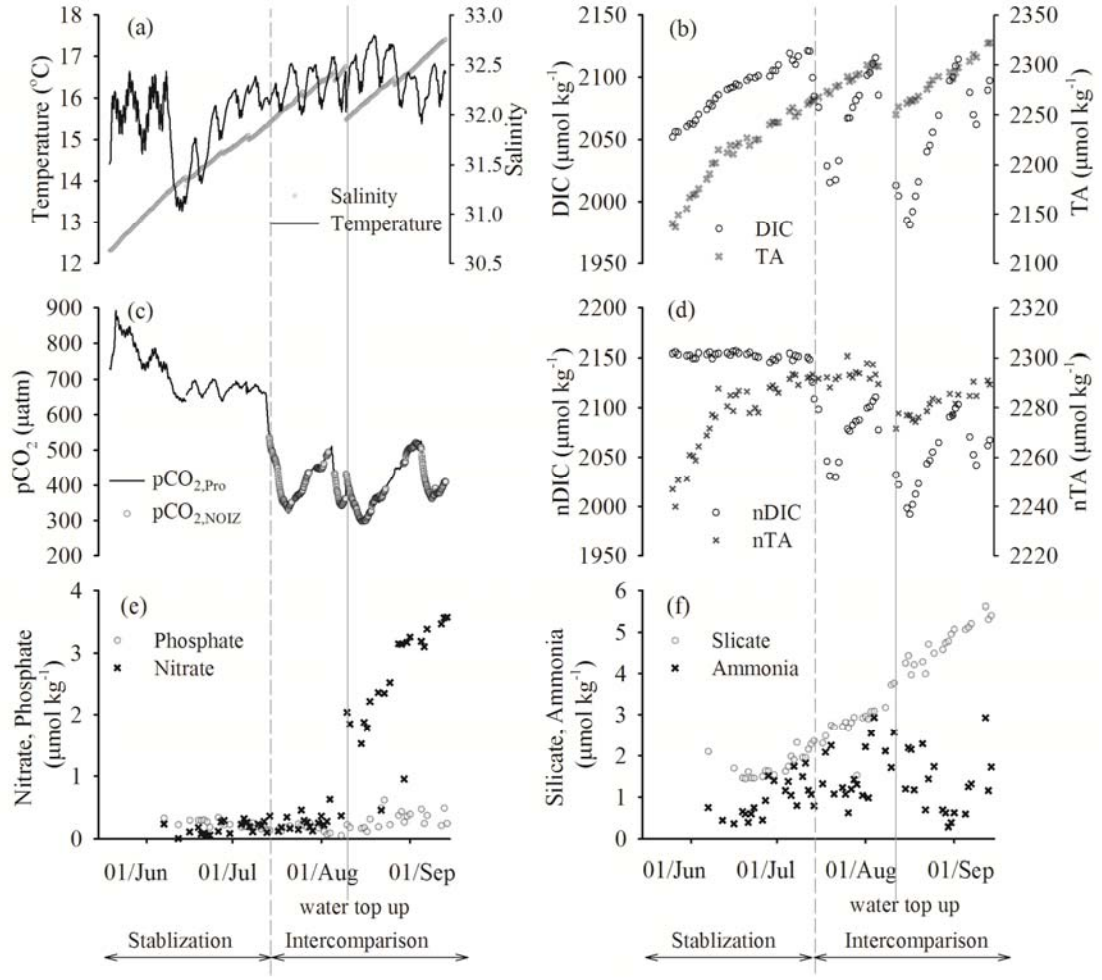

Figure 3.6 The variations of (a) temperature and salinity, (b) DIC and TA, (c) pCO_2 measured by the CO_2-Pro and the NOIZ system, (d) salinity normalized nDIC and nTA, (e) nitrate and phosphate, and (f) silicate and ammonia during the Aquatron test. The dashed line and the solid line correspond to the starting of the intercomparison and the substantial top up event respectively.

The intercomparison of the pCO_2 measurements by the SNOMS and NOIZ systems is presented in Figure 3.7. The CO_2-Pro functioned properly throughout the Aquatron test while the NOIZ system suffered from malfunctions on a few occasions (the failed measurements are not included in the intercomparison, Figure 3.7a). Both measurements were averaged to 5 minute internal and $pCO_{2,NOIZ}$ was normalized to the temperature in the SNOMS tank to eliminate the temperature influence on the comparison (the average temperature difference is ~0.08°C, which corresponds to ~1.5 μatm in pCO_2). There may be a slight delay in $pCO_{2,Pro}$ when responding to the pCO_2 disturbances (bubbling, water top up) as these events occurred in the Aquatron

tank were first observed by the NOIZ system. Overall, the pCO_2 measured by the two systems shows a tight correlation ($pCO_{2,Pro}$ = 0.9987 * $pCO_{2,NOIZ}$, R^2 = 0.99, not shown). The mean and SD of the differences between the two measurements (ΔpCO_2 = $pCO_{2,Pro}$ - $pCO_{2,NOIZ}$) are -3.0 ± 4.4 µatm (n = 13847, Figure 3.7c). ΔpCO_2 doesn't show a constant drift over the two month test (Figure 3.7c) but appears to change with the absolute pCO_2 concentration (Figure 3.7b), which may be due to a linear error in the sensor calibration. When the CO_2-Pro measurements are calibrated against $pCO_{2,NOIZ}$, the differences between the calibrated $pCO_{2,ProCorr}$ and $pCO_{2,NOIZ}$ ($\Delta pCO_{2,corr}$ in Figure 3.7d, 0 ± 2.9 µatm) show a random distribution around the mean value throughout the intercomparison experiment, which suggests no instrumental drift of the CO_2-Pro during the two-month period.

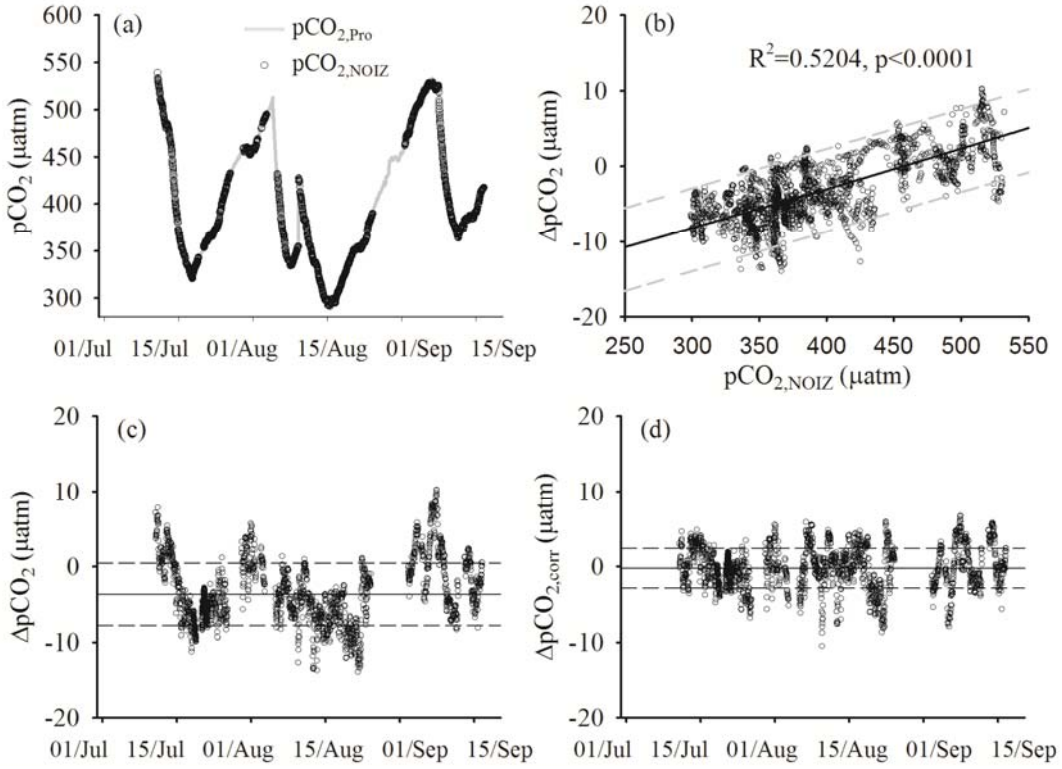

Figure 3.7 The results of the two-month intercomparison between the CO_2-Pro and the calibrated NOIZ system: (a) pCO_2; (b) the pCO_2 differences (ΔpCO_2 = $pCO_{2,Pro}$ - $pCO_{2,NOIZ}$) vs. $pCO_{2,NOIZ}$, the linear fit and the 95% prediction bands are shown; (c) ΔpCO_2 vs. time; (d) $\Delta pCO_{2,corr}$ is the pCO_2 differences after the correction of $pCO_{2,Pro}$ against $pCO_{2,NOIZ}$.

An interesting phenomenon observed in the Aquatron test is the abnormal changes in alkalinity. The increase in nTA during the stabilization period (2240 to 2290 μmol kg^{-1}, Figure 3.6d) cannot be explained by the changes in inorganic carbon content and nutrients: (1) the small changes in nDIC and nutrients indicate minor TA changes resulted from biological activities such as precipitation and dissolution of $CaCO_3$ (which changes TA and DIC at a ratio of 2:1) and nutrient uptake and release by algae (which changes TA following the nutrient-H^+-compensation principle) [Wolf-Gladrow et al., 2007]; (2) air-sea gas exchange of CO_2 changes DIC but doesn't affect the concentration of TA [Wolf-Gladrow et al., 2007]; (3) the oxygen saturation varied between 86 to 104% (not shown) which suggests no TA changes induced by anaerobic processes. Similarly, increases in nTA observed after the top up event on 7 August (2270 to 2290 μmol kg^{-1}) also did not match the changes in nDIC and nitrates: the increasing concentrations of nDIC and nitrates during this period (Figure 3.6d, e) suggests the occurrence of remineralization processes which would decrease TA.

In order to examine the TA anomaly in the Aquatron test, alkalinity was calculated from the measured DIC and pCO_2 using the CO2SYS. The calculated Alk_{sys} (uncertainty estimated to be ± 3.5 μmol kg^{-1}) is the alkalinity expected at the equilibration state of the carbonate system, which accounts for the major inorganic buffering acid-base pairs. It is shown in Figure 3.8a that the concentrations of Alk_{sys} are 3-24 μmol kg^{-1} lower than the measured values of TA_{meas}. This excess of TA_{meas} over the Alk_{sys} (Alk_{excess}) suggests substances or processes which affect the concentration of alkalinity and/or the titration process of alkalinity. This may be due to: waste water or mineral/clay reactions in the harbour, contamination during the pumping process, reaction with the fibreglass wall of Aquatron tank, or the existence of organic alkalinity. Although the source(s) of the alkalinity anomaly cannot be clearly identified, it is shown that using the measured TA_{meas} for carbonate calculation would result in underestimates in pCO_2 (Figure 3.8b). The $pCO_{2,DICTA}$ calculated from TA_{meas} and DIC is 7-90 μatm lower compared to the direct pCO_2 measurement, and this underestimation ($pCO_{2,bias} = pCO_{2,Pro} - pCO_{2,DICTA}$) shows a similar trend to that of Alk_{excess} (Figure 3.8c). Closer investigation shows that the percentage bias in pCO_2 ($\%pCO_{2,bias} = pCO_{2,bias} / pCO_{2,Pro}$) is positively correlated to

the percentage bias in alkalinity ($\%Alk_{excess} = Alk_{excess} / TA_{meas} = 12.54 * \%pCO_{2,bias}$, Figure 3.8d).

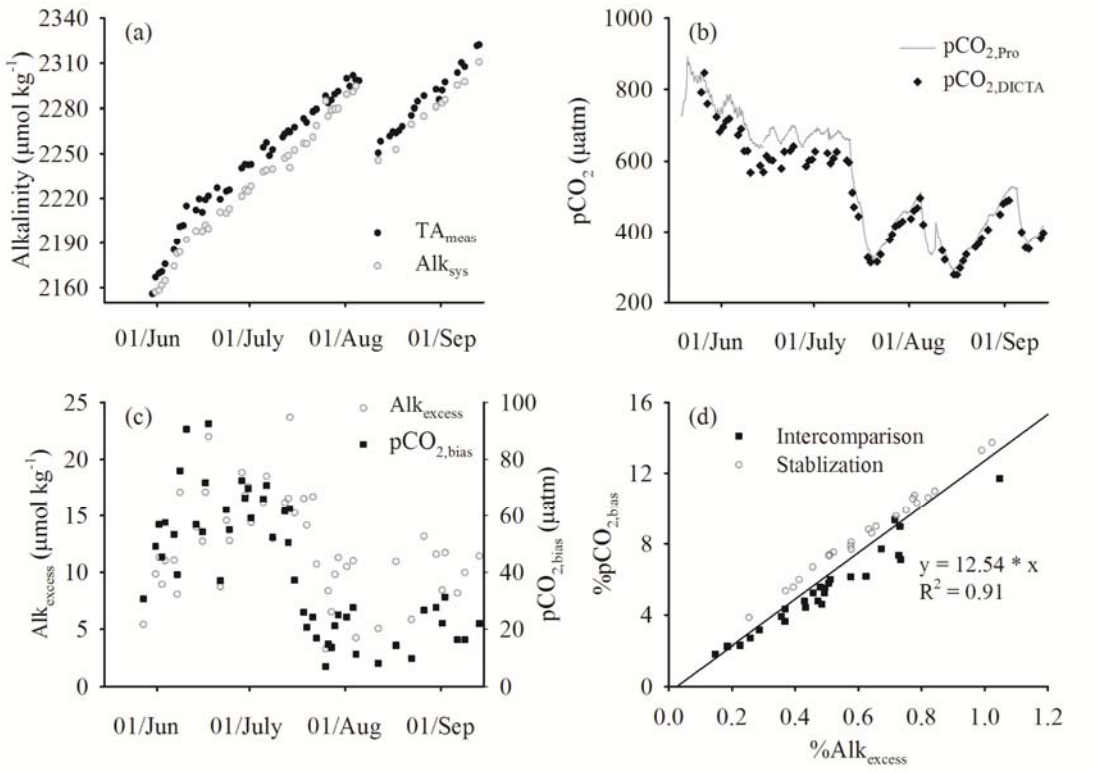

Figure 3.8 (a) The concentrations of TA_{meas} from direct measurement and Alk_{sys} calculated from the measured DIC and pCO_2; (b) pCO_2 measured by the CO_2-Pro ($pCO_{2,Pro}$) and $pCO_{2,DICTA}$ calculated from the measured DIC and TA; (c) the differences of TA and pCO_2 between direct measurements and the carbonate calculations ($Alk_{excess} = TA_{meas} - Alk_{sys}$, $pCO_{2,bias} = pCO_{2,Pro} - pCO_{2,DICTA}$); (d) the correlation between the percentage of $pCO_{2,bias}$ and Alk_{excess} in comparison to the measured values ($\%pCO_{2,bias} = pCO_{2,bias} / pCO_{2,Pro}$, $\%Alk_{excess} = Alk_{excess} / TA_{meas}$).

3.4.4 Results of the in-situ operation on the PAP mooring

Since the first deployment in June 2010, a CO_2-Pro continuously worked at the PAP site until January 2011 when a communication cable of the hub controller broke. A calibrated unit replaced the original sensor in July 2011 and operated until March 2012 when the controlling hub was flooded. A frustratingly short deployment during May to July 2012 was due to the communication failure when the sensor frame detached from the mooring. The deployment of CO_2-Pro at PAP was successful for

up to 7 months while the failure of longer measurement was due to problems at the hub controller rather than the sensor malfunction.

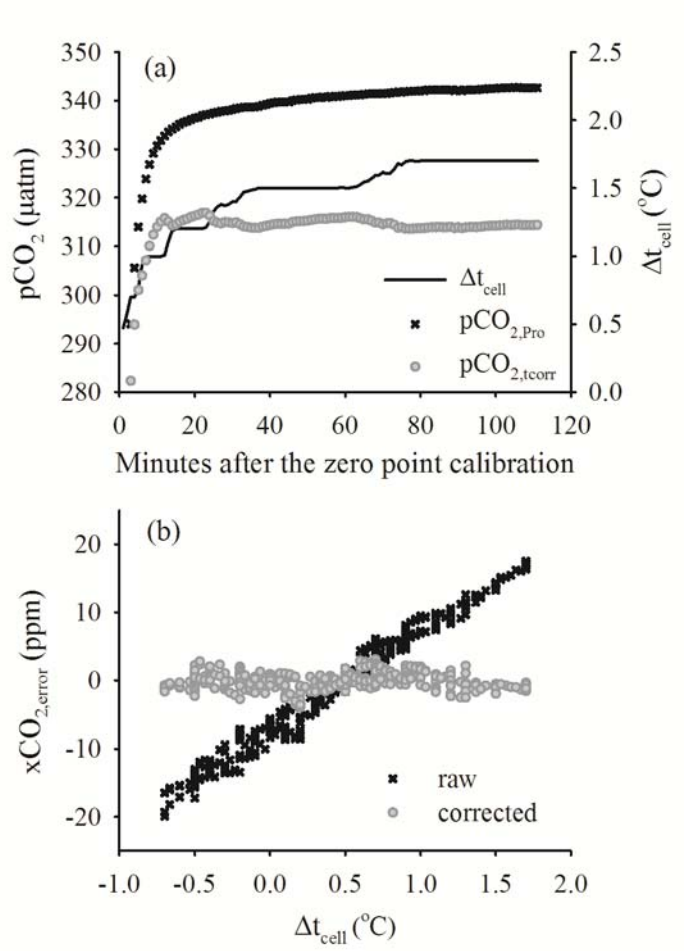

Figure 3.9 (a) A typical measuring cycle of CO_2-Pro on PAP mooring, Δt_{cell} is optical cell temperature deviation during the measurement in compared to that during the ZPC, $pCO_{2,Pro}$ and $pCO_{2,tcorr}$ are the raw sensor outputs and those corrected by the influence of Δt_{cell}; (b) the errors in xCO_2 measurements result from Δt_{cell} for the three standard gases in the laboratory test, and those after correction for the temperature influence.

In contrast to continuous measurement on SOO, the CO_2-Pro on the PAP mooring was operated intermittently (1 to 4 times a day) due to the limitation of power supply. Each measurement lasted for 45 to120 minutes which assures a full equilibrium with the seawater (typically within 15 minutes). The pCO_2 of the oligotrophic surface water around PAP site is expected to show minor variability during the short time length of each measurement. However, the pCO_2 measured by CO_2-pro showed a

consistent increase throughout each measurement (Figure 3.9a presents a typical measuring cycle of the CO_2-Pro) while the in-situ temperature and salinity remained unchanged. It is noted that the optical cell temperature of the detector shows an increasing trend similar to that of pCO_2 (Figure 3.9a). Moreover, the cell temperature during the measurement (t_{meas}) is found to be much higher than that during the ZPC ($\Delta t_{cell} = t_{meas} - t_{ZPC}$, Figure 3.9a). As the NDIR measurement is affected by the optical cell temperature, this temperature fluctuation would result in errors in pCO_2 detection.

In order to examine the influence of optical cell temperature, a laboratory test was carried out when the sensor was recovered from deployment. A series of CO_2 standard gases (256, 363 and 459 ppm) were connected to the detector bypassing the equilibrator for direct NDIR measurements. In addition, a CO_2-free gas (N_2 passing through CO_2 absorbance) was used to simulate the baseline measurement of C_{zero} during the ZPC. Measurements of these gases were carried out following a ZPC at 40°C, while the temperature of the optical cell during the measurement of each gas was perturbed by heating with an electric breeze and cooling with a cold pack (Δt_{cell} was adjusted to be -0.7 to 1.8°C). The test results show that the inferred signals of all measured gases decrease linearly with increasing optical cell temperature (not shown). As the zero-CO_2 signal also changes with temperature, using baseline measured at t_{zero} as the blank reference for measurements at different cell temperature would result in errors in calculating ε and xCO_2. As shown in Figure 3.9b, the errors in xCO_2 ($xCO_{2,error}$ = measured xCO_2 – certified value) were linearly correlated with Δt_{cell}, and the temperature effects are similar for the three standard gases at 15 ppm $°C^{-1}$. It is also shown that the errors in xCO_2 can be removed if the influence of Δt_{cell} is considered in the calculations of ε and xCO_2 (Figure 3.9b). The scatter of the data should mainly be caused by the uneven heating or cooling on the optical cell in this test.

When this correction of Δt_{cell} is applied to the PAP measurement, the corrected $pCO_{2,tcorr}$ stabilizes at 15 minutes after the ZPC as expected from the equilibrium time and shows minor changes afterward (Figure 3.9a). It is notable that the Δt_{cell} at PAP mooring is quite large (up to 1.5°C), which corresponds to error in pCO_2 as large as 25 μatm. This is because of the early ZPC at low t_{ZPC} when the optical cell

was not sufficiently warmed up, as well as the poor thermostat control of the optical cell, i.e. the cell temperature kept on increasing after ZPC. In contrast, this issue is not significant for the continuous measurements as the long-term operation allows the optical cell to be fully warmed up and minimize the temperature difference between ZPC and measurement. The Δt_{cell} during the SNOMS and Aquatron operations was ~ 0.2°C corresponding to an error of 3 μatm in pCO_2, and corrections of Δt_{cell} are applied to the SNOMS and Aquatron data before assessment.

3.5 Discussion and recommendations

Overall, the CO_2-Pro is suitable for onboard and in-situ measurements on platforms with limited working space and on platforms that could not be serviced regularly. The sensor's capacity for long-term operation was demonstrated by the successes of the SNOMS operation and PAP mooring deployment. One significant limit of CO_2-Pro is the lack of regular calibration against standard gases, which make it difficult to assess the accuracy of the measurement when it is deployed alone. In this study, the performance of CO_2-Pro is evaluated extensively under field and laboratory conditions and the results are summarized in Table 3.4. The CO_2-Pro agreed with a calibrated water-air equilibrator system during a 2-month side-by-side laboratory intercomparison (-3.0 ± 4.4 μatm). When used at sea, the direct sensor outputs differed from the calculated pCO_2 reference at 6.4 ± 12.3 μatm (on a SOO) and 8.7 ± 14.1 μatm (on a mooring). These differences result from a number of factors including the sensor error, the uncertainties in the reference and the comparison process, how well the sensor was set up, contamination issues et al. This study suggests that, when pCO_2 reference is available for correction, the uncertainty of the corrected sensor result is similar to and largely determined by the uncertainty of the reference.

Table 3.4 Summary of the assessment results of the CO_2-Pro in this study

	Application	**Mode**	**Time length**	**Reference and its uncertainty**	**Difference with the reference (μatm)**	
					direct output	**corrected output**
ACT	mooring test	in-situ	16-day	calculation from pH and TA (± 7.5 μatm)	8.7 ± 14.1	0 ± 7.4
SNOMS	SOO	underway	several	calculation from DIC and TA (± 8.1 μatm)	6.4 ± 12.3	0.2 ± 7.8
	observation		months	direct and calibrated measurement (± 2 μatm)		-0.3 ± 3.9
Aquatron	laboratory test	underway	2 months	direct and calibrated measurement (± 2 μatm)	-3.0 ± 4.4	0 ± 2.9

Moreover, this study reveals that error in pCO_2 measurement of CO_2-Pro can result from the changes in optical cell temperature between ZPC and measurement. This problem may be significant for the early versions of CO_2-pro whose optical cell are not well thermostat controlled. However, this error is correctable and can be avoided by better temperature control on the detector optical cell (the cell temperature fluctuation is within ± 0.05°C in the upgraded version of CO_2-Pro). This work also reveals that the inaccuracy of the sensor may be related to the calibration error. This may be due to that the empirical corrections are not able to accurately account for the differences of conditions between calibration and measurement. One significant factor is that the calibration is carried out on dry standard gas while the measured gas is nearly saturated with water vapour. The measured gas is recommended to be dried to minimize the differences between the calibration and measurement, and also to eliminate the influence of water vapour on the NDIR measurement on CO_2. This can be easily done by passing the gas through a desiccant before it goes into the optical cell, while wet CO_2 mole fraction and pCO_2 can be calculated as suggested by Pierrot et al. [2009]. An automatic calibration function using standard gases, if possible, is highly demanded in the future to optimize the accuracy of the measurement.

For the users of this sensor, calibration before and after long-term deployment should be carried out to examine any potential drift. Collection of discrete samples over a wide range of pCO_2 for the determination of other carbonate variables is recommended to provide quality control on the sensor, also for additional information on biogeochemical variability. If the sensor is only used for onboard or laboratory measurements, it is suggested that the users should contact the manufacturer to customize the sensor to enable an easy way for external manual calibration using standard gases.

In order to fulfill the target of constraining the regional air-sea CO_2 fluxes to 0.2 Pg C $year^{-1}$, pCO_2 measuring systems need to be accurate to within 2 μatm for seawater pCO_2 (Pierrot et al. 2009). This is presently a high requirement for pCO_2 sensors. As demonstrated in this work, the current accuracy of CO_2-pro has not met the golden standard of 2 μatm. However, considering the large variability of pCO_2 in time and space, there is great value in expanding in-situ observations by using sensors with a known and reasonably good accuracy. The developing sensor technology provide a

very effective way to increase the capability for global and regional ocean monitoring. This can provide useful information on the surface ocean where no or few measurements have been made or other extreme marine environments such as the deep ocean or the hydrothermal vent [Nakano et al., 2006; Willcox et al., 2009]. Moreover, the long-term time series data from fixed-station sensor deployment is the most powerful tool to understand the controlling mechanisms regulating the changes in ocean CO_2.

Another interesting finding in this study is the alkalinity anomaly and the mismatch in carbonate calculation in the Aquatron test. Excess of measured TA (up to 24 μmol kg^{-1}) are found in comparison to that calculated from DIC and pCO_2, while the carbonate calculation of pCO_2 using measured TA and DIC result in underestimation in pCO_2 (up to 90 μatm). Although the causes of this TA anomaly cannot be confirmed in this study, one possible explanation is the organic contribution to alkalinity. Many previous studies have proved the existent of organic alkalinity in both laboratory cultures (up to 800 μmol kg^{-1}) and natural coastal environments (tens of μmol kg^{-1}) [Cai et al., 1998; Hernandez-Ayon et al., 2007; Kim and Lee, 2009; Muller and Bleie, 2008]. Since the use of alkalinity including organic bases could lead to errors in the carbonate calculation, care should be taken when making calculations for the marine carbonate system in environments with high concentration of organic matter, e.g. estuary, coastal water and incubation culture solution. When studying the organic matter-rich waters, alkalinity is recommended to be measured using method proposed by Cai et al. [1998] or Hernández-Ayón et al. [1999] to identify the organic alkalinity.

Chapter 4: Variability of alkalinity and alkalinity-salinity relationship in the tropical and subtropical surface ocean

This chapter is adapted from a manuscript submitted to Global Biogeochemical Cycles by Jiang, Z.-P., T. Tyrrell, D. J. Hydes, M. Dai, and S. Hartman: 'Variability of alkalinity and alkalinity-salinity relationship in the tropical and subtropical surface ocean'.

4.1 Abstract

The variability of TA and its relationship with salinity in the (sub)tropical surface ocean were examined using data collected in various marine environments by a ship of opportunity. In the open ocean regions in the Atlantic, Pacific and Indian Ocean, the sea surface TA variability is mainly controlled by the simple dilution or concentration (SDC) effect of precipitation and evaporation, and the measured concentrations of TA agreed well with those predicted from salinity and temperature. The non-SDC changes in alkalinity in ocean margins and inland seas were examined by comparing the salinity-normalized alkalinity (NTA) with that of the open ocean end member. The non-SDC alkalinity additions to the western North Atlantic margin, eastern North Pacific margin and Mediterranean Sea were identified, which mainly resulted from river input and shelf current. In contrast, removal of TA into the formation and sedimentation of calcium carbonate was observed to be an important control in the Red Sea. In addition, the influences of these processes on the intercept of TA-salinity regression (TA_{S0}) were discussed. The concentration of river end member can only be accurately derived from TA_{S0} in river-dominated systems such as estuaries and river plumes. In coastal regions where other processes (evaporation, shelf current, upwelling, calcification etc.) are more influential, TA_{S0} can significantly deviate from the river water concentration. Furthermore, negative values of TA_{S0} can result from the non-SDC removal at the low salinity end (relative to the salinity of oceanic end member) and/or the non-SDC addition of TA at the high salinities (e.g. the Mediterranean Sea).

4.2 Introduction

TA is an important variable in the study of the marine carbonate system and $CaCO_3$ cycling in the ocean [Feely et al., 2004; Sarmiento et al., 2002]. In the surface ocean, the global distribution of TA generally matches that of salinity. This is because TA in the open ocean is mainly controlled by freshwater addition or removal which is reflected by salinity changes [Lee et al., 2006; Millero et al., 1998]. In the tropical and subtropical open ocean, changes in salinity account for more than 80% of the surface TA variability [Millero et al., 1998]. In high latitude regions, convective mixing of TA rich deep water plays an important role in affecting the surface TA

concentration. This process can be indicated by the changes in SST: the intensified convection during the cooling season acts to increase the surface TA concentration while this effect is minimal during summertime when SST is high [Lee et al., 2006; Millero et al., 1998]. Using salinity and SST as proxies for the main processes inducing surface TA variations in the open ocean Lee et al. [2006] categorized the global ocean into five regimes and proposed empirical algorithms to estimate the surface TA concentrations with an area-weighted uncertainty of ± 8.1 μmol kg^{-1}. Meanwhile, the concentration of TA can also be modulated by various biogeochemical processes, e.g., precipitation and dissolution of $CaCO_3$, uptake and release of nutrients, and anaerobic processes [Brewer and Goldman, 1976; Chen, 2002; Wolf-Gladrow et al., 2007]. Significant deviations from the expected TA-S relationship can be caused by biological activities, e.g., calcification during blooms of carbonate-secreting organisms [Bates et al., 1996; Harlay et al., 2010, 2011;]. Moreover, TA variability in coastal environments is more complex due to biophysical interactions among riverine inputs, shelf currents, upwelling, groundwater and biological processes [Abril et al., 2003; Cai et al., 2010; Cao et al., 2011; Chen, 2002; Friis et al., 2003; Liu et al., 2012].

Identifying the controlling mechanisms of TA variability and TA-S relationship in different marine environments is important for understanding marine biogeochemistry. This is particularly true in the context of ocean acidification caused by the oceanic absorption of anthropogenic CO_2, i.e. the decreases in pH and Ω in the ocean [Doney, 2009; Doney et al., 2009a; Orr et al., 2005]. Moreover, understanding the TA-S relationship is important either to estimate the end member properties from field observations (two-end member regression or multiple-end member analysis) or to examine the in situ biogeochemically-induced changes (by comparing the measurements to the values predicted from conservative mixing). Taking advantage of the wide sampling coverage of a SOO, this study looked into more details on the surface TA distribution in various characteristic oceanographic regions spanning open ocean, marginal seas and inland seas. The measured concentrations of TA were compared to the historical measurements from Carbon Dioxide Information Analysis Center (CDIAC) and values estimated from empirical algorithms [Lee et al., 2006]. In order to reveal the major controlling mechanisms of TA variability, the TA-S relationships in different marine environments were

examined, with special attention paid to the intercept of the TA-S regression (TA_{S0}). Moreover, salinity-normalized alkalinity (NTA) was used as an indicator to examine the addition and removal of alkalinity by processes other than dilution or concentration.

4.3 Methodology

4.3.1 Sampling, measurement and external data

Discrete samples for salinity and TA were collected on a daily basis on the SOO *MV Pacific Celebes* during the SNOMS operation (Chapter 2.2) and were analyzed under stable laboratory conditions at National Oceanography Centre, Southampton (Chapter 2.4). The ship traveled around the globe four times between June 2007 to March 2009: from Canada across the North Atlantic, Mediterranean, around India to Indonesia, across the Equatorial Pacific, through the Panama Canal into the Gulf of Mexico and then back to Canada. From March to September 2009, the ship worked one triangular route from Indonesia to North America via the Cape of Good Hope. After October 2009, the ship changed route to trade between Australia, New Zealand and North America. As shown in Figure 4.1, sample collections (n = 717) were carried out along the ship's route, except for June-October 2008 when a system failure occurred and January-April 2011 when the system was removed for calibration. The wide spatial coverage of sampling positions along the ship's route (Figure 4.1) thus provides a good opportunity to examine the distribution and variability of TA and its relationship with salinity in different environmental settings.

In order to compare the SNOMS data to previous measurements and to better constrain the oceanic end members, historical data were downloaded from CDIAC (Figure 4.1), including datasets from several data synthesis projects such as GLobal Ocean Data Analysis Project (GLODAP v1.1) [Key et al., 2004], CARbon dioxide IN the Atlantic Ocean (CARINA v1.2) [Tanhua et al., 2008], PACIFic ocean Interior Carbon (PACIFICA) [Suzuki et al., 2013], and cruise data from the Global Coastal Program in the North American west and east coasts [Feely and Sabine, 2011; Wanninkhof et al., 2011] and the Mediterranean Sea [Schneider and Roether., 2007; Tanhua et al., 2012]. Surface data were selected from waters within

20 m depth in the (sub)tropics (30°S - 30°N) and 30 m depth in regions with a latitude higher than 30 [Lee et al., 2006].

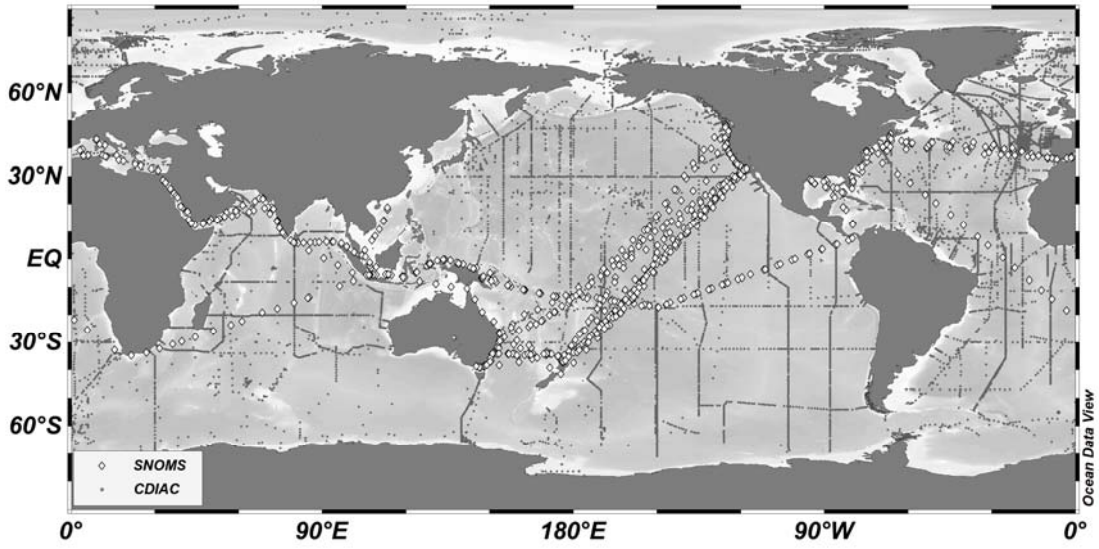

Figure 4.1 Sampling positions during the SNOMS project from 2007-2012 and the historical measurements from the Carbon Dioxide Information Analysis Center.

4.3.2 Salinity-normalized alkalinity (NTA), simple dilution or concentration (SDC) vs. non-SDC processes

Specific alkalinity, defined as the ratio of alkalinity to chlorinity, was used to compare alkalinity from different locations and depths; to identify the production of $CaCO_3$; and to characterize water masses [Koczy, 1956; Park, 1966, 1968]. In a similar way, salinity-specific alkalinity can be defined as the ratio of alkalinity to salinity. For each pair of TA and salinity, salinity-specific alkalinity is actually the slope of the line connecting the sample point and the origin. This mixing line is referred to as the 'Simple Dilution or Concentration' (SDC) line, which reflects TA variability caused by the addition or removal of zero-alkalinity freshwater (e.g. precipitation and evaporation). By multiplying salinity-specific alkalinity with a constant salinity (S_{ref}), salinity-normalized alkalinity (NTA) was widely used to adjust and compare TA data measured at different salinities (see Friis et al. [2003] and references therein). S_{ref} of 35 was used in this study.

Chapter 4. Variability of TA and TA-salinity relationship in the surface ocean

TA is a conservative quantity with respect to mixing [Wolf-Gladrow et al., 2007]:

$$TA_{mix} = \sum_i (TA_i M_i) / \sum_i M_i \quad (4.1)$$

where TA_{mix} is the concentration of TA in the mixture, TA_i and M_i refer to the concentrations of TA and masses of different water parcels, respectively. The alkalinity of a particular water parcel can be considered as a mixing product (TA_{mix}) with additional biogeochemical alterations (ΔTA_{bgc}):

$$TA = TA_{mix} + \Delta TA_{bgc} \quad (4.2)$$

TA_{mix} is a salinity-related term as mixing processes in the ocean are associated with changes in salinity (S), except for the mixing among water parcels with same salinity but different biogeochemical properties. In contrast, biogeochemical changes of ΔTA_{bgc} (e.g., precipitation and dissolution of $CaCO_3$, uptake and release of nutrients) result in little change in salinity. As typical values of ΔTA_{bgc} are much smaller than the mean concentration of TA [Sarmiento and Gruber, 2006], TA_{mix} tends to have a larger impact on the variability of TA. Therefore, TA-S relationship is commonly observed as an approximately linear mixing line with scatter reflecting the existence of additional biogeochemical contributions. If we consider a simple linear relationship between TA and salinity:

$$TA = slope * S + TA_{S0} \quad (4.3)$$

NTA is then calculated as:

$$NTA = TA * S_{ref}/S = slope * S_{ref} + TA_{s0} * S_{ref}/S \quad (4.4)$$

The schematic diagrams in Figure 4.2 demonstrate the influences of SDC and non-SDC processes on TA-S relationship and NTA. SDC processes change TA along the SDC line:

$$TA_{mix}^{SDC} = TA_{ocean} * S/S_{ocean} \text{ (the SDC line)} \quad (4.5)$$

where TA_{mix}^{SDC} is the alkalinity result from the SDC mixing between the oceanic end member (S_{ocean}, TA_{ocean}, O in Figure 4.2) and the zero-alkalinity freshwater (the

origin). This results in a zero TA_{S0} and a uniform NTA at all salinities ($NTA = NTA_{ocean} = TA_{ocean} * S_{ref}/S_{ocean}$, see the position of x axis in Figure 4.2b, d). In contrast, non-SDC changes in TA cause deviations in the TA-S relationship from the SDC line. This can be attributed to non-SDC mixing (ΔTA_{mix}^{nonSDC}) and biogeochemical processes (ΔTA_{bgc}). Therefore, TA can be broken down into:

$$TA = TA_{mix}^{SDC} + \Delta TA_{mix}^{nonSDC} + \Delta TA_{bgc} \quad (4.6)$$

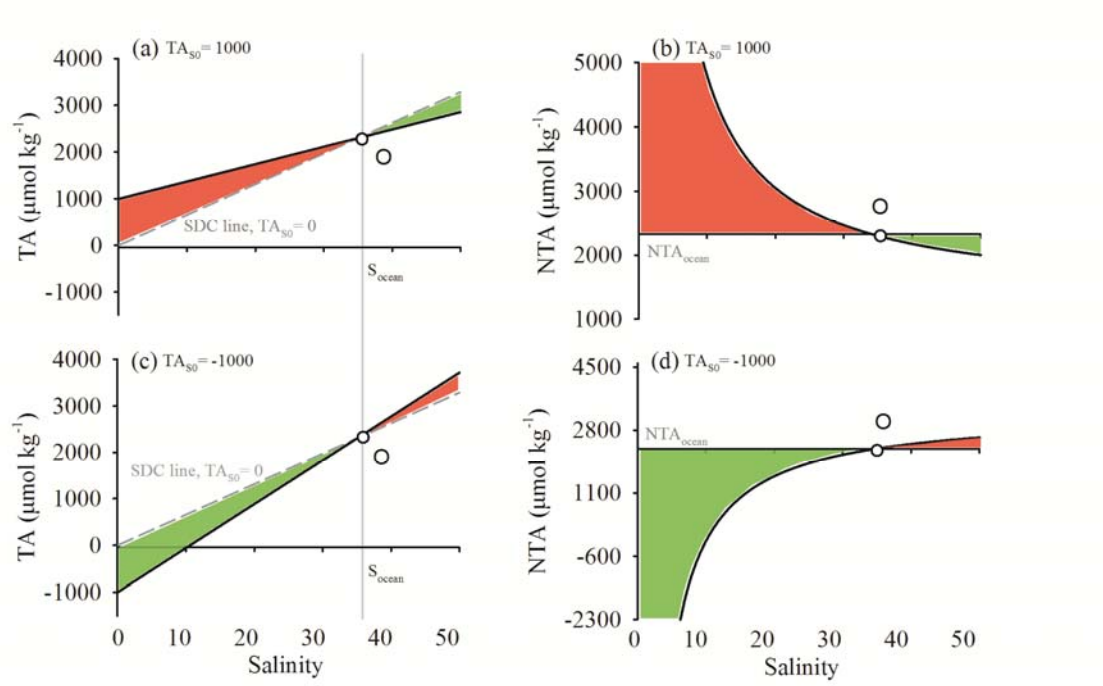

Figure 4.2 Schematic diagrams showing the influence of simple dilution or concentration (SDC) and non-SDC processes on the TA-S relationships. Here a mean oceanic surface end member O is assumed: S = 35, TA = 2300 µmol kg^{-1}, NTA = 2300 µmol kg^{-1} and (a, b) a positive intercept TA_{S0} of 1000 µmol kg^{-1} and (c, d) a negative intercept TA_{S0} of -1000 µmol kg^{-1}. The dashed SDC line shows the TA-S changes due to the SDC effect on the oceanic end member. The non-SDC additions and removals of TA are indicated by the red and green shaded areas respectively. In panel (b) and (d), the position of the x axis corresponds to the NTA_{ocean} of the oceanic end member; NTA > NTA_{ocean} suggests the non-SDC TA addition, and vice-versa.

Table 4.1 The influences of simple dilution or concentration (SDC) and non-SDC processes on TA, salinity normalized TA (NTA) and the intercept of TA-S relationship (TA_{S0}) under different salinity conditions. This study assume a well-defined oceanic end member (S_{ocean}, TA_{ocean}, NTA_{ocean}) and TA_{mix}^{SDC} is the alkalinity resulting from the SDC mixing between the oceanic end member and the zero-alkalinity freshwater.

Controlling processes	**TA**	**NTA**	**Condition**	**TA_{S0}**	**Example**
SDC only	$TA = TA_{mix}^{SDC}$	$NTA = NTA_{ocean}$	any salinity	$TA_{S0} = 0$	Precipitation/evaporation only
SDC + non-SDC addition	$TA > TA_{mix}^{SDC}$	$NTA > NTA_{ocean}$	$S > S_{ocean}$	$TA_{S0} < 0$	Mediterranean Sea
			$S < S_{ocean}$	$TA_{S0} > 0$	Western North Atlantic margin, Eastern North Pacific margin
SDC + non-SDC removal	$TA < TA_{mix}^{SDC}$	$NTA < NTA_{ocean}$	$S > S_{ocean}$	$TA_{S0} > 0$	Red Sea
			$S < S_{ocean}$	$TA_{S0} < 0$	

As shown in Figure 4.2 and Table 4.1, the influences of non-SDC processes on TA_{S0} are closely related to salinities condition. A positive TA_{S0} can result from the non-SDC removal of TA at salinity higher than S_{ocean} and/or the non-SDC alkalinity addition at salinity lower than S_{ocean} (Figure 4.2a). On the contrary, the non-SDC TA addition at the high salinity end and/or the non-SDC TA removal at the low salinity end result in a negative TA_{S0} (Figure 4.2c). With a non-zero TA_{S0} resulting from non-SDC processes, NTA-S distribution is a power function as suggested by Equation4.4 (Figure 4.2b, d). For this reason, it was argued that this traditional normalization concept could cause an 'overcorrection' and 'artificial variance' by ignoring non-SDC processes [Friis et al., 2003]. Instead, a salinity normalization considering a constant and regional-specific term for zero salinity was proposed by Friis et al. [2003]:

$$NTA_{eS} = (TA_{obs} - TA_{s0}) * S_{ref}/S_{obs} + TA_{s0} \quad (4.7)$$

where NTA_{eS} is the normalized alkalinity which accounts for the non-zero TA_{S0}, and T_{obs} and S_{obs} are the alkalinity and salinity from observation. While the frequent occurrence of non-SDC processes rules out NTA as a universally appropriate salinity normalization technique [Friis et al., 2003], NTA can be used as a good indicator of non-SDC changes in alkalinity. At any salinity, non-SDC addition of TA causes a deviation of the TA-S relationship above the SDC line ($TA > TA_{mix}^{SDC}$ in Table 4.1) and an NTA higher than NTA_{ocean}, and vice-versa (Figure 4.2b, d).

4.4 Results

4.4.1 General pattern

For all the SNOMS data, the measured TA varies strongly with salinity (Figure 4.3). Most open ocean data follow the SDC line through the global mean surface water end member (S = 35, TA = 2300 μmol kg^{-1}). However, different slopes and intercepts of the TA-S relationships were observed in the Mediterranean Sea and the Red Sea (Figure 4.3)., Deviations of TA from the SDC line are especially large at low salinities (Figure 4.3), which indicates the influences of terrestrial inputs, biological and physical processes in coastal regions [Cai et al., 2010; Chen, 2002;

Friis et al., 2003]. Accordingly, the results were divided into three geographic regimes: open ocean, marginal seas and inland seas. The observational results were summarized in Table 4.2. A detailed examination of the variability of TA, TA-S relationship and NTA for each regime is presented below.

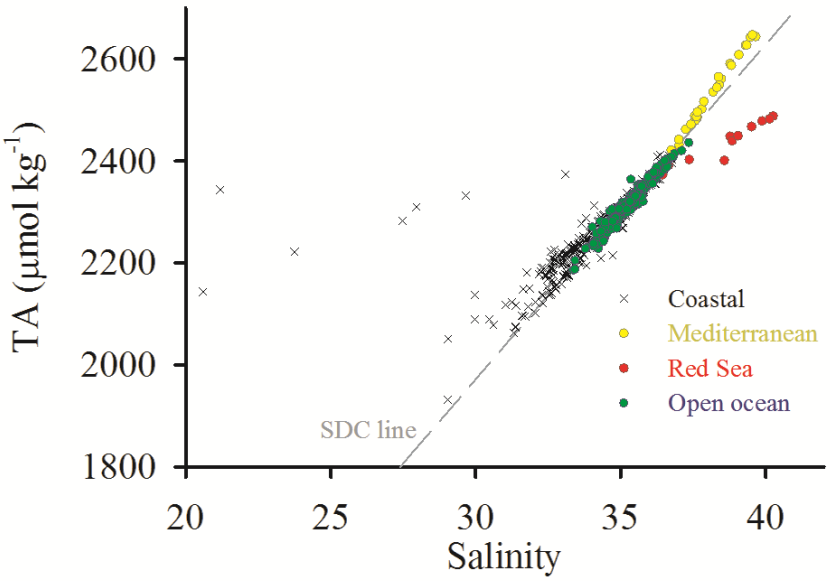

Figure 4.3 TA-S distributions in the open ocean, Mediterranean Sea, Red Sea and coastal regions. All the SNOMS measurements (n = 717) are shown here. The dashed line shows the TA-S changes due to the simple dilution or concentration effect on the mean oceanic surface water (S = 35, TA = 2300 µmol kg^{-1}).

Table 4.2 The observations in the surface waters of the (sub)tropical ocean by the SNOMS project. Sea surface temperature (SST, °C), salinity, total alkalinity (TA), the salinity-normalized alkalinity (NTA) are presented as 'mean ± one SD, minimum to maximum'. The concentrations of alkalinity are in units of μmol kg-1. NTA is compared to that of the oceanic end member (NTA_{ocean}).

(Sub)tropics	**Region**	**SST**	**Salinity**	**TA**	**NTA**	**NTA_{ocean}[c]**
Open ocean	Atlantic[a] 30°S-45°N, 70°W-20°E	22.23 ± 3.69 16.20 to 28.40	36.31 ± 0.35 35.57 to 37.34	2377 ± 22 2315 to 2436	2291 ± 5 2276 to 2302	2296 ± 8
	Pacific[b] 30°S-30°N, 180°W-130°W	26.76 ± 2.31 19.43 to 30.48	35.19 ± 0.61 33.36 to 36.58	2313 ± 40 2185 to 2404	2301 ± 9 2271 to 2341	2301 ± 10
	Indian Ocean 35°S-0°N, 20°E-100°E	24.93 ± 3.33 16.51 to 28.99	34.89 ± 0.55 34.19 to 35.66	2282 ± 37 2230 to 2336	2289 ± 6 2283 to 2304	2295 ± 7
Marginal Seas	Western North Atlantic margin 25°N-45°N, 155°W-115°W	17.28 ± 3.98 9.85 to 25.69	33.63 ± 0.85 31.25 to 35.43	2242 ± 45 2123 to 2336	2333 ± 15 2286 to 2378	2307 ± 5
	Eastern North Pacific margin 20°N-45°N, 100°W-45°W	21.10 ± 7.97 3.65 to 30.72	34.19 ± 3.98 13.64 to 37.34	2319 ± 89 2051 to 2449	2426 ± 521 2279 to 6285	2290 ± 6
Inland Seas	Mediterranean Sea 30°N-45°N, 7°W-40°E	21.84 ± 4.11 15.28 to 27.68	38.14 ± 0.88 36.74 to 39.65	2532 ± 73 2420 to 2647	2323 ± 15 2285 to 2344	2290 ± 4
	Red Sea 10°N-30°N, 30°E-45°E	29.15 ± 3.24 22.85 to 32.76	38.67 ± 1.33 36.43 to 40.24	2438 ± 40 2373 to 2488	2208 ± 44 2164 to 2284	2286 ± 9

[a] Excluding the Mediterranean Sea. [b] Excluding the equatorial upwelling Pacific. [c] For the open ocean, NTA was estimated from the CDIAC measurements in the defined region excluding the coastal data. For the marginal seas, NTA_{ocean} was estimated from the CDIAC measurements in the open ocean waters adjacent to the marginal seas under study. For the Mediterranean Sea and the Red Sea, NTA_{ocean} was estimated from the CDIAC measurements in the inflowing water from the North Atlantic adjacent to the Strait of Gibraltar and that in the Arabian Sea adjacent to the Gulf of Aden respectively. See the text for details.

4.4.2 (Sub)tropical open ocean

The surface TA in the open ocean regions in the (sub)tropical Atlantic (Figure 4.4c) and Pacific (Figure 4.5c) both show a minimum at 10°N and maxima at 15°S and 25°N. The latitudinal distribution of TA is similar to that of salinity (Figure 4.4b, Figure 4.5b), which is mainly determined by the rates of precipitation and evaporation at different latitudes [Millero et al., 1998]. It is also shown that the SNOMS data are well within the variation ranges of the CDIAC measurements (Figure 4.4, Figure 4.5).

Atlantic: Previous work has shown that most of the TA variations in the Atlantic subtropical gyres (30°S - 30°N) are associated with salinity changes and the NTA is remarkably invariant [Millero et al., 1998]. Estimated from the CDIAC open ocean data (30°S - 30°N, 70°W - 20°E, excluding the coastal regions, Figure 4.4a), the NTA_{ocean} of the (sub)tropical Atlantic is 2296 ± 8 μmol kg^{-1} (mean ± one SD, the same hereafter, n = 1015, Figure 4.4d). It was also found that NTA in the Atlantic increases towards high latitudes due to the intensified vertical mixing of the TA rich deep water [Millero et al., 1998]. SST is a potential proxy of the intensity of convective mixing and 20°C was used as the threshold to distinguish the high latitude regime from the (sub)tropical regime [Lee et al., 2006; Millero et al., 1998]. For the SNOMS measurements, the NTA along the west-east North Atlantic transects (35°N - 45°N, 60°W - 0°, Figure 4.4a) is 2292 ± 4 μmol kg^{-1} (n = 31, Figure 4.4d), which is not significantly different from that along the south-north Atlantic transect from Cape of Good Hope to North America (2289 ± 7 μmol kg^{-1}, n = 18, Figure 4.4d). This suggests a minor TA addition from deep water convection at these mid-latitude North Atlantic transects, which is supported by the relatively warm SST observed (16.2 to 28.4°C). As a whole, the SNOMS measurements in the low and mid latitude Atlantic open ocean (30°S - 45°N) showed a tight TA-S correlation (R^2 = 0.94, n = 49) and a relative constant NTA similar to the NTA_{ocean} estimated from CDIAC data.

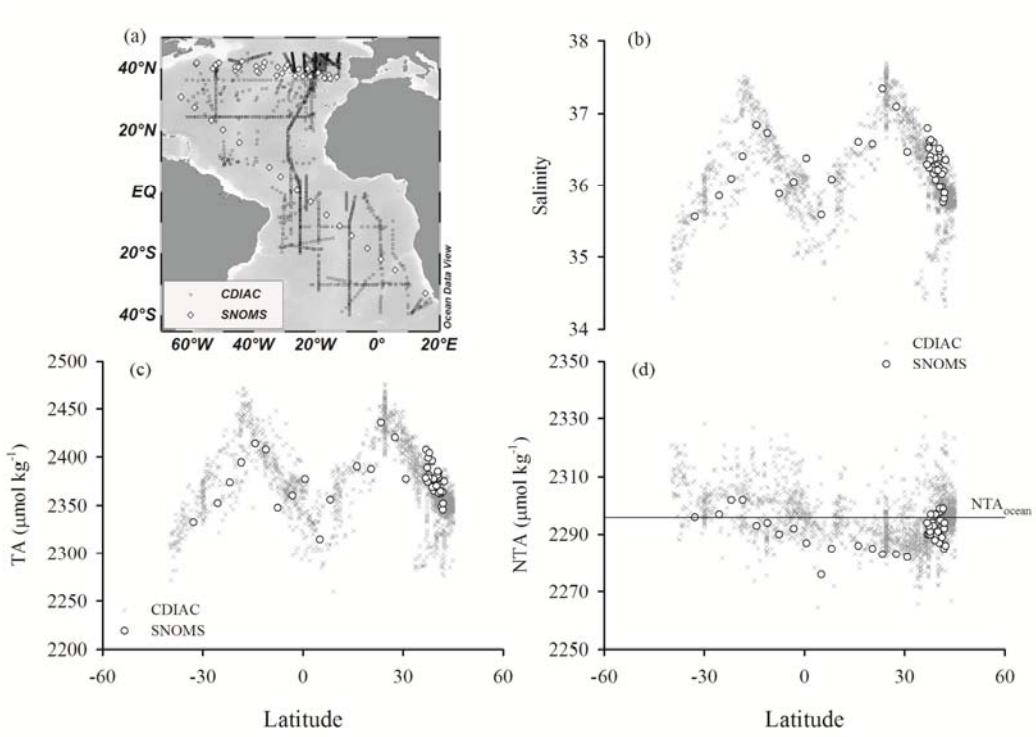

Figure 4.4 (a) The sampling positions of the SNOMS project in the (sub)tropical Atlantic, and the CDIAC measurements in the similar area excluding the coastal region; the latitudinal distributions of (b) salinity, (c) TA and (d) salinity-normalized alkalinity (NTA) from the SNOMS and CDIAC data. The reference NTA_{ocean} line in panel (d) is the mean value of the CDIAC measurements.

Pacific: In the subtropical Pacific gyres, Millero et al. [1998] reported a constant NTA of 2300 ± 6 μmol kg^{-1}. This is close to the NTA_{ocean} estimated from the CDIAC open ocean data adjacent to the SNOMS route (2301 ± 10 μmol kg^{-1}, n = 2245, yellow dots in Figure 4.5a). In the eastern equatorial Pacific, higher NTA associated with the equatorial upwelling was observed and the NTA decreases westward from the upwelling site [Millero et al., 1998]. The SNOMS measurements covered the eastern North Pacific, the central equatorial Pacific, and the western South Pacific (Figure 4.5a). As the sampling locations in the central equatorial Pacific were located far from the site of upwelling (Figure 4.5a), the influence of the equatorial upwelling is expected to be minor. For the SNOMS data in the (sub)tropical Pacific open ocean (30°S-30°N, 180°W-130°W excluding the eastern North Pacific margin, red dots in Figure 4.5a), the observed NTA (2301 ± 9 μmol kg^{-1}, n = 195) is close to the NTA_{ocean} (Figure 4.5d). With very limited riverine inputs from Australia, the coastal

data in the western South Pacific also showed an NTA similar to that in the Pacific open ocean (Figure 4.5d). On the other hand, higher NTA was observed in the eastern North Pacific margin (Figure 4.5d) and its cause is discussed below.

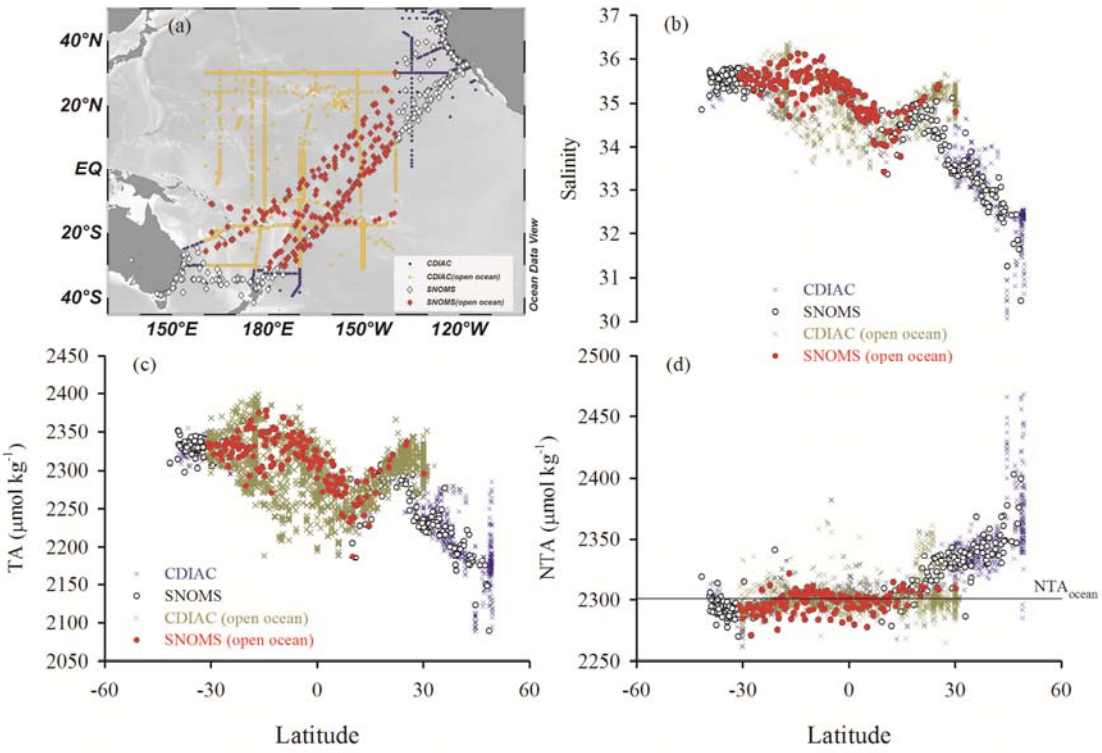

Figure 4.5 (a) The sampling positions of the SNOMS project in the (sub)tropical Pacific excluding the equatorial upwelling Pacific, and the CDIAC measurements in the similar area; the latitudinal distributions of (b) salinity, (c) TA and (d) salinity-normalized alkalinity (NTA) from the SNOMS and CDIAC data. The open ocean data were highlighted in yellow and red colors for the SNOMS and CDIAC data respectively. The reference NTA_{ocean} line in panel (d) is the mean value of the CDIAC open ocean data.

Indian Ocean: There were only a few SNOMS measurements in the open ocean in the Indian Ocean (Figure 4.1). As shown in Table 4.2, the measurements show an NTA of 2289 ± 6 μmol kg^{-1} (n = 16) which was not significantly different from the NTA_{ocean} of the Indian open ocean water estimated from the CDIAC data (2295 ± 7 μmol kg^{-1}, n = 420).

Overall, the SNOMS data in the (sub)tropical open ocean show a good TA-S correlation along the SDC line (Figure 4.3) and relatively constant values of NTA which are similar to those of NTA_{ocean} (Table 4.2). This suggests that the TA variability in this region is mostly due to the SDC effect of precipitation and evaporation while the non-SDC processes only play a minor role. The TA predicted from salinity and SST following Lee et al. [2006] generally agreed with the measured alkalinity (not shown). The difference between the predicted values and the measurements is 0.3 ± 10 μmol kg^{-1} (n = 304), which is similar to the uncertainty of the prediction (± 8.1 μmol kg^{-1}, [Lee et al., 2006]).

4.4.3 Marginal Seas

Western North Atlantic margin: The TA distribution and TA-S relationship in the western North Atlantic margin have been extensively examined by Cai et al. [2010]. They identified a river-dominated two end member mixing type of TA-S relationship, as well as an alongshore current-dominated type which exhibits a segmented mixing line with a shared mid-salinity end member [Cai et al., 2010]. They also found that the intercepts of the TA-S regressions roughly match the concentrations of TA of the local rivers [Cai et al., 2010]. The open ocean end member for this region (NTA_{ocean} = 2290 ± 6 μmol kg^{-1}, n = 181) was estimated from the CDIAC measurement in the Atlantic water adjacent to the western North Atlantic margin (25-40°N, 60-30°W, S > 36). During the SNOMS operation, samples were collected in the US east coast and in the Gulf of Mexico (Figure 4.1). As shown in Figure 4.6, the SNOMS results agree well with those measured during the North American Carbon Program (NACP) US east coast cruise from CDIAC. Data with salinity values lower than 35 are above the SDC line (Figure 4.6a) with NTA higher than the NTA_{ocean} (Figure 4.6b). The TA-S regression in the US east coast (Figure 4.6a) shows an intercept of 740 μmol kg^{-1} which is similar to the average concentration of the rivers entering the Mid Atlantic Bight (700 μmol kg^{-1}) [Cai et al., 2010]. The TA-S distribution in the Gulf of Mexico (Figure 4.6a) is also well constrained by the mixing lines of the oceanic end member and the local rivers (Atchafalaya: 1960 μmol kg^{-1}, Mississippi; 2375 μmol kg^{-1}, data from Water Quality Data for the Nation and Cai et al. [2010]). This river-dominated pattern shows that the mixing between river waters and seawater is

the dominant controlling factor of the TA-S relationship in the western North Atlantic Ocean margin. The riverine non-SDC addition (NTA > NTA_{ocean}, Figure 4.6b) at the low salinity end results in the positive values of TA_{S0} that are close to TA concentrations of the local rivers (Figure 4.6a).

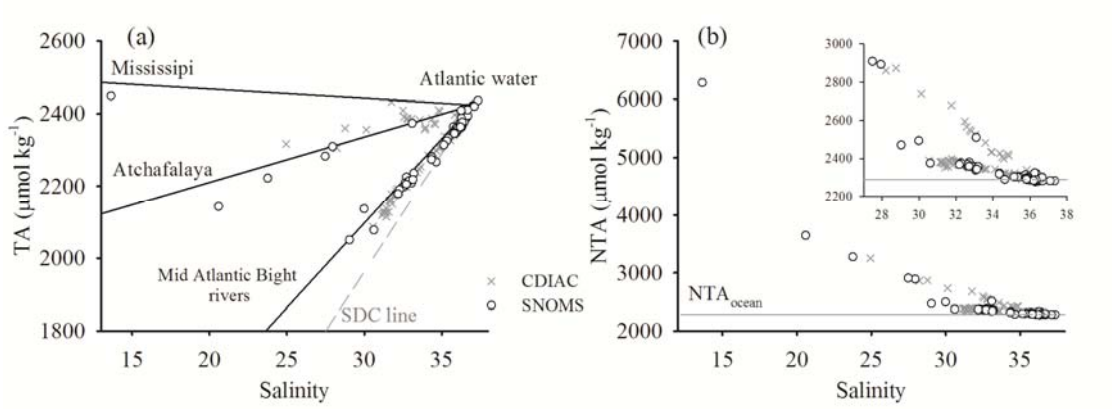

Figure 4.6 The (a) TA-S and (b) salinity-normalized alkalinity (NTA)-S relationships in the western North Atlantic margin from the SNOMS and CDIAC data. Panel (a) adapted from Figure 2 by Cai et al. [2010]. In panel (a), the dashed SDC line shows the TA-S changes due to the simple dilution or concentration effect on the North Atlantic open ocean water, while the solid lines show the TA-S distributions assuming a two-end member conservative mixing between the Atlantic water and the individual rivers. In panel (b), the reference line shows the NTA_{ocean} of the Atlantic open ocean water, and the NTA-S distribution at high salinities is highlighted in the inset.

Eastern North Pacific margin: As shown in Figure 4.7, the SNOMS and CDIAC data in the eastern North Pacific margin clearly show the influences of the low-salinity Columbia River plume off the coast of Oregon, the mid-salinity California Current that moves south along the western coast of North America [Batteen et al., 1995; Schneider et al., 2005], and the low-temperature and high salinity coastal upwelling off northern California [Feely et al., 2008]. As the Columbia River plume was separated from the open ocean water by the California Current, a segmented TA-S mixing line with a shared California Current end member at salinity ~32 was observed (Figure 4.8a). This TA-S distribution shows a mixing between the river water and the California Current at low salinities (S < 32) and a mixing between the California Current and the open ocean water at high salinities (S > 32). The TA-S

regression for the low-salinity data off the coast of Oregon (S < 32, Figure 4.8a) generates an intercept of 957 μmol kg^{-1} (R^2 = 0.89, n = 27), which agrees well with the TA concentration of the Columbia River (1000 μmol kg^{-1}) [Park, 1966, 1968; Park et al., 1970].

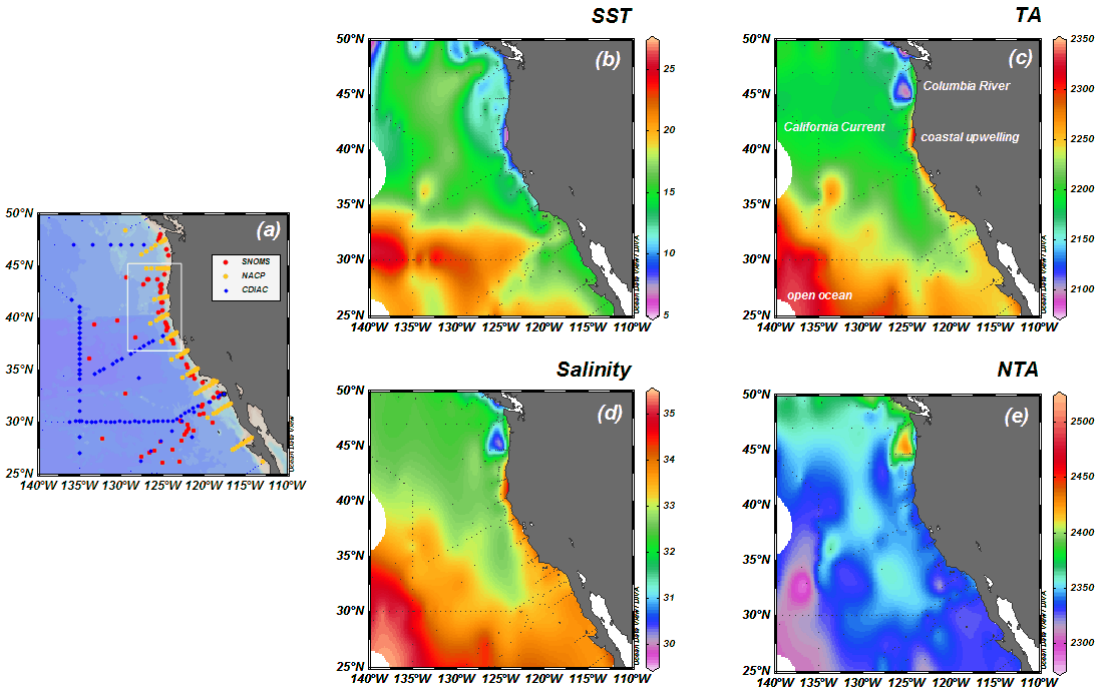

Figure 4.7 (a) The sampling positions of the SNOMS project in the western North Pacific margin, and the CDIAC measurements in the similar region including the NACP US west coast cruise 2007 [Feely and Sabine, 2011]; the sea surface distributions of (b) sea surface temperature (SST), (c) TA, (d) salinity and (e) salinity-normalized alkalinity (NTA). The low salinity water off Oregon is mainly from the Columbia River (panel d); the coastal upwelling off northern California is indicated by the low SST (panel b) and high salinity (panel d); the mid-salinity California Current is also shown. The NACP data in the white rectangle (panel a) were highlighted in the inset of Figure 4.8b. Figure produced by the Ocean Data View [Schlitzer, 2011].

The data measured in the eastern North Pacific margin generally fall above the SDC line (Figure 4.8a) with NTA higher than the NTA_{ocean} of the adjacent Pacific open ocean water (120-45°N, 155-130°W, S > 35, 2307 ± 5 μmol kg^{-1}, n = 69). The non-SDC TA additions from the Columbia River and the California Current are clearly shown in the NTA distribution (Figure 4.7e) and the NTA-S relationship (Figure

4.8b). Moreover, coastal upwelling of 'corrective' water ($\Omega_{aragonite} < 1$) was observed off the northern California during the NACP US west coast cruise [Feely et al., 2008]. As this upwelled water was undersaturated with respect to aragonite, the potential occurrence of the dissolution of $CaCO_3$ may be an additional non-SDC source for the surface alkalinity. In order to examine the importance of this biogeochemical effect, the results of the four NACP transects covering the Columbia River plume and the coastal upwelling (see the rectangle in Figure 4.7a) were highlighted in the inset of Figure 4.8b. It is shown that only a small increase in NTA was observed in the low-SST and high-salinity upwelled water, and the upwelling-induced increase in NTA is much lower than that resulting from river and current (Figure 4.8b).

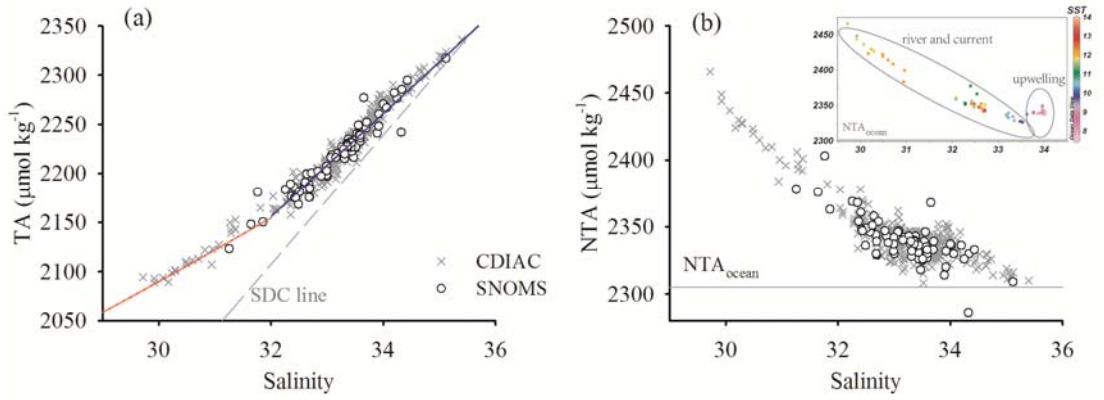

Figure 4.8 The (a) TA-S and (b) salinity-normalized alkalinity (NTA)-S relationships in the eastern North Pacific margin from the SNOMS and the CDIAC data. In panel (a), the dashed SDC line shows the TA-S changes due to the simple dilution or concentration effect on the North Pacific open ocean water; the segmented TA-S mixing a shared mid salinity end member at salinity ~32. In panel (b), the reference line shows the NTA_{ocean} of the North Pacific open ocean water. The NACP measurements covering the river plume and coastal upwelling (within the white rectangle in Figure 4.7a) are highlighted in the inset of panel (b).

4.4.4 Inland Seas

The Mediterranean Sea and the Red Sea are adjacent semi-enclosed inland seas both located in arid regions with high evaporation and little precipitation. One notable feature for the two inland seas is that their TA-S variations are more significantly

affected by evaporation than freshwater addition. As shown in Figure 4.9a and Table 4.2, the two inland seas are both characterized by very high salinity and TA. Despite the similar variation in the range of salinity (36.4 to 40.2, Figure 4.9a), the concentrations of TA in the Mediterranean Sea (2420 to 2647 μmol kg^{-1}) are much higher than those in the Red Sea (2373 to 2488 μmol kg^{-1}). The TA-S relationships in the two seas deviate from the SDC line in different directions (Figure 4.9a) and the NTA clearly suggests different non-SDC processes (Figure 4.9b): one adding TA to the Mediterranean Sea ($NTA > NTA_{ocean}$), and the other removing TA from the Red Sea ($NTA < NTA_{ocean}$).

Mediterranean Sea: The Mediterranean Sea is characterized by an anti-estuarine thermohaline circulation resulting from a negative freshwater balance [Lascaratos et al., 1999]. The surface water in the Mediterranean Sea is from the inflowing Atlantic water through the Strait of Gibraltar [Lascaratos et al., 1999]. The Atlantic water adjacent to the Strait of Gibraltar was thus used as the ocean end member (NTA_{ocean} = 2290 ± 4 μmol kg^{-1}, n = 49). In the Mediterranean Sea, salinity and TA increase eastwards away from the Atlantic inflow due to evaporation (Figure 4.9a, c). The NTA also increases with longitude (Figure 4.9c) and the high NTA ($NTA > NTA_{ocean}$) suggests additional TA sources due to non-SDC processes. This can be explained by the alkalinity inputs from the local rivers: the Rhone, Po, Nile, Ebro, Tiber and Adige (S = 0, discharge-weighted TA = 2820 μmol kg^{-1}) and from the Black Sea and Sea of Marmara (S = 29.3, TA = 2909 μmol kg^{-1}) [Schneider et al., 2007]. Although the coral reefs in the Mediterranean Sea [Aguilar, 2007] may result in calcification-induced decreases in TA, this TA sink (0.4×10^{12} mol yr^{-1}) [Copin-Montégut, 1993] is much smaller than the TA influx from rivers and the Black Sea (2.7×10^{12} mol yr^{-1}) [Schneider et al., 2007].

The TA and salinity in the Mediterranean Sea show a good correlation (TA = 79.84 * S – 510, R^2 = 0.97, n = 92, Figure 4.9a), but the negative intercept does not represent the local riverine input. Negative TA_{S0} was also observed at the Dyfamed site in the northwest Mediterranean Sea by Copin-Montégut and Bégovic [2002] (-1038 μmol kg^{-1}), and at a west-east transect in the Mediterranean Sea by Schneider et al. [2007] (-682 μmol kg^{-1}). This phenomenon is caused by the exceptional Mediterranean environment: the non-SDC alkalinity additions from the local rivers and the Black

Sea mainly occur in the eastern Mediterranean where salinity is higher than the S_{ocean} (strong evaporation effect). As demonstrated in Figure 4.2c, the non-SDC addition of TA at high salinity end ($S > S_{ocean}$) results in a steeper TA-S slope than the SDC line and a negative intercept.

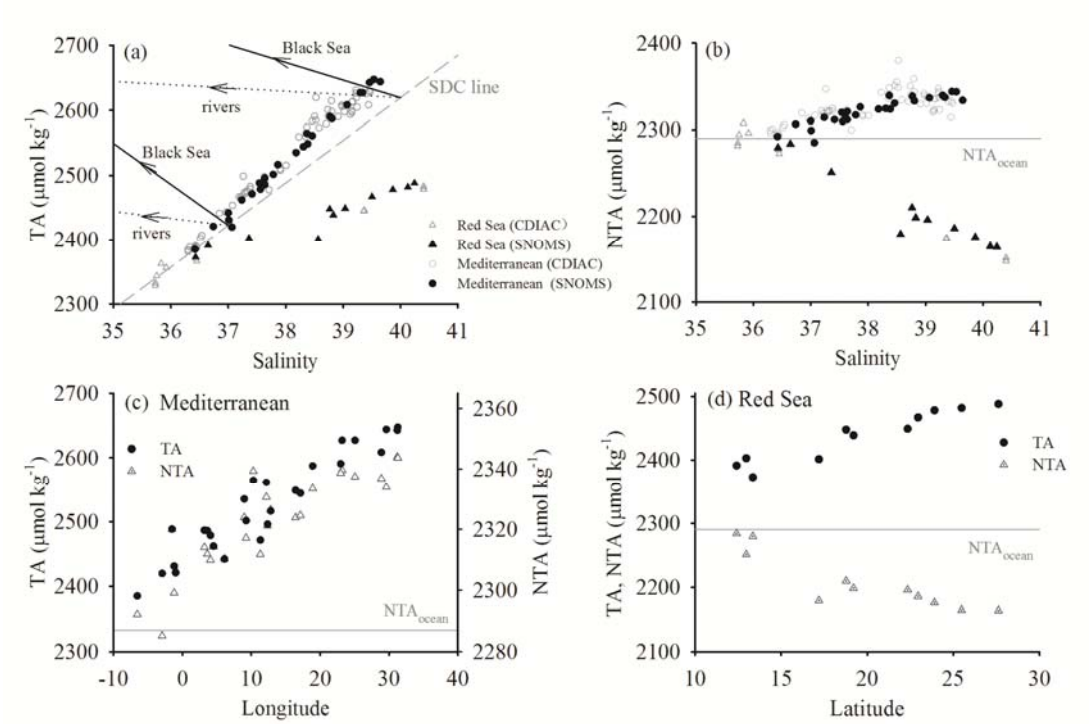

Figure 4.9 The (a) TA-S and (b) salinity-normalized alkalinity (NTA)-S relationships in the Mediterranean Sea and the Red Sea from the SNOMS and CDIAC data; the distributions of TA and NTA along (c) longitude in the Mediterranean Sea and (d) latitude in the Red Sea. In panel (a), the dashed line shows the TA-S change due to the simple dilution or concentration effect on the mean open ocean water, and the arrow lines demonstrate TA-S variations in the Mediterranean Sea caused by mixing with alkaline waters from the local rivers and the Black Sea. In panel (b), (c) and (d), the reference lines show the NTA_{ocean} of the inflowing waters from the North Atlantic into the Mediterranean Sea and from the Arabian Sea into the Red Sea respectively.

Red Sea: The Red Sea lies between the Mediterranean Sea and the Indian Ocean. It is a deep trench resulting from the separation of the Arabian plate from the African plate [Bosworth et al., 2005]. The water circulation pattern in the Red Sea is similar to that in the Mediterranean Sea. The major source of the surface water in the Red

Sea is the inflowing water from the Arabian Sea through the Gulf of Aden (NTA_{ocean} = 2289 ± 9 μmol kg^{-1}, n = 22). Due to the evaporation during the northward advection of the surface water, the salinity and TA in the northern Red Sea are higher than those in the southern part (Figure 4.9d). In contrast, NTA decreases northwardly to concentrations lower than NTA_{ocean} (Figure 4.9d) indicating a non-SDC alkalinity removal in the Red Sea.

The Red Sea is a simpler system for examining the alkalinity cycling because there are no major rivers entering it. Therefore, the non-SDC alkalinity removal is attributed to biogeochemical processes. Coral reefs are widely distributed in the Red Sea, and the coral diversity is considered amongst the highest in the India Ocean region [PERSGA, 2000, 2010]. The surface water in the Red Sea is oversaturated with respect to $CaCO_3$ ($\Omega_{aragonite}$ = 4.08 ± 0.26, n = 22) which may promote the biological formation of calcareous shells and skeletons. Ellis and Milliman [1985] suggested that the suspended $CaCO_3$ particles in the Red Sea are either biogenic or detrital rather than formed by inorganic precipitation. Production of $CaCO_3$ would decrease the concentrations of carbonate ion and TA in the water column [Wolf-Gladrow et al., 2007]. Because of the biogenic precipitation of $CaCO_3$ and sinking of surface water due to the high evaporation, the depth profiles of salinity specific alkalinity in the Red Sea showed lower values compared to those in the adjacent Gulf of Aden [Anderson and Dyrssen, 1994]. As undersaturation of $CaCO_3$ is never reached in the whole water column of the Red Sea [Elageed, 2010], the sedimentation and accumulation of $CaCO_3$ are favored and deep-sea carbonate sediments were found in the Red Sea [Al-Fukaha, 1994; Al-Rousan, 1998; Gevirtz and Friedman, 1966]. The Red Sea is estimated to be a sink of TA of 1.65×10^{12} mol yr^{-1} [Anderson and Dyrssen, 1994]. As discussed above, the loss of TA in the Red Sea should be mainly attributed to biogenic calcification and $CaCO_3$ sedimentation. Moreover, this non-SDC TA removal at high salinity end results in a positive intercept although there is no notable freshwater influx to the Red Sea.

4.5 Discussion

It has been shown that the surface TA in the world's major oceans can be estimated from salinity and SST with a reasonable accuracy [Lee et al., 2006]. When

combining TA with the existing pCO_2 observations, the whole carbonate system in the surface ocean can be characterized [Millero et al., 1998]. As the global fields of SST (http://www.ospo.noaa.gov/Products/ocean/sst.html) and salinity (http://aquarius.nasa.gov/) are now available from remote sensing, it is possible to use satellite data to improve studies of the global distribution and variability of TA, although the accuracy of such approach has yet to be established.

However, no global empirical algorithms can be developed for coastal regions due to the complex physical and biological interactions in these dynamic environments. For instance, under the influences of various rivers, different concentrations of TA can be observed at the same salinity in the western North Atlantic margin (Figure 4.6a). It is also difficult for the algorithms to account for the non-SDC biological changes in TA, particularly during the episodic blooms of phytoplankton or coccolithophores. Moreover, phytoplankton and bacterial cells [Kim et al., 2006] and chemically reactive particles [Sejr et al., 2011] could affect the TA measurement, while organic bases could contribute to alkalinity in biologically productive waters or waters with high organic loads [Cai et al., 1998; Hernandez-Ayon et al., 2007; Muller and Bleie, 2008]. These biochemical effects are usually minor in the open ocean but can be significant in the more biogeochemically active coastal waters. In coastal regions, the locally observed TA-S relationship is recommended to be used to estimate TA at salinity that is not directly measured. A typical example of this application is to use the intercept of TA-S regression to estimate the river water TA concentration. However, this study have demonstrated that TA_{S0} can either be positive or negative depending on the non-SDC changes in TA at different salinities (Figure 4.2, Table 4.1). As a result, river end member can only be reliably estimated from TA_{S0} when river input dominates as the mechanism controlling the TA-S relationship (e.g. in estuaries and river plumes).

Figure 4.2 and Table 4.1 assume a simple two-end member linear mixing. However, the mixing processes in the ocean often consists of more than two end members. Take the coastal systems with multiple river inputs and a shelf current as an example (Figure 4.10), this study discuss how mixing schemes with multiple end members would affect TA_{S0}. It should be noted that the discussion here focuses only on the physical aspect and doesn't take the biogeochemical effect into account (assuming

$\Delta TA_{bgc} = 0$ in Equation 4.2). In Figure 4.10a, for simplicity this work assume two river end members R_1 and R_2 ($TA_{R2} > TA_{R1}$); Z and O refer to the end members of the zero-alkalinity freshwater and the open ocean water respectively; and any straight line connecting two end members represents the mixing between the two water masses.

In most estuaries, salinity and TA changes due to the SDC processes can be safely ignored when compared to riverine inputs. As a result, the mixture (M in Figure 4.10a) falls within the range constrained by the triangle R_1R_2O while its position depends on the contributions of the different end members. If river R_1 is the more dominant contributor to the mixing (e.g. near the estuary of river R_1), the data will be closer to the line OR_1 and the TA-S regression will give an intercept closer to TA_{R1}. If R_1 and R_2 are well mixed before they mix with seawater (e.g. R_1 and R_2 are tributaries of a big river), the TA_{S0} at zero salinity will be a flow-weighted mean concentration of the two rivers. In Figure 4.10b and c, a shelf current end member (C) is added in addition to the integrated river end member (R). As shown by the observation in the eastern North Pacific margin (Figure 4.8a), the current-dominated type of mixing shows a segmented TA-S line with a shared shelf current end member at mid-salinity [Cai et al., 2010], i.e. the line RCO in Figure 4.10b and c. If the mixture (M) consist of waters from the three end members, M will fall in the triangle RCO (Figure 4.10). It is demonstrated that the difference between TA_{S0} and the river water concentration (TA_R) depends on the deviation of the current end member from the mixing line of the oceanic water and the river water (line OR in Figure 4.10b, c). If C is above the line OR, TA_{S0} would be higher than TA_R (Figure 4.10b), and vice versa (Figure 4.10c). In the western North Atlantic margin, the segmented TA-S mixing line observed by Cai et al. [2010] was not clearly seen in this study (Figure 4.6a). This is probably due to the lack of data points at low salinities. However, the reasonably good agreement between the values of TA_{S0} and the river TA concentrations (Figure 4.6a) suggests that the shelf current end member should not lie far from the river-oceanic water mixing line.

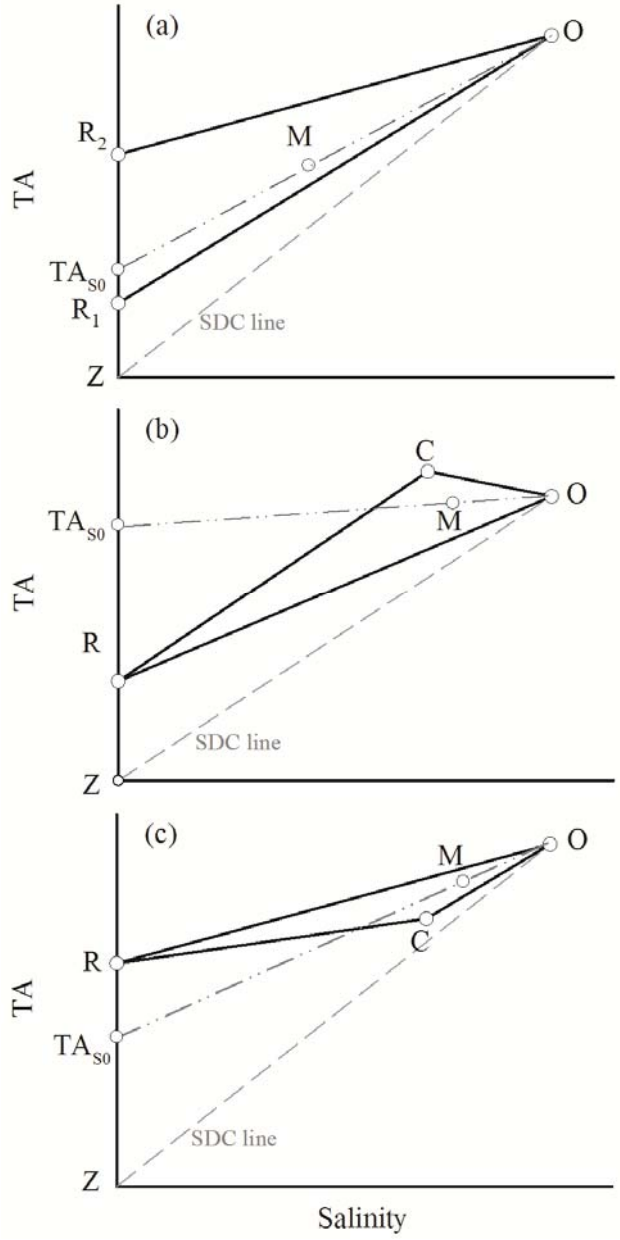

Figure 4.10 Schematic of the TA-S relationship in the coastal systems with (a) two river end members R_1 and R_2; (b, c) one river end member R and one shelf current end member C with different concentrations of TA. Adapted from Figure 12 by Cai et al. [2010]. The points Z and O refer to the end members of zero-alkalinity freshwater and oceanic water respectively. The dashed SDC lines show the TA-S changes due to the simple dilution or concentration effect on the oceanic water. It is assumed that the TA-S regression line goes through the oceanic end member and the mixing product (M) generating an intercept at TA_{S0}. See the text for detail.

4.6 Conclusions

The SNOMS project provided surface measurements across a large and diverse range of (sub)tropical marine environments. This large dataset was used to analyse the variability of TA, the TA-S relationship, and NTA in response to SDC and non-SDC processes (as summarized in Table 4.1). In the low and mid latitude open ocean waters of the Atlantic, Pacific (excluding the equatorial upwelling) and Indian Oceans, the TA variability is mostly controlled by the SDC effect of precipitation and evaporation. In ocean margins and inland seas, deviations of the TA-S relationship from the SDC line indicate the occurrences of non-SDC processes. Using NTA as an indicator, the non-SDC additions ($NTA > NTA_{ocean}$) and removal ($NTA < NTA_{ocean}$) of alkalinity can be identified. The non-SDC TA additions in the western North Atlantic margin and eastern North Pacific margin are caused by inflow of rivers and shelf currents, and the high NTA in the Mediterranean Sea is attributed to the alkalinity inputs from rivers and the Black Sea. Conversely, the low NTA in the Red Sea results from TA removal into newly formed (and subsequently exported) $CaCO_3$. These non-SDC changes in alkalinity generate either positive or negative TA_{S0} depending on the salinities at which they take place (Figure 4.2 and Table 4.1). In river-dominated marginal systems, the non-SDC TA addition at $S < S_{ocean}$ lead to positive values of TA_{S0} which are close to the TA concentrations of the local rivers. In contrast, the non-SDC TA addition in the Mediterranean Sea and the non-SDC TA removal in the Red Sea, both occurring at $S > S_{ocean}$, result in negative and positive TA_{S0} respectively.

The analyses of these diverse systems lead to several recommendations. When TA_{S0} is not zero, NTA shows a power function with salinity (Figure 4.2b, d). This is the reason why NTA is not a universally appropriate salinity normalization method, and why it is important that, where the outcome of regression is a non-zero TA_{S0}, that this be included in the normalization [Friis et al., 2003]. However, NTA was found to be a useful indicator of the activity of non-SDC processes (Figure 4.2 and Table 4.1). In coastal regions, this study suggests that estimating the river water TA concentration from TA_{S0} is likely to be successful only in river-dominated systems. In contrast, where there are large impacts from other physical (e.g. evaporation, shelf

currents, upwelling) and biological processes (e.g. calcification, uptake and release of nutrients), they act to decouple TA_{S0} from the river water concentration.

Chapter 5: Key controls on the seasonal and interannual variations of the carbonate system and air-sea CO_2 flux in the Northeast Atlantic (Bay of Biscay)

This chapter is adapted from a published paper: Jiang, Z.-P., D. J. Hydes, T. Tyrrell, S. E. Hartman, M. C. Hartman, C. Dumousseaud, X. A. Padin, I. Skjelvan, and C. González-Pola (2013), Key controls on the seasonal and interannual variations of the carbonate system and air-sea CO_2 flux in the Northeast Atlantic (Bay of Biscay), *Journal of Geophysical Research: Oceans*, *118*, 1-16.

5.1 Abstract

Biogeochemical variations of surface water in the Northeast Atlantic (Bay of Biscay) were examined using high-frequency underway measurements combined with monthly sampling of carbon-related variables. The mechanisms controlling seasonal CO_2 variability were investigated by distinguishing the contributions of biological and physical processes to the monthly changes in DIC and pCO_2. The seasonality of DIC (47-81 μmol kg^{-1}) had a single peak with a winter maximum primarily driven by vertical mixing and a summer minimum driven by spring biological removal. Non-Redfield C:N uptake was observed in the nutrient-depleted summer but not during the spring bloom. In the North Atlantic, pCO_2 seasonality shows a latitudinal transition: from the temperature-dominated oligotrophic subtropical gyre to the subpolar region where pCO_2 is dominated by changing concentrations of DIC. In the mid-latitude Bay of Biscay, the annual cycle of pCO_2 (61-75 μatm) showed a double-peak distribution. The summer pCO_2 peak was mainly driven by temperature increase, while the winter peak resulted from the dominant effect of entrainment of subsurface water. Interannual variations of DIC were more pronounced in winter and were driven by the changes in the strength of winter mixing. Higher wintertime concentrations and seasonal amplitudes of DIC were observed in cold years when the mixed-layer depths were deeper, which appears to be associated with negative phases of the North Atlantic Oscillation. The Bay of Biscay shows a decrease of CO_2 uptake in 2008-2010 (-0.97 and -0.75 mol m^{-2} yr^{-1}) compared to 2002-2004 (-1.47 and -1.68 mol m^{-2} yr^{-1}) .

5.2 Introduction

The ocean is an important sink taking up about a quarter of the anthropogenic CO_2 released each year [Le Quere et al., 2009; McKinley et al., 2011]. Oceanic carbon uptake slows the buildup of atmospheric CO_2 and mitigates human-driven climate change [Fung et al., 2005; Tyrrell, 2011]. Meanwhile, the CO_2 invasion is acidifying the ocean and could have deleterious impacts on marine ecosystems [Gattuso and Hansson, 2011; Orr et al., 2005]. There are large spatial and temporal variations in surface seawater biogeochemistry and air-sea CO_2 exchange across heterogeneous ocean regions (Chapter 1.4). Knowledge of this spatial and temporal variability is

critical in order to understand the current carbon cycle and to predict the future oceanic response to climate change.

The North Atlantic is one of the strongest ocean sinks for natural and anthropogenic atmospheric CO_2 [Sabine et al., 2004; Takahashi et al., 2009; Watson et al., 2009]. Much invaluable knowledge has been gained from the long-term measurements of carbon-related variables at marine time series stations in the North Atlantic, such as at BATS in the western North Atlantic subtropical gyre [Bates, 2001, 2007; Bates et al., 1996], at ESTOC in the eastern part of the North Atlantic subtropical gyre [González-Dávila et al., 2003, 2007a; Santana-Casiano et al., 2007], and at OWSM in the high latitude Norwegian Sea [Skjelvan et al., 2008]. In recent years, acquisition of surface ocean pCO_2 has been greatly expanded by the use of SOO equipped with underway measuring systems. Based on the observations obtained from time series stations and coordinated networks of SOO, several studies have tracked the changing CO_2 sink in the North Atlantic basin [Corbiere et al., 2007; Schuster et al., 2009; Watson et al., 2009]. These studies suggested substantial variations in the carbonate system and annual CO_2 fluxes on seasonal to decadal scales in the North Atlantic, and also showed that interannual variability tends to be influenced by changes in large-scale climatic patterns.

The Bay of Biscay is situated on the eastern side of the North Atlantic at mid-latitudes; it is bounded by the Azores current from the subtropical gyre and the North Atlantic current from the subpolar gyre [Lavín et al., 2006]. The water masses of the Bay of Biscay mostly originate from the North Atlantic, and it is an area of deep winter mixing due to strong vertical convection [Lavín et al., 2006; Pollard et al., 1996]. Using data obtained from SOOs, Padin et al. [2008] examined the variability of oceanic CO_2 concentrations and CO_2 flux in the Bay of Biscay during 2002-2004. Based on an empirical algorithm developed from in-situ observations, Padin et al. [2009] estimated the seawater pCO_2 from remotely sensed SST and chlorophyll-a (Chl-a). However, most SOO measurements were limited to pCO_2 and basic ancillary environmental parameters such as temperature and salinity. Tracking the mechanisms controlling the variability of pCO_2 and CO_2 flux was difficult because of the lack of information on other important biogeochemical variables.

To overcome this problem, monthly sampling of carbon-related variables in addition to high-frequency underway measurements were carried out since 2003 along the route of the *MV Pride of Bilbao* between Portsmouth and Bilbao (Chapter 2.3). This operation enabled some earlier studies of biogeochemical dynamics of surface waters on this route, particularly analyses of new production based on DO [Bargeron et al., 2006], variability of the carbonate system during 2005-2007 [Dumousseaud et al., 2010], and seasonal changes in the morphotypes of the coccolithophore *Emiliania huxleyi* [Smith et al., 2012].

In this chapter, the records of two full annual cycles (SOO observations coupled with satellite data and subsurface data from Argo floats, September 2008 to September 2010) provide more details on the seasonal variations of the carbonate system, nutrients, and air-sea CO_2 flux in the Bay of Biscay. The mechanisms controlling seasonal carbon variability were investigated by separating the contributions of biological and physical processes to the monthly changes in DIC and pCO_2. The data also allow us to follow the elemental stoichiometry of biological uptakes of carbon and nutrients to evaluate the existence of 'carbon overconsumption' [Sambrotto et al., 1993; Toggweiler, 1993] in the Northeast Atlantic. To look at regional differences in seasonal patterns in the carbonate system in the North Atlantic, the data from the Bay of Biscay were compared to the time series observation results at BATS ([Bates, 2001, 2007; Bates et al., 1996], http://bats.bios.edu/), ESTOC [González-Dávila et al., 2003, 2007; Santana-Casiano et al., 2007] and OWSM [Skjelvan et al., 2008]. Furthermore, trends in 2008-2010 were compared to those inferred from the 2005-2007 data along the same route [Dumousseaud et al., 2010] and the 2002-2004 data along an orthogonal route [Padin et al., 2008] (Figure 5.1). This extends the time series to cover the years from 2002 to 2010. The interannual variability was investigated focusing on the role of winter mixing and its link with the large-scale climate variability such as the North Atlantic Oscillation (NAO) and the Eastern Atlantic pattern (EA).

5.3 Materials and methods

5.3.1 Observations and measurements

The observational data in this study were obtained mainly from the *MV Pride of Bilbao* (Chapter 2.3 and 2.4). This study focus on the Bay of Biscay defined as latitudes 45-46.5 ºN along the ferry's route (Figure 5.1) where the riverine influence is relatively small Figure 5.2.

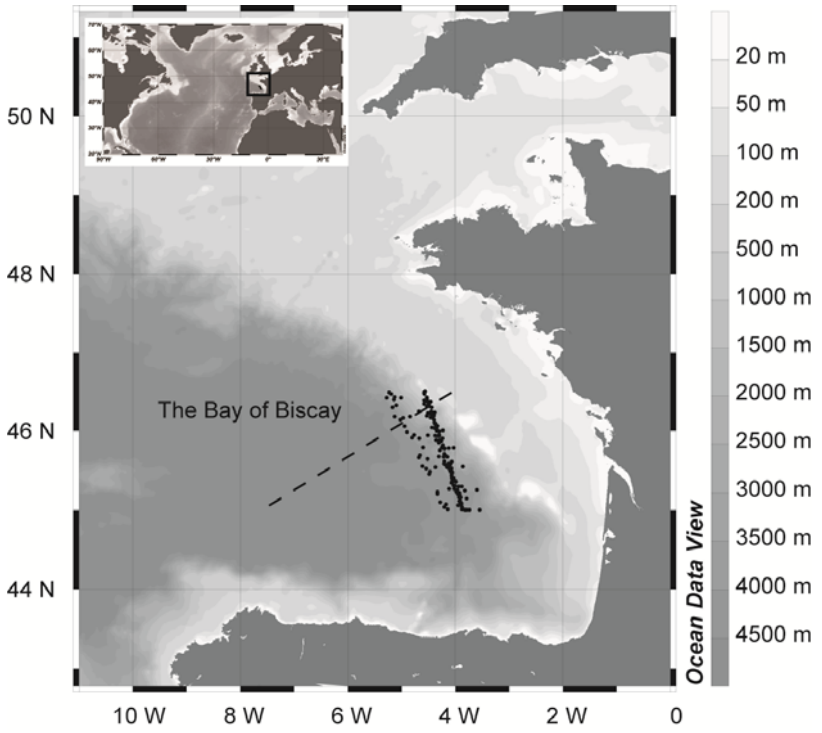

Figure 5.1 Map of the study region. The sampling positions of discrete samples in the Bay of Bay are shown as dots (latitude 45-46.5ºN along the route of *MV Pride of Bilbao*). The dashed line shows the route of underway CO_2 observations during 2002-2004 by Padin et al. [2008].

5.3.2 External data

A number of other data sources were used to develop the interpretation of the data from the *MV Pride of Bilbao*. Argo floats (http://www.coriolis.eu.org) provide temperature profiles in the Bay of Biscay for the estimation of the MLD following the fitting algorithm developed by González-Pola et al. [2007]. The monthly area-

averaged Chl-a data (45-46ºN, 5-3ºW) from the 4 km global products of MODIS-Aqua (Giovanni online data system by the NASA GES DISC, http://reason.gsfc.nasa.gov/Giovanni/) provide a consistent indication of the phytoplankton biomass in the surface layer of the study region against which to compare the fluorescence measurements made on the ship. The atmospheric CO_2 measurements were obtained at three land stations (Mace Head: 53.33ºN, 9.90ºW, Ile Grande: 48.80ºN, 3.58ºW, and Pic du Midi: 42.94ºN, 0.14ºE) adjacent to the study region from the World Data Centre for Greenhouse Gases (http://gaw.kishou.go.jp/wdcgg/wdcgg.html). The in-situ wind speed data came from the Gascogne Buoy moored in the Bay of Biscay (45.3ºN, 5ºW, UK's Met Office) and it was corrected to 10 m height assuming neutral stability [Hoffman, 2011]. The remotely measured wind speed data were collected from the QuikSCAT product provided by the Physical Oceanography Active Archive Center of the NASA Jet Propulsion Laboratory (http://poet.jpl.nasa.gov/). The 2002-2004 data in the Bay of Biscay were measured by Padin et al. [2008].

5.3.3 Calculations

Although the study region is potentially affected by riverine fresh water, Equation 1.13 was used to normalize DIC and TA because of the high uncertainties of the $X^{S=0}$ of the river end members and their changes in the estuary processes [Abril et al., 1999, 2003, 2004]. Suggested by the underway salinity measurements along the ship's route (Figure 5.2) and salinities of the discrete samples (Figure 5.3b), using of Equation 1.13 for salinity normalization is applicable during winter and spring when the riverine influence was minor. Although the signals of the riverine input were observed in summer months (Figure 5.2 and Figure 5.3b), the uncertainty associated with the normalization did not significantly affect the discussion as the changes in DIC and pCO_2 during this period were only discussed in a qualitative fashion (Chapter 5.4).

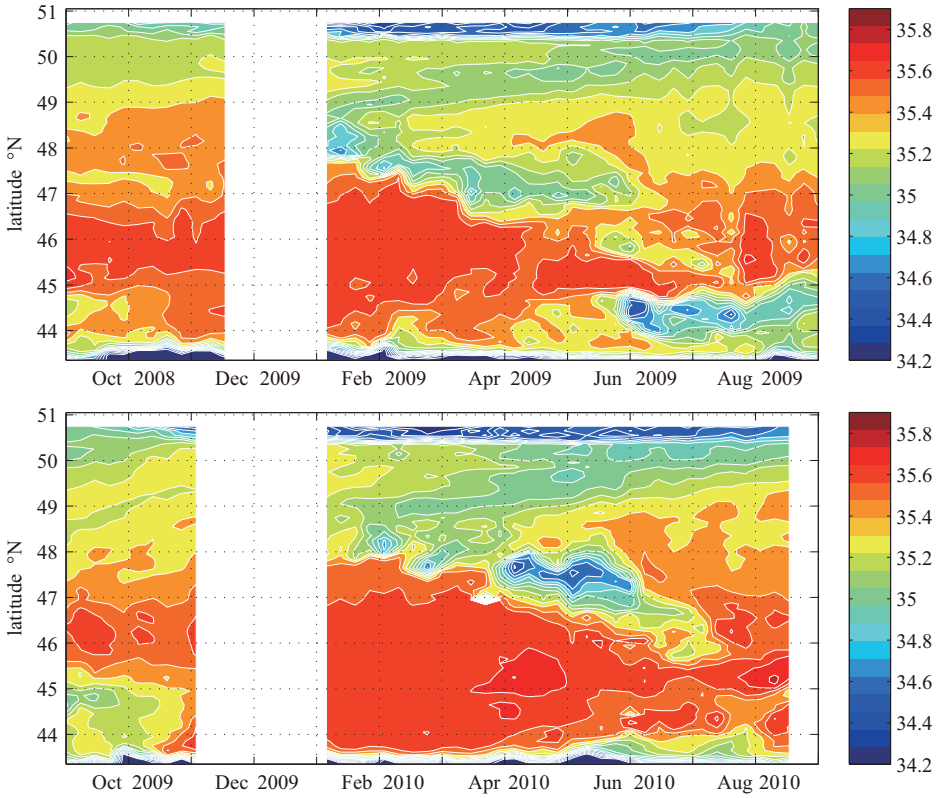

Figure 5.2 High resolution salinity measurements along the route of *MV Pride of Bilbao* during 2008-2010.

Carbonate chemistry calculation: concentrations of different components of the carbonate system were calculated using the program 'CO2SYS' from the measured DIC, TA, and ancillary data (Chapter 2.5).

DO anomaly: the DO anomaly (DO_{anom}) was calculated as the difference between the measured DO concentration (DO_{obs}) and the saturated value (DO_{sat}) [Benson and Krause, 1984]:

$$DO_{anom} = DO_{obs} - DO_{sat} \qquad (5.1)$$

Air–sea flux: the air–sea flux of CO_2 (F_{CO2}) and O_2 (F_{O2}) were calculated as:

$$F_{CO2} = k_{(CO2)} * \alpha * \Delta pCO_{2,sea-air}, \quad F_{O2} = k_{(O2)} * DO_{anom} \qquad (5.2)$$

where α is the gas solubility of CO_2 as a function of seawater temperature and salinity [Weiss, 1974b], $\Delta pCO_{2,sea-air}$ is the partial pressure difference of CO_2 between the seawater (calculated from the measured DIC and TA using 'CO2SYS') and the atmosphere (measured by the adjacent land stations), and k is the gas transfer

velocity which can be calculated from Schmidt number of CO_2 or O_2 and wind speed [Wanninkhof, 1992]. The wind speed data were obtained from in-situ buoy measurement or remote sensing (QuikSCAT). In addition, three algorithms [McGillis et al., 2001; Nightingale et al., 2000; Sweeney et al., 2007a] were used for calculation and the results were compared to assess the uncertainty resulting from different parameterizations of the gas transfer velocity.

Contributions to the monthly DIC changes: the observed changes in the concentration of salinity-normalized DIC ($\Delta nDIC_{obs}$) in the mixed-layer can be attributed to three groups of physical and biogeochemical processes - gas exchange (ΔDIC_{gas}), biological production (ΔDIC_{BP}), and mixing processes (ΔDIC_{mix}):

$$\Delta nDIC_{obs} = \Delta DIC_{gas} + \Delta DIC_{BP} + \Delta DIC_{mix} \qquad (5.3)$$

Since ΔDIC_{gas} and ΔDIC_{BP} can be estimated from the measurements but ΔDIC_{mix} is difficult to estimate directly, ΔDIC_{mix} was calculated by difference as:

$$\Delta DIC_{mix} = \Delta nDIC_{obs} - \Delta DIC_{gas} - \Delta DIC_{BP}$$

$$= \Delta nDIC_{obs} - F_{CO2} / MLD - NCP_{MLD} / MLD \qquad (5.4)$$

where ΔDIC_{gas} is estimated from the air-sea CO_2 flux and MLD, and NCP_{MLD} is the MLD-integrated net community production (NCP). For the biological term ΔDIC_{BP}, this study only considered the effect of NCP but ignored the influence of calcification because of the relatively low coccolithophore abundance [Smith et al., 2012]. NCP_{MLD} can be estimated from the changes in the concentrations of nitrate plus nitrite (NO_x), DIC, or DO. The frequency of DO measurements (1-3 days at a given position) have better temporal resolution than those of NO_x and DIC (monthly) in this study. Therefore, NCP_{MLD} was calculated from the changes in the gas transfer-corrected DO_{anom} ($DO_{anom}^{GasCorr}$).

$$DO_{anom}^{GasCorr} = DO_{anom} + \Delta DO_{gas} = DO_{anom} + F_{O2} / MLD \qquad (5.5)$$

where the DO_{anom} is corrected for the effect of gas exchange (ΔDO_{gas}). Considering the relative quick equilibration time of oxygen, the monthly air-sea O_2 flux (F_{O2}) was calculated as the mean value of the 3-day fluxes. NCP_{MLD} was then estimated as:

$$NCP_{MLD} = (DO_{anom}{}^{GasCorr}{}_{m+1} - DO_{anom}{}^{GasCorr}{}_{m}) (MLD_{m+1} + MLD_{m}) / 2 * (C:O)_{NCP} \quad (5.6)$$

where $(DO_{anom}{}^{GasCorr}{}_{m+1} - DO_{anom}{}^{GasCorr}{}_{m})$ is the difference in $DO_{anom}{}^{GasCorr}$ between two consecutive months, $(MLD_{m+1} + MLD_{m}) / 2$ is the average MLD in those two months and the Redfield $(C:O)_{NCP}$ ratio of 106:138 was used to convert the changes in oxygen to those of carbon.

During the spring bloom, the effect of entrainment was insignificant (shoaling of MLD) and the riverine influence was also minor (Figure 5.2 and Figure 5.3b). Therefore, the estimates of NCP_{MLD} during spring were little affected by the mixing effects. During autumn and winter with a deepening MLD, Equation 5.6 underestimated the NCP_{MLD} since it did not account for the portion of production that balances the DO decrease induced by convection. However, this did not affect our ability to identify the major controlling factor of DIC variations (see the discussion below). In the stratified conditions from May to September/October, changes in concentrations of DIC are sensitive to small changes in biological or physical processes (including the riverine influence) acting on the small volume of water above the summer thermocline. Consequently, the biological and mixing effects in this period were not separated and their combined effect was presented instead (ΔDIC_{BP+mix} in Figure 5.6a).

Temperature effect on pCO_2: the thermally forced pCO_2 variation ($pCO_{2,Temp}$, Equation 1.18) was calculated under isochemical conditions (DIC and TA fixed at their mean values of 2093 and 2350 μmol kg^{-1} respectively) but with CO_2 solubility varying as a function of the measured temperature. Additionally, the temperature-normalized pCO_2 ($pCO_{2,NT}$, Equation 1.17) was calculated from the measured DIC and TA at the mean temperature (16.0°C).

Contributions to the monthly changes in pCO_2: seawater pCO_2 is mainly a function of temperature, DIC, TA, and salinity [Takahashi et al., 1993]. All the processes affecting DIC would result in corresponding changes in pCO_2, and pCO_2 is further modulated by the changes in TA and temperature. In a similar way to Equation 5.3, the monthly variability of the calculated pCO_2 was broken down into the contributions of different biological and physical processes.

$$\Delta pCO_2 = \Delta pCO_{2,(\Delta DICgas)} + \Delta pCO_{2,(\Delta DIC_{BP})} + \Delta pCO_{2,(\Delta DICmix)} + \Delta pCO_{2,(\Delta TAmix)} + \Delta pCO_{2,(\Delta Temp)} \quad (5.7)$$

where the subscripts of ΔpCO_2 correspond to the factors controlling variations in pCO_2 resulting from the changes in DIC (ΔDIC_{gas}, ΔDIC_{BP}, ΔDIC_{mix}), TA (ΔTA_{mix}) and temperature ($\Delta Temp$). ΔDIC_{gas}, ΔDIC_{BP} and ΔDIC_{mix} were estimated from the Equation 5.3. ΔTA_{mix} was calculated from changes in the observed TA which were corrected for the uptake or release of nutrients according to the nutrient-H^+-compensation principle [Wolf-Gladrow et al., 2007]. $\Delta Temp$ was calculated from the observed temperature changes.

Each term in Equation 5.8 was calculated on a monthly basis assuming that each process acted on the seawater carbonate system individually. The changes in DIC, TA, and temperature caused by each process were considered in turn while the other variables were held constant. The difference in pCO_2 between the original state and the modified conditions were then calculated. Uncertainties of the calculations of Equations 5.3 and 5.8 were estimated from the errors of measurements and as was their propagation through the calculations [Taylor, 1982].

5.4 Seasonal variations

The plots in Figure 5.3 show the seasonal cycles in the Bay of Biscay covering the two full annual cycles between September 2008 and September 2010.

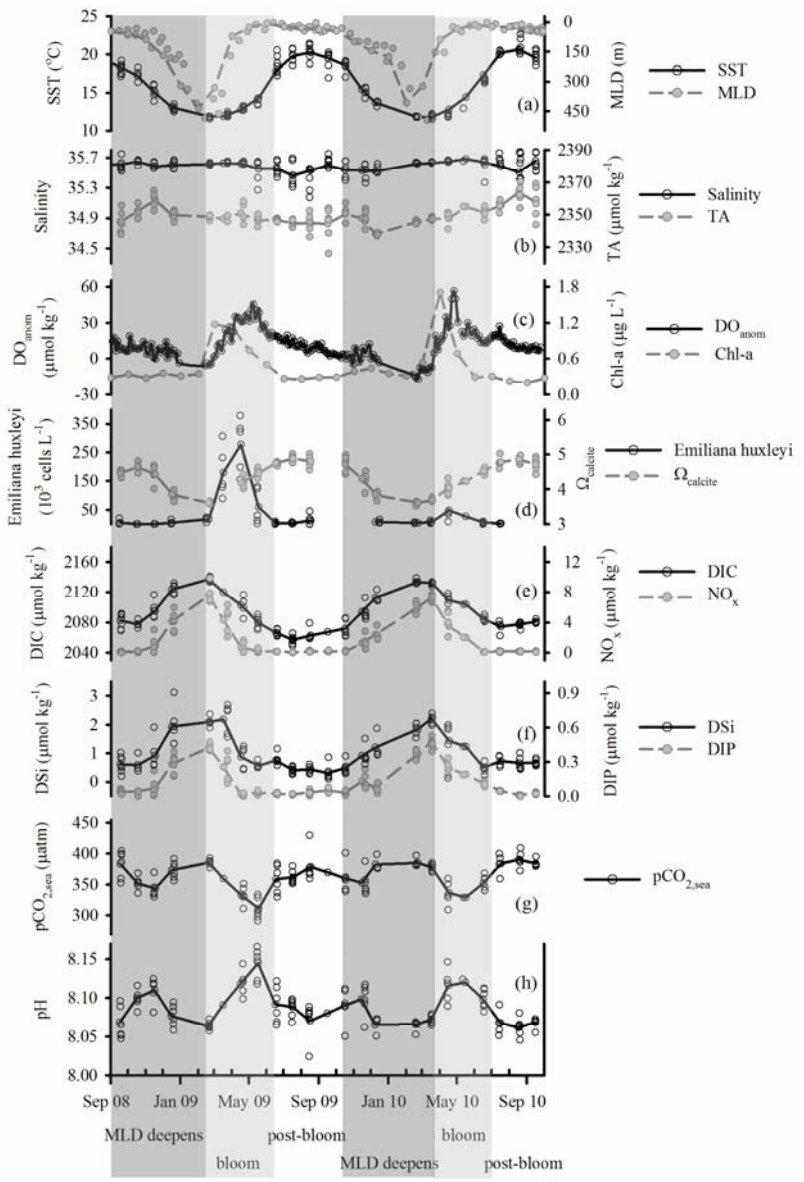

Figure 5.3 The biogeochemical variations of the surface water in the Bay of Biscay from September 2008 to September 2010: (a) sea surface temperature (SST) and mixed-layer depth (MLD); (b) salinity and TA; (c) DO_{anom} and remotely sensed Chl-a concentration; (d) DIC and NO_x; (e) *Emiliania huxleyi* cellular abundance and $\Omega_{calcite}$, (f) silicate (DSi) and phosphate (DIP); (g) pCO_2 calculated from DIC and TA; and (h) calculated in-situ pH in total scale. The monthly-averaged values were connected for a better visualization of the seasonal trend. The annual cycle was divided into three periods with different dominant controlling mechanism on DIC and pCO_2 variability (see the text for details).

5.4.1 Hydrography and environmental variables

The seasonal amplitudes of the monthly mean SST (Figure 5.3a) were 8.4 and 8.9°C in the two years, respectively. Winter minima in SST occurred in February 2009 (11.9°C) and March 2010 (11.8°C) and summer maxima occurred in August in both years (20.3 and 20.6°C). The seasonal evolution of MLD was coupled to the changes in SST (Figure 5.3a). The deepening of the MLD progressed from autumn along with decreasing SST and developed to 400 to 500 m in the coldest months. A transition from deep winter mixing to shallow stratification was observed in spring, and stable stratification (~20 m) developed in May and then remained throughout the summer. The monthly mean salinity ranged from 35.46 to 35.68 without an obvious seasonal trend, but most low salinities were observed during the post-bloom summer months (Figure 5.2 and Figure 5.3b). The low salinity surface water along this SOO route and its movement relating to the wind and current was discussed by Kelly-Gerreyn et al. [2006].

The remotely sensed Chl-a (Figure 5.3c) peaked during the spring blooms (up to 1.2 and 1.7 mg m^{-3} in 2009 and 2010 respectively) compared to the low concentrations in other seasons (~0.3 mg m^{-3}). Coccolithophore abundance showed a similar pattern to that of Chl-a (Figure 5.3c, d). The concentration of the dominant specie of coccolithophores (*Emiliana huxleyi*) peaked in April (2.77×10^5 and 0.46×10^5 cells L^{-1} in 2009 and 2010 respectively) but well below bloom levels (10^6 cells L^{-1}). Together with the increasing phytoplankton biomass, DO_{anom} increased during spring reaching 33.4 μmol kg^{-1} in May 2009 and 35.5 μmol kg^{-1} in April 2010. It then decreased towards winter to a slight undersaturation in February (Figure 5.3c).

5.4.2 Carbonate system and nutrients

The ranges of the monthly averaged TA were 15 and 26 μmol kg^{-1} in 2008/2009 and 2009/2010 respectively, but there was not a clear seasonal trend in TA variations (Figure 5.3b). Salinity normalization ($nTA_{35.6}$ in Figure 5.4b) did not explain the TA variations. The local calcification influence on TA was expected to be minor because of the low abundance of coccolithophores (Figure 5.3d). The small difference between $nTA_{35.6}$ and the potential TA ($pTA = nTA + NO_x$) in Figure 5.4b indicated

that uptake or release of nutrients during the organic production also did not have a significant influence on the TA variability. Therefore, mixing processes (i.e. riverine influence or advection of water mass with calcification signals) appear to be more important than the local biological processes affecting the TA concentration in the study region. The measured values of TA were generally higher than those predicted using a published algorithm for the north Atlantic open ocean based on SST and salinity (TA_{Lee} in Figure 5.4a) [Lee et al., 2006]. This suggests additional TA sources to the study region, which may be related to the high TA concentrations of the rivers Loire and Gironde and the addition of TA in the estuary [*Abril et al.*, 1999, 2003, 2004].

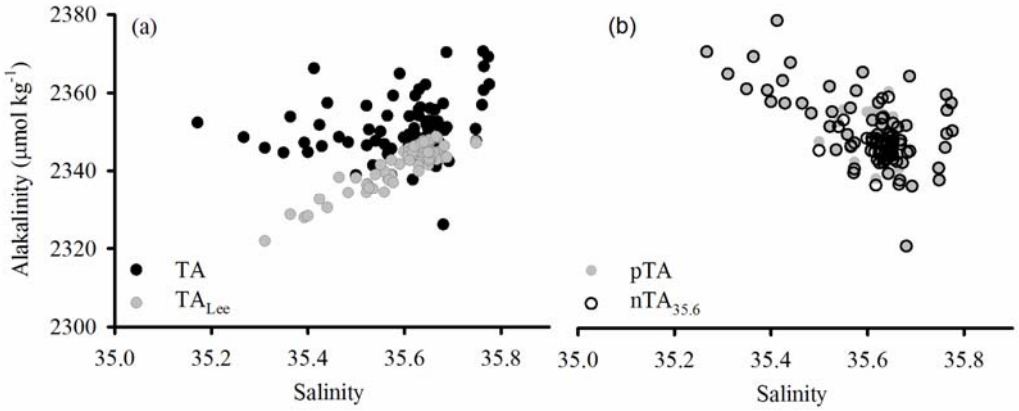

Figure 5.4 Alkalinity vs. salinity: (a) measured TA and TA_{Lee} predicted from SST and salinity using Lee et al. [2006]'s algorism; (b) TA normalized to the mean salinity of 35.6 ($nTA_{35.6}$) and potential TA ($pTA = TA + NO_x$).

In contrast, DIC showed a clear seasonality (Figure 5.3e) that varied inversely with SST and MLD (Figure 5.3a). The concentrations of DIC increased in autumn and winter, at a time when there was decreasing SST and deepening of the MLD. The annual maximum concentrations of DIC in February (2137 μmol kg^{-1} in 2009 and 2134 μmol kg^{-1} in 2010) were followed by decreases through spring to summer minima in July (2057 μmol kg^{-1} in 2009 and 2072 μmol kg^{-1} in 2010) (Figure 5.3e). Figure 5.3d presents the calculated saturation state of the calcite form of $CaCO_3$: $\Omega_{calcite} = [Ca^{2+}]\,[CO_3^{2-}]/K'_{sp(calcite)}$, where $[Ca^{2+}]$ and $[CO_3^{2-}]$ are the concentrations of Ca^{2+} and CO_3^{2-}, and $K'_{sp(calcite)}$ is the stoichiometric solubility product of calcite.

Higher values of Ω favor the formation of $CaCO_3$ shells and skeleton while values lower than 1 are corrosive to $CaCO_3$ [Feely et al., 2008]. The $\Omega_{calcite}$ was constantly above 1 in the study region, and its seasonal cycle was opposite to that of DIC with higher values in summer (~5.2) and lower values in winter (~3.6). The potential effects of these changes on coccolithophores have been considered in the associated study of Smith et al. [2012].

Similarly to DIC, concentrations of nutrients (Figure 5.3e, f) increased from autumn to maxima in late winter (7.6 and 7.3 μmol kg^{-1} for NO_x, 0.43 and 0.48 μmol kg^{-1} for dissolved phosphate, 2.20 and 2.22 μmol kg^{-1} for dissolved silicate in 2008/2009 and 2009/2010, respectively). During spring, nutrients showed parallel declines associated with DIC drawdown and corresponding increases in Chl-a and DO_{anom} (Figure 5.3). Concentrations of NO_x and DIP decreased to a depleted level at the onset of stratification and remained low throughout the summer (< 0.15 μmol kg^{-1} for NO_x and < 0.05 μmol kg^{-1} for DIP respectively), while the concentrations of DSi remained at ~0.5 μmol kg^{-1} in the summer (Figure 5.3e, f).

In contrast to the single annual peak in DIC, the calculated seawater pCO_2 was characterized by a double-peak annual cycle (Figure 5.3g). One peak in pCO_2 was observed in the late winter (386 and 385 μatm in February 2009 and 2010 respectively) together with the annual maxima of DIC and nutrients, while the second peak in summer (379 and 390 μatm in August 2009 and 2010 respectively) corresponded to the annual maximum SST. The corresponding two minima in pCO_2 were observed in early winter (343 and 352 μatm in November 2009 and 2010 respectively) and late spring (311 and 329 μatm in May 2009 and 2010 respectively). The calculated in-situ pH ranged from 8.02 to 8.17 showing a mirror image of the distribution of pCO_2 (Figure 5.3h).

5.4.3 Air-sea CO_2 flux

The air-sea CO_2 exchange is driven by the pCO_2 differences across the air-sea interface ($\Delta pCO_{2,sea\text{-}air}$ in Figure 5.5a). The atmospheric pCO_2 showed a seasonal variability of ~16 μatm in 2008-2010 (not shown), which is lower than that in the seawater (75 and 61 μatm, Figure 5.3g). Therefore, $\Delta pCO_{2,sea\text{-}air}$ were determined

more by the greater variations in the seawater $pCO_{2,sea}$. Figure 5.5a shows that surface seawater in the Bay of Biscay was undersaturated in pCO_2 in autumn (October to November) and spring (March to June) in both years. In contrast, pCO_2 in seawater was close to equilibrium with the atmosphere in winter (December to February) and became slightly supersaturated in CO_2 in summer (July to September). The second factor determining the rate of CO_2 exchange is wind speed [Wanninkhof, 1992]. Over the Bay of Biscay, winds tend to be governed by the Azores High and Iceland Low [Lavín et al., 2006]. The wind speeds measured at the Gascogne Buoy had similar patterns in both years (Figure 5.5b): higher in winter and weaker in spring and summer. The QuikSCAT wind speeds showed similar trends when compared to the buoy measurements and were ~0.5 m s^{-1} lower than the in-situ wind speed.

Due to the similarity of the patterns in variation of $\Delta pCO_{2,sea-air}$ and wind speed between years, the air-sea CO_2 flux seasonal patterns were also similar in 2008/2009 and 2009/2010 (Figure 5.5c). Two periods of greater oceanic CO_2 uptakes were observed: at the end of spring bloom and at the onset of winter turnover. The former period was mainly associated with more negative $\Delta pCO_{2,sea-air}$ and the other with high wind speed. The Bay of Biscay became neutral or turned into a weak CO_2 source to the atmosphere at the times of the two peaks in $\Delta pCO_{2,sea}$ towards the end of winter and in summer (Figure 5.5c).

The annual CO_2 flux was integrated from the monthly fluxes. The three algorithms of gas transfer calculation [McGillis et al., 2001; Nightingale et al., 2000; Sweeney et al., 2007a] and the two sets of wind speed data (in-situ buoy measurement and remotely QuikSCAT data) were used to estimate the uncertainty for the CO_2 flux estimation (Table 5.1). When the in-situ wind speed was used, the annual CO_2 fluxes calculated following the three algorithms were -1.05 ± 0.04 and -0.88 ± 0.06 mol m^{-2} yr^{-1} in 2008/2009 and 2009/2010, respectively. The annual fluxes estimated from the QuikSCAT data were -1.01 ± 0.03 mol m^{-2} yr^{-1} in 2008/2009 and -0.81 ± 0.05 mol m^{-2} yr^{-1} in 2009/2010 (gaps in the QuikSCAT record in 2009/2010 were filled by estimation based on the in-situ measurements and their correlation with QuikSCAT data during 2005 to 2009, $R^2 = 0.89$).

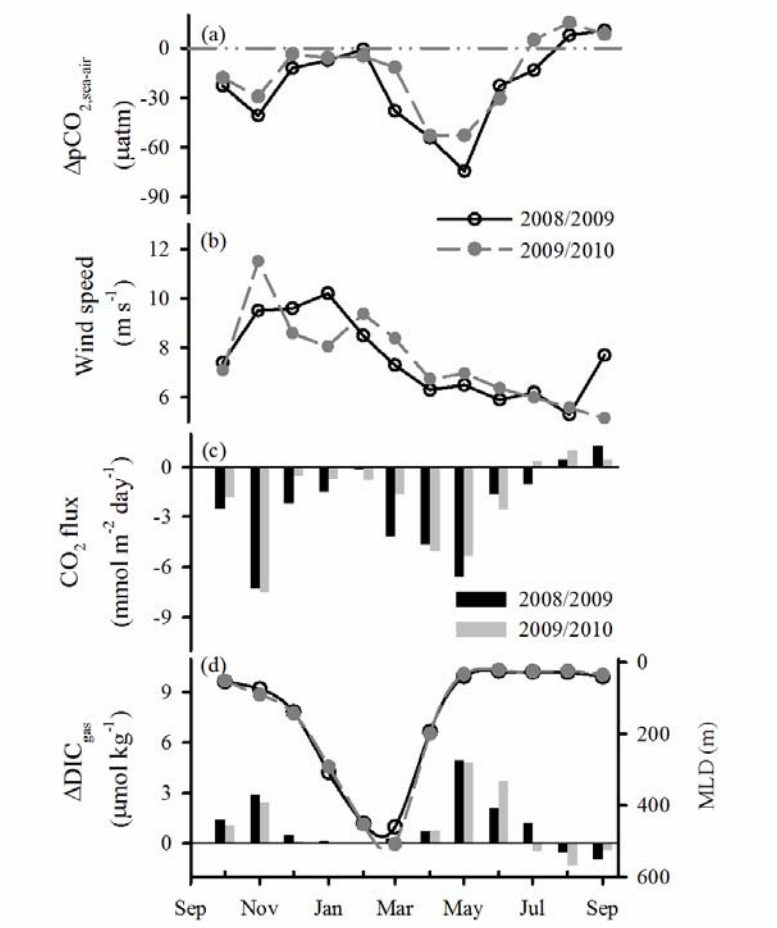

Figure 5.5 (a) pCO_2 difference between surface seawater and atmosphere ($\Delta pCO_{2,sea-air}$); (b) in-situ wind speed by buoy measurement; (c) air-sea CO_2 flux calculated using in-situ wind speed and parameterization following Nightingale et al. [2000] - the negative fluxes refer to the gas transfer from atmoshphere to sea; (d) MLD and gas exchange-induced changes in DIC (ΔDIC_{gas}).

Table 5.1 The annual CO_2 flux (mol m^{-2} yr^{-1}) calculated from different wind speeds and parameterizations of gas transfer velocity. The wind speed data were from QuikSCAT remote sensing and in-situ buoy measurements (no available data in 2002-2004). Three parameterizations of the gas transfer velocity were used: McGillis et al., [2001] (M01), Nightingale et al., [2000] (N00), Sweeney et al., [2007] (S07).

Wind speed Parameterization	**QuikSCAT**			**Buoy measurement**		
	N00	**M01**	**S07**	**N00**	**M01**	**S07**
2002/2003	-1.47	-1.60	-1.59			
2003/2004	-1.68	-1.80	-1.81			
2008/2009	-0.97	-1.02	-1.04	-1.01	-1.05	-1.08
2009/2010	-0.75	-0.85	-0.82	-0.82	-0.94	-0.89

Figure 5.5d shows the gas transfer-induced DIC changes and their relationship with the air-sea CO_2 flux and MLD. It suggests that gas exchange had little influence on changing concentrations of DIC between December and April as the CO_2 influx from gas exchange was diluted into a large volume of water as the mixed-layer was relatively deep. In contrast, CO_2 invasion from the atmosphere noticeably increased concentrations of DIC in the post-bloom period (May to July) and autumn (October and November). These were times of a high air-to-sea CO_2 flux entering a shallow mixed-layer.

5.5 Controlling mechanisms of the seasonal variations of DIC and pCO_2

To better examine the seasonal variability, the annual cycle is divided into three periods (Figure 5.3). This is similar to the division in 'pre-bloom, bloom, and post-bloom' periods made by Padin et al. [2008] but is here based on the evolution of MLD and concentrations of nutrients. The first period - 'MLD deepens', covers autumn and winter with the progressive deepening of the MLD (October to February/March). The second period - 'spring bloom', is from the month with the maximum nutrient concentrations to when nutrients were depleted (February/March to May). The third period - 'post-bloom', is summer with surface stratification from June to September. In Figure 5.6, monthly changes in DIC and pCO_2 were partitioned into the contribution from the individual biological and physical controlling factors using Equations 5.3 and 5.8.

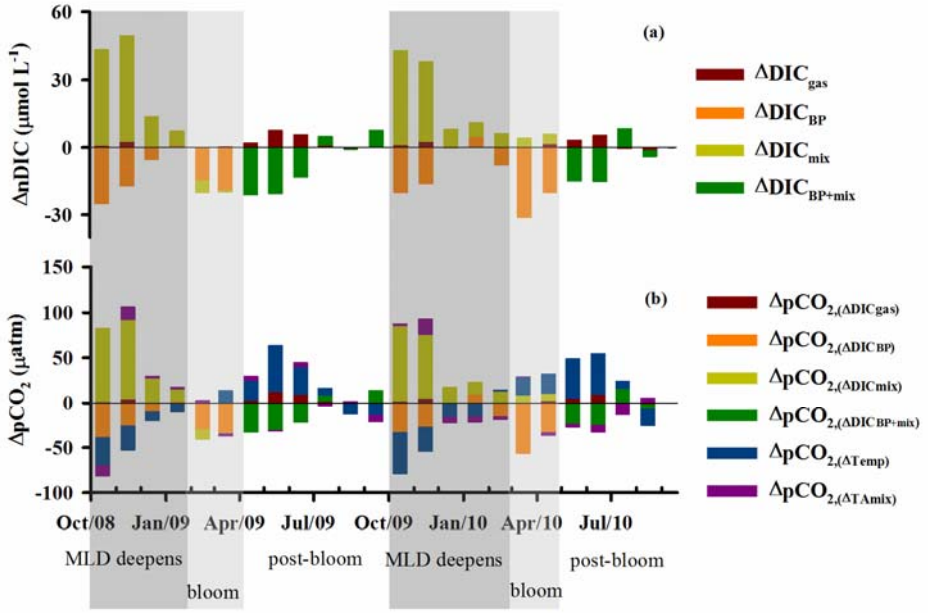

Figure 5.6 (a) Contributions to monthly changes in the salinity-normalized DIC (ΔDIC) from individual processes as indicated by the subscripts: gas exchange ('gas'), mixing ('mix'), biological production ('BP'). The biological and mixing influence were not separated during the stratified post-bloom period and their combined effect ('BP+mix') was shown. The corresponding changes in pCO_2 resulted from these changes in DIC were presented in panel (b) together with those resulted from the changes in temperature ($\Delta pCO_{2,(\Delta Temp)}$) and mixing-induced TA changes ($\Delta pCO_{2,(\Delta TAmix)}$). See the text for details.

5.5.1 Key controls on the seasonality of DIC

During the period of 'MLD deepens', concentrations of DIC showed an increasing trend along with the deepening of the MLD (Figure 5.3). As DIC increases with depth (Figure 5.7), the entrainment of deep water enriched in CO_2 elevated the concentration of DIC in the surface layer. As shown in Figure 5.6a, the net increases in DIC during this period mainly resulted from the effect of mixing processes (ΔDIC_{mix}) which overcame the influences of biological activities (ΔDIC_{BP}) and gas transfer (ΔDIC_{gas}). If a well-mixed state of the upper 420 m (the maximum MLD in the two winters) water column was assumed, the DIC concentration (2132 μmol kg^{-1}) calculated from the vertical profiles (measured in September 2005, Figure 5.7)

corresponded well with the observed winter peaks (2137 and 2134 μmol kg^{-1} in 2009 and 2010 in Figure 5.3e). Therefore, the convection-induced DIC increase was the major driver of the increasing DIC concentration in the 'MLD deepens' period.

During the 'spring bloom' period, concentrations of Chl-a increased significantly fueled by the nutrients supplied from the preceding winter mixing (Figure 5.3). The autotrophic biological production (ΔDIC_{BP} in Figure 5.6a) resulted in declines in DIC and nutrients (Figure 5.3e, f) accompanied by the production of DO (Figure 5.3c). Meanwhile, the mixing effect (ΔDIC_{mix} in Figure 5.6a) is small as the MLD is shoaling. Photosynthetic uptake was thus the dominant process resulting in the drawdown of DIC and nutrients in the productive 'spring bloom' period.

The mixed-layer during the 'post-bloom' period was characterized by depleted nutrients and strong stratification, and the concentration of DIC was unusually prone to change because of the shallow MLD. During this period, biological production was limited by nutrient scarcity; vertical mixing was suppressed by stratification; but the salinity data suggested the influence of river water(Figure 5.3b). DIC variability in the 'post-bloom' period was controlled by a combination of biological and physical effects without a single dominant controlling factor. Therefore, the effects of biological and mixing were not separated in this period and their combined effect was presented (ΔDIC_{BP+mix} in Figure 5.6a).

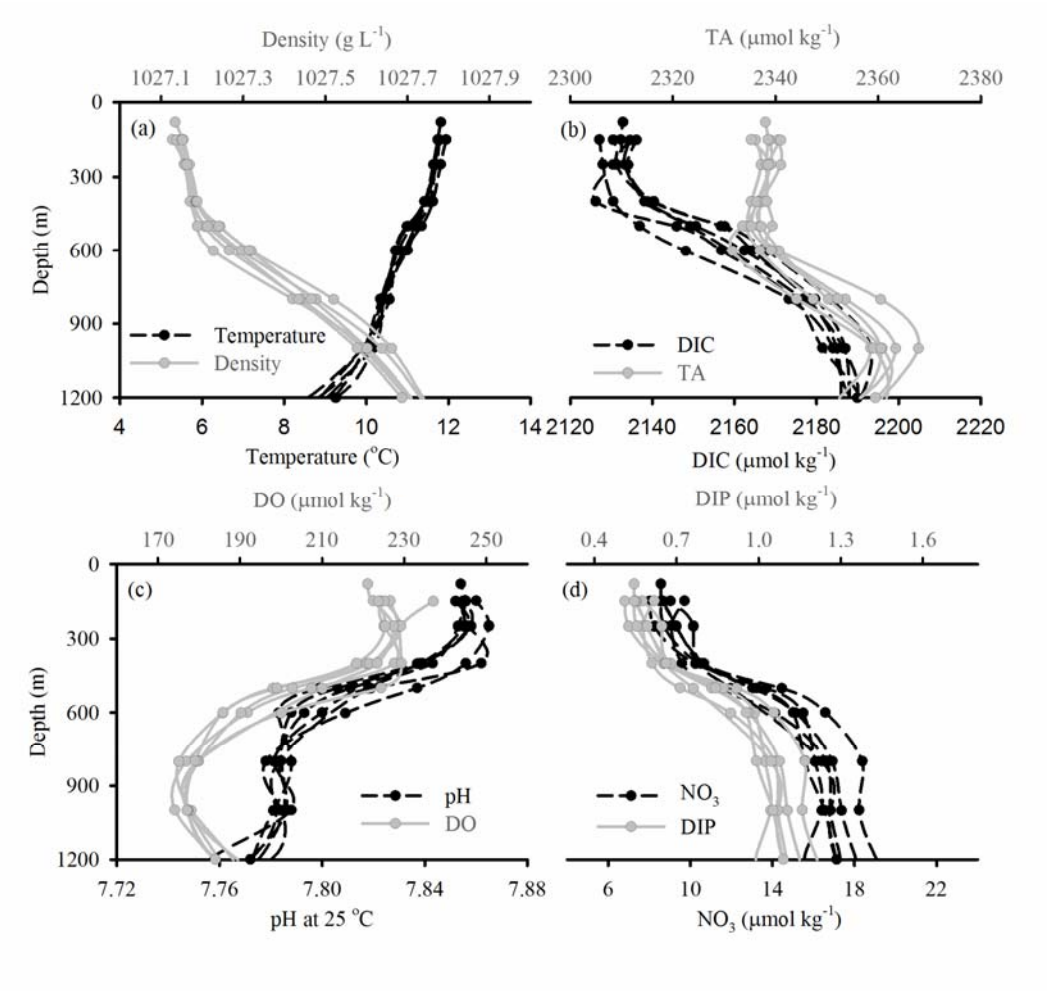

Figure 5.7 Vertical profiles of (a) temperature and density; (b) DIC and TA; (c) pH at 25°C and DO; (d) NO_3 and DIP in the Bay of Biscay in September 2005.

5.5.2 Key controls on the seasonality of pCO_2

The seasonal ranges in SST in the Bay of Biscay resulted in corresponding thermally-driven pCO_2 variations ($pCO_{2,Temp}$ in Figure 5.8a) of 126 and 136 μatm in 2008/2009 and 2009/2010 respectively. On the other hand, the temperature-normalized $pCO_{2,NT}$ (Figure 5.8a) reflects the influence of non-thermal processes (i.e. air-sea CO_2 transfer, biological activity, and mixing) on pCO_2 variability [Körtzinger et al., 2008]. $pCO_{2,NT}$ displays an annual cycle similar to the concentration changes in DIC (Figure 5.3e), and its seasonal amplitudes were 154 and 143 μatm in 2008/2009 and 2009/2010 respectively (Figure 5.8a). The opposite trend between $pCO_{2,Temp}$ and $pCO_{2,NT}$ (Figure 5.8a) suggests a competing effect of temperature and the non-thermal processes on the pCO_2 variability. Figure 5.8a also shows that

temperature was the dominant driver of changes in pCO_2 in summer ($pCO_{2,Temp} > pCO_{2,NT}$) while the non-thermal forcing of pCO_2 exceeded the temperature effect in other seasons ($pCO_{2,Temp} < pCO_{2,NT}$).

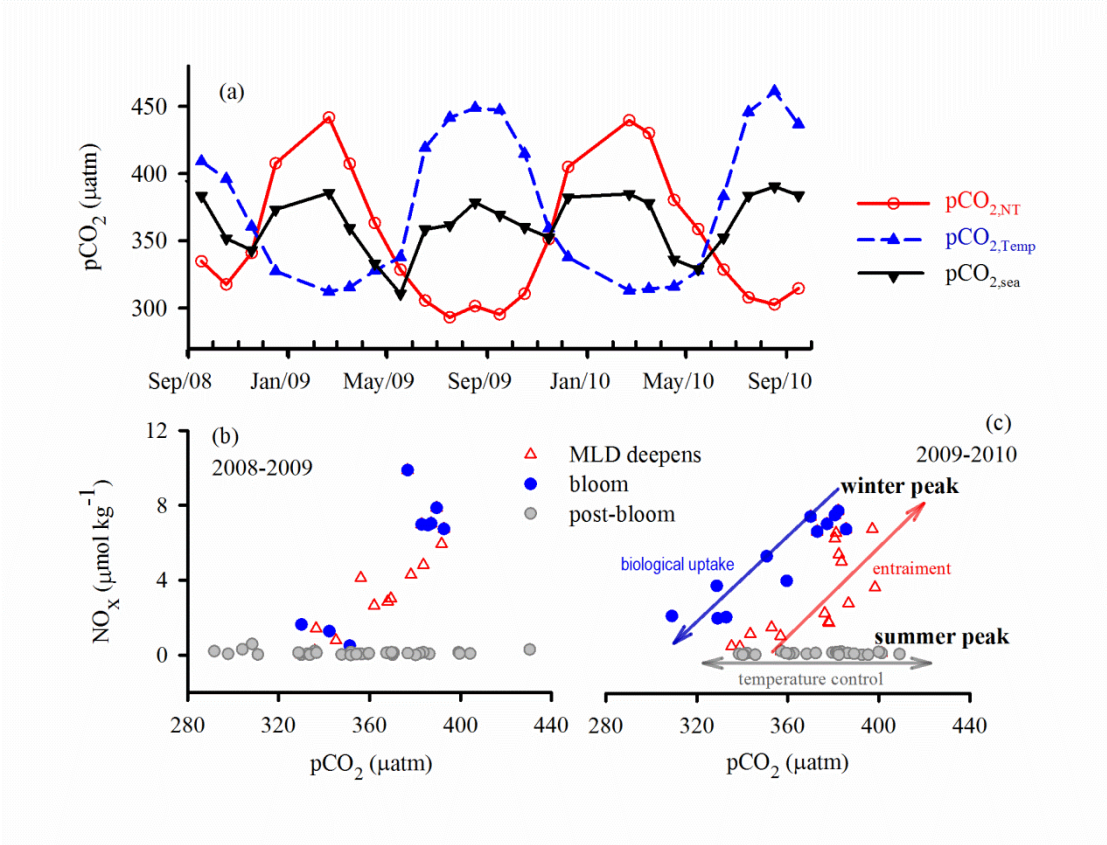

Figure 5.8 The monthly averaged seawater $pCO_{2,sea}$, temperature-normalized $pCO_{2,NT}$, and thermally-driven pCO_2 variations ($pCO_{2,Temp}$). The variations of NO_x and pCO_2 in (b) 2008-2009 and (c) 2009-2010; the major controls resulting in the summer and winter peaks in pCO_2 were showed in panel (c).

Considering the contributions of the various processes to the monthly changes in pCO_2 (Equation 5.8), the result shown in Figure 5.6b suggests that the influence of temperature ($\Delta pCO_{2,(\Delta Temp)}$), biological production ($\Delta pCO_{2,(\Delta DIC_{BP})}$), and mixing-induced changes in DIC ($\Delta pCO_{2,(\Delta DICmix)}$) were more important than gas transfer ($\Delta pCO_{2,(\Delta DICgas)}$) and mixing-induced changes in TA ($\Delta pCO_{2,(\Delta TAmix)}$) throughout the annual cycle. During the 'MLD deepens' period, $\Delta pCO_{2,(\Delta DIC\text{-}mix)}$ was the dominant driver of the pCO_2 increases (Figure 5.6b). The entrainment of the CO_2-rich subsurface water led to a net increase in pCO_2 overriding the pCO_2 decreases resulting from the seasonal cooling ($\Delta pCO_{2,(\Delta Temp)}$) and biological $\Delta pCO_{2,(\Delta DIC_{BP})}$.

During the 'spring bloom' period, pCO_2 drawdown was mostly explained by the photosynthetic uptake of $\Delta pCO_{2,BP}$ which exceeded the increasing tendency due to surface warming (Figure 5.6b). From autumn to spring, the major controlling factors on pCO_2 were the same as those acting on concentrations of DIC, therefore pCO_2 varied in phase with DIC during these periods (Figure 5.3e, g). However, the $\Delta pCO_{2,(\Delta Temp)}$ and CO_2 invasion ($\Delta pCO_{2,(\Delta DICgas)}$) exceeded the combined effects of biological production and mixing ($\Delta pCO_{2,(\Delta DICBP+mix)}$) during the stratified summer conditions (Figure 5.6b). The dominance of the temperature effect over other non-thermal processes resulted in the summer pCO_2 peak occurring at the same time as the highest SST.

The key controls on the double-peak distribution of the pCO_2 annual cycle were also shown by the relationship between pCO_2 and NO_x (Figure 5.8b, c). The peaks of pCO_2 and NO_x (as well as DIC) in late winter were mainly generated by convection-driven winter increases and biological-induced spring decreases. In contrast, low biological production during the stratified 'post-bloom' period results in temperature becoming the dominant control on the pCO_2 variations in summer.

5.6 C:N stoichiometry

The Redfield stoichiometry [Redfield et al., 1934] is a basic paradigm in ocean biogeochemistry relating the fluxes of carbon and nutrients through the production and remineralization cycle. Recent studies have suggested that the stoichiometry of NCP may differ from the Redfield ratio. 'Carbon overconsumption', i.e. the elevated consumption of carbon relative to the Redfield equivalent (C:N = 6.6) of nutrient uptake, has been reported for the surface ocean including the North Atlantic [Sambrotto et al., 1993; Toggweiler, 1993]. The C:N ratio of NCP, $(C: N)_{NCP}$, estimated from the mixed-layer regression of DIC and nitrate in the 1989 North Atlantic Bloom Experiment (NABE) was well above the Redfield value (up to 14.2 ± 0.2, Sambrotto et al. 1993). Along an Atlantic transect (30-60°N, 20°W) covering different trophic states with migrating spring bloom conditions, Körtzinger et al. [2001] reported an increasing $(C: N)_{NCP}$ from pre- or early bloom condition (5 to 6) to the post-bloom/oligotrophic system (10 to 16). At a single point, the $(C: N)_{NCP}$ estimated from observations of pCO_2 and nitrate on a mooring (49°N, 16.5°W) was

11.0 ± 0.7 [Körtzinger et al., 2008]. On a basin-integrated scale in the North Atlantic (40-65°N), the C:N ratio of new production estimated from climatological data (11.4 ± 1.4) also far exceeds the Redfield value [Koeve, 2006]. However, a re-analysis of the NABE data and the 20°W transect data [Koeve, 2004] suggested that the average seasonally integrated cumulative $(C: N)_{NCP}$ between winter mixing and the end of bloom is not significantly different from the Redfield ratio. *Koeve* [2004] also suggested that the elevated $(C: N)_{NCP}$ in the temperate and subarctic Northeast Atlantic was probably generated from carbon overconsumption in summer rather than during spring bloom.

The NABE data are only from observations over a 2 weeks period [Sambrotto et al., 1993], and extrapolation from spatial patterns along the 20°W transect to a model for seasonal progression [Körtzinger et al., 2001] is open to question. *Koeve* [2004] also pointed out that the estimations of $(C: N)_{NCP}$ critically depend on determination of the pre-formed winter DIC and nutrient concentrations. In this study, the wintertime concentrations of DIC and nutrients were directly observed and the subsequent changes in their concentrations month by month. This enables a reliable and direct evaluation of the progression of elemental stoichiometry of $(C: N: P)_{NCP}$.

To accurately estimate the $(C: N: P)_{NCP}$, the salinity-normalized DIC concentrations were corrected for the air-sea exchange ($nDIC^{GasCorr}$, Figure 5.9a, b) to account for the biasing effect of gas exchange. The effect of calcification was neglectable on the basis of the low coccolithophores abundance and the small TA variability as discussed above. The relative changes in $nDIC^{GasCorr}$, NO_x and DIP during the three periods are shown in Figure 5.9. The slopes estimated from linear regression during the spring bloom period reflect the time integrated uptake ratios of DIC and nutrients. The samples with NO_x concentrations lower than 0.5 μmol kg^{-1} were discarded in the regression to avoid the effect of nutrient limitation [Sambrotto et al., 1993].

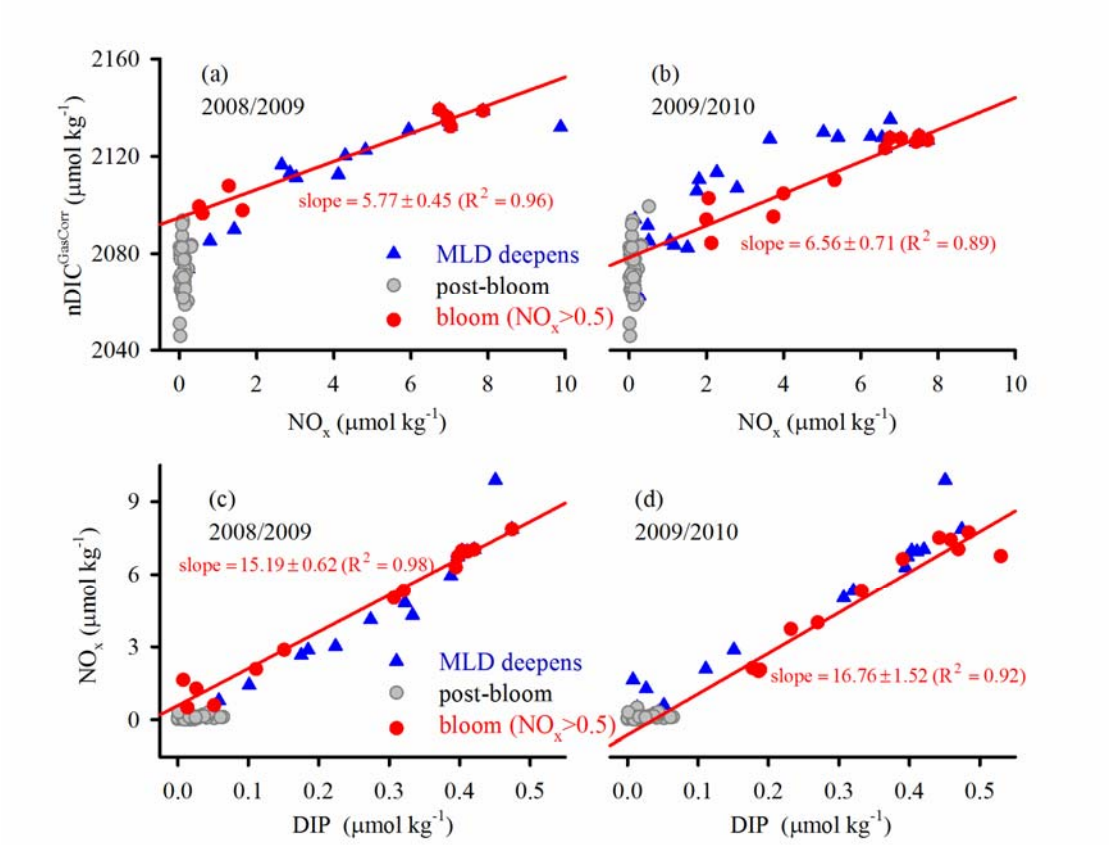

Figure 5.9 The concentrations of salinity-normalized DIC corrected for gas exchange ($nDIC^{GasCorr}$) and NO_x in different periods in year 2008-2009 (a) and 2009-2010 (b); the concentrations of NO_x and DIP in different periods in year 2008-2009 (c) and 2009-2010 (d). The regressions were based on data collected during the spring bloom period with NO_x concentration higher than 0.5 µmol kg^{-1}.

The ratios of $(C: N)_{NCP}$ were 5.77 ± 0.45 (R^2 = 0.96) and 6.56 ± 0.71 (R^2 = 0.89) in the two years (Figure 5.9a, b), respectively. These values didn't show 'carbon overconsumption' during the spring bloom when nutrients were not limiting. However, closer inspection shows that DIC continued to decrease after the end of bloom when NO_x was undetectable (Figs. 5.3 and 5.9a, b). So non-Redfield consumption of carbon versus nitrogen appear to be observed in the 'post-bloom' period with nutrient stress. This may possibly be attributed to the riverine influence, or preferential recycling of nutrients or the autotrophic pathway [Bozec et al., 2006; Koeve, 2006], or other potential nutrient inputs such as nitrogen fixation [Chou et al., 2006; Rees et al., 2009] and the short-lived transportation of nitrate from deep stocks [Johnson et al., 2010].

Our observations confirm *Koeve* [2004]'s suggestion that apparent overconsumption of carbon relative to nitrogen occurs after the spring bloom in the Northeast Atlantic. Moreover, $(C: N)_{NCP}$ ratio in this study would have been overestimated if it had been calculated simply based on DIC and NO_x at two timepoints which included the 'post-bloom' period. This demonstrates that care needs to be taken when using sparse data sets to infer discrepancies relative to the Refield ratio. Meanwhile, the $(N: P)_{NCP}$ in the two years (15.19 ± 0.62 and 16.76 ±1.52, Figure 5.9c, d) was not significantly different from the classic Redfield ratio value of 16, apparently contrary to the suggestions that 'bloom-formers' should have low N:P ratio (≤ 10) [Klausmeier et al., 2004; Quigg et al., 2003].

5.7 Comparison of the seasonal carbon variability in the North Atlantic

In Figure 5.10 and Table 5.2, the seasonal variations of SST, DIC, and pCO_2 in the Bay of Biscay are compared to other time-series observations in the North Atlantic from the subtropical gyre (BATS, ESTOC) and from the subpolar region (OWSM). The SST is lower at high latitudes and shows a similar seasonal pattern at all three locations in the North Atlantic (Figure 5.10a). In all areas, the seasonality of DIC is similarly characterized by winter-spring maxima associated primarily with entrainment of subsurface water and summer-autumn minima generated from biological uptake. The intensity of winter mixing is stronger in the higher latitude regions compared to the North Atlantic subtropical gyre. Accordingly, winter maxima in DIC and nutrients have higher values at OWSM and in the Bay of Biscay compared to those at BATS (Figure 5.10b). As a result of higher winter-preformed concentrations of DIC and stronger biological removal stimulated by the higher winter upward nutrient supply, the seasonal amplitudes of DIC at OWSM and in the Bay of Biscay were also higher than those at BATS (Figure 5.10b).

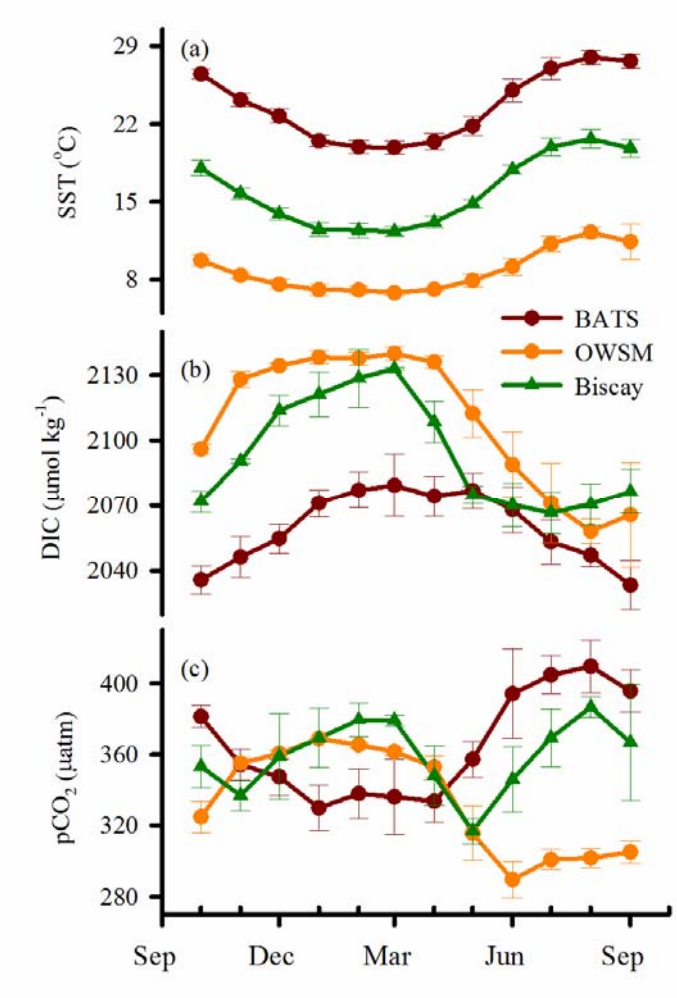

Figure 5.10 The seasonal variations of (a) SST, (b) DIC, and (c) pCO_2 in regions at different latitudes in the North Atlantic: BATS, OWSM, and Bay of Biscay. The available data during 2003-2010 are presented and the error bars show the standard deviations of the monthly averaged values in different years.

As shown in Figure 5.10c, the seasonal variation in pCO_2 has a different pattern at different latitudinal locations. In the oligotrophic subtropical gyre with low biological production rate (BATS and ESTOC), seawater pCO_2 is dominated by temperature with a single summer maximum and a single winter minimum [Bates et al., 1996; González-Dávila et al., 2003]. In contrast, in the high latitude North Atlantic it has generally been reported that changes in pCO_2 occur in parallel to those of DIC with a single-peak annual cycle which is opposite to that in the oligotrophic subtropical gyre [Körtzinger et al., 2008; Olsen et al., 2008; Takahashi et al., 1993].

The Bay of Biscay is located in the transition region between the northern seasonally stratified subpolar gyre and the southern permanently stratified subtropical gyre [McKinley et al., 2011]. The 'double-peak' annual cycle of pCO_2 in the Bay of Biscay displayed a seasonal evolution between the DIC-dominated variability and the temperature-dominated variability (Figure 5.10c). As discussed above, the pCO_2 variations in the Bay of Biscay followed the changes in DIC from autumn to spring, which was similar to that at OWSM. However, the winter upward supply of nutrients in the Bay of Biscay was lower than that at OWSM (Table 5.2), which resulted in an earlier nutrient depletion (started from May associated with surface stratification, Figure 5.3). During the post-bloom period, the nutrient-depleted and stratified condition in the Bay of Biscay was similar to that in the oligotrophic subtropical gyre. Therefore the pCO_2 variability displayed a temperature-dominated pattern in summer months similar to the BATS (Figure 5.10c).

Table 5.2 Comparison of the seasonal biogeochemical variations of the surface water in the North Atlantic

Region/Site	Type	SST (°C)	Salinity	TA (umol kg^{-1})	MLD[e] (m)	DIC (μmol kg^{-1})	NO_x (μmol kg^{-1})	pCO_2 (μatm)
ESTOC[a]	variation range	18 to 24	36.6 to 37.0	2399 to 2424	25 to 200	~2085 to ~2105	ND[f] to 1.5	~320 to ~400
29° 10' N, 15° 30' W	seasonal amplitude	4 to 6	0.4	25		20 to 30	1.5	60 to 70
BATS[b]	variation range	19 to 28	36.2 to 36.9	2365 to 2405	10 to 250	2010 to 2065	ND to detectable	310 to 410
31° 50' N, 64° 10' W	seasonal amplitude	7 to 10	0.6	20 to 30		40 to 50		90 to 100
Bay of Biscay[c]	variation range	11.8 to 21.5	35.5 to 35.7	2336 to 2364	20 to 500	2060 to 2135 (cold winter) 2060 to 2110 (warm winter)	ND to 7.9 (cold winter) ND to 3.9 (warm winter)	~320 to ~390
45-46.5°N, 4-6°W	seasonal amplitude	6.4 to 9.5	0.2	15 to 26		47 (warm winter) to 80 (cold winter)	3.9 (warm winter) to 7.9 (cold winter)	~50 to 75
OWSM[d]	variation range	6 to 14	34.8 to 35.2		20 to 300	~2040 to ~2140	ND to 12	~290 to ~370
66°N, 2 °W	seasonal amplitude	5 to 8	0.4			~80 to ~100	~12	~80

a) Gonzalez-Davila et al. [2003], Santana-Casiano et al. [2007]; b) Bates et al. [1996], Bates [2001; 2007]; c) Padin et al. [2008], Dumousseaud et al. [2010], and this study; d) Skjelvan et al. [2008]; e) MLDs in different studies may be estimated from various criteria; f) ND: not detectable.

5.8 Interannual variability of DIC, pCO_2, and air-sea CO_2 flux

The time series of carbon system observations in the Bay of Biscay can be extended back from 2010 to 2002 by including earlier observations [*Padin et al.*, 2008; *Dumousseaud et* The available comparable data from 2002 to 2010 are shown in Figure 5.11 and the key points are summarized in Table 5.3. The evolutions of SST, MLD, DIC, and nutrients in the Bay of Biscay showed similar seasonal trends in all years in 2002-2010 as described in Chapter 5.4. However, their seasonal amplitudes showed notable year-to-year variations which were mainly due to the differences in winter conditions (Figure 5.11 and Table 5.3). The winter minima in SST ranged from 11.8 to 13.1°C from 2002 to 2010. Higher winter SSTs were observed in the warmer winters of 2006/2007 and 2007/2008 when the surface air temperature was the warmest on record for 500 years [Luterbacher et al., 2007]. The SST anomalies were related to the changes in oceanic convection: a regression analysis of winter minima in SST and maxima in MLD results in a negative correlation ($R^2 = 0.72$). In the warmer-than-average years, shallower winter MLDs were developed and decreased winter mixing results in lower wintertime concentrations and seasonal amplitudes of DIC and nutrients (Figure 5.11, Table 5.3). Similar correlations between the winter anomalies of SST, MLD, and DIC have also been established in the North Atlantic subtropical gyre [Bates, 2007; González-Dávila et al., 2007a; Gruber et al., 2002]. In contrast, in the North Atlantic subpolar gyre the largest differences in DIC between years have tended to be observed during summer [Corbiere et al., 2007; Findlay et al., 2008; Skjelvan et al., 2008].

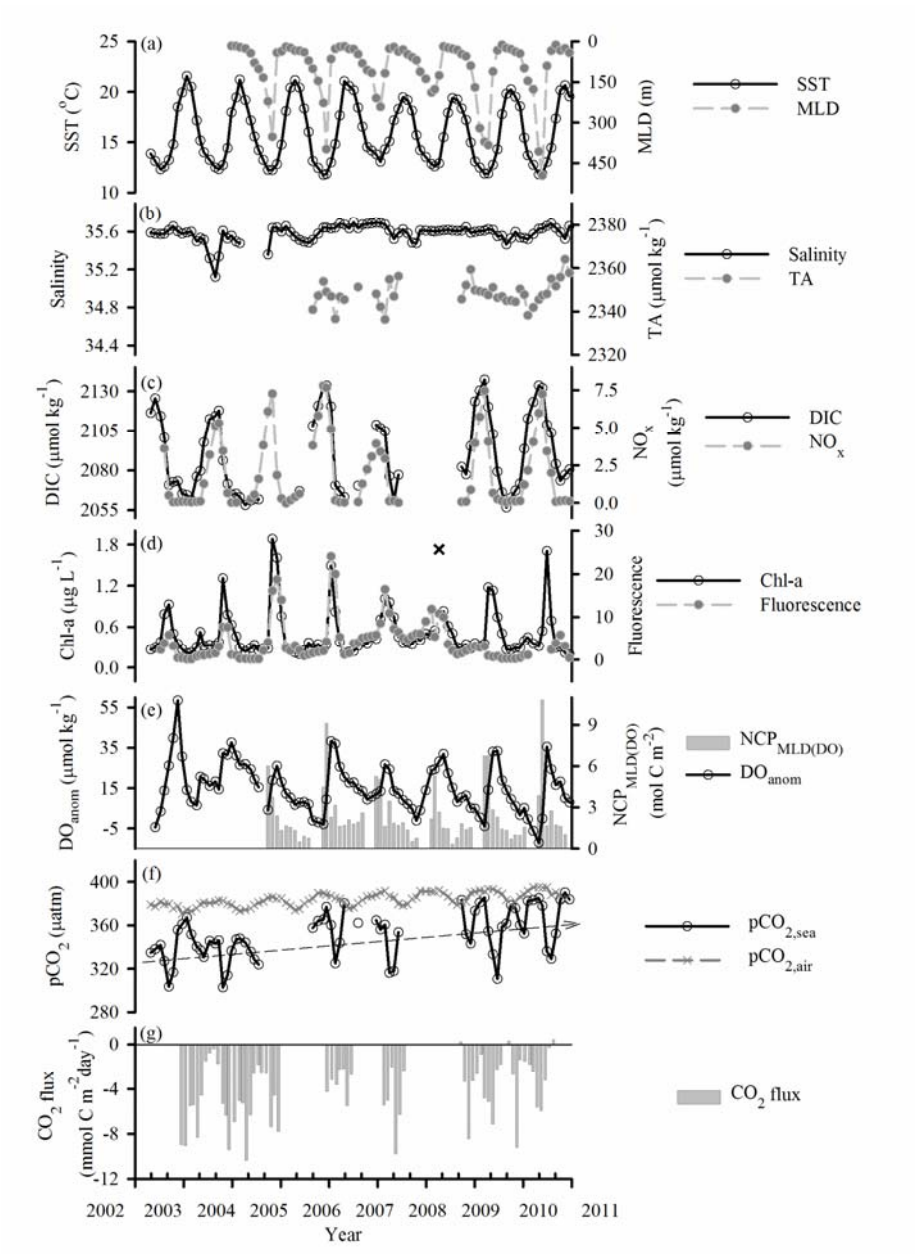

Figure 5.11 The interannual variability in the Bay of Biscay from 2003 to 2010: (a) SST and MLD; (b) salinity and TA; (c) DIC and NO_x; (d) remotely sensed Chl-a and underway fluorescence; (e) DO_{anom} and mixed-layer integrated net community production (NCP_{MLD}); (f) atmospheric $pCO_{2,air}$ and seawater $pCO_{2,sea}$; (g) air-sea CO_2 flux. Comparison between the remotely sensed Chl-a concentration and the underway fluorescence suggested an outliner in the remotely sensed Chl-a in spring 2008 which was highlighted as a cross in panel (d).

In the Bay of Biscay, seasonal patterns of pCO_2 in 2008-2010 and 2002-2004 were similar: with high values observed later in winter and summer (Figure 5.11f). The seasonal ranges in 2008-2010 (75 and 61 μatm) were also similar to those in 2002-2004 (72 μatm in both years). Compared to the simple correlation between variations of DIC and winter mixing, the interannual variability in seawater pCO_2 is more complicated due to the counteracting effects of temperature versus non-thermal processes. The net changes in pCO_2 depend on the balance of the opposing effects of changes in SST and DIC which may cancel each other out. For example, higher SST in a warmer winter will support a higher pCO_2, but the decreased concentrations of DIC will lead to a lower pCO_2.

An increase in annual averaged seawater $pCO_{2,sea}$ was found from 2002-2004 (340 and 335 μatm) to 2008-2010 (359 and 369 μatm). This rise of 20-30 μatm is considerably more rapid than the rate of increase in the atmosphere over the same time interval (~13 ppm estimated from measurements at land stations). In order to examine the changes in the annual air-sea CO_2 flux, an identical calculation method was applied to all the data sets obtained between 2002 and 2010 in the Bay of Biscay. The annual flux estimated using the QuikSCAT wind data and the *Nightingale et al.*, [2000] parameterization (Table 5.1) suggests that the capacity of CO_2 uptake of the Bay of Biscay has decreased from 2002-2004 (-1.47 and -1.68 mol m^{-2} yr^{-1}) to 2008-2010 (-0.97 and -0.75 mol m^{-2} yr^{-}). These results are similar to those obtained in several other studies which also found reduced rates of ocean CO_2 uptake in the North Atlantic in recent years [Corbiere et al., 2007; Schuster et al., 2009; Watson et al., 2009]. However, a study based on data from 1981 to 2009 [McKinley et al., 2011] suggests that trends in oceanic CO_2 concentration converge with atmospheric trends over the 29-year period, overcoming the influence of variability on decadal scale.

5.9 Interannual variability and its link with large-scale climate variations

Understanding of the link between local interannual variability and large-scale climate patterns is thought to be critical for improving our knowledge of both the controls on natural ocean biogeochemistry and the potential impact of future climate change [Bates, 2007; Corbiere et al., 2007]. The North Atlantic Oscillation (NAO) is

the dominant mode of the atmospheric pressure variation over the North Atlantic [Marshall et al., 2001; Visbeck et al., 2003]. In the western North Atlantic subtropical gyre, interannual variations of SST, MLD, DIC, and NCP appear to be correlated with the variability of NAO [Bates, 2001, 2007; Gruber et al., 2002]. *Gruber et al.* [2002] concluded that the carbon variability at BATS is largely driven by variations in winter SST and MLD linked to the NAO, and suggested that the entire North Atlantic may vary in a basin-wide coordinated pattern. However, studies at ESTOC suggested that the oceanic response in the eastern North Atlantic subtropical gyre is apparently delayed by 3 years relative to the shifts in the NAO and was instead more directly related to the East Atlantic pattern (EA) [*González-Dávila et al.*, 2003, 2007; *Santana-Casiano et al.*, 2007].

The NAO is most strongly expressed in the atmosphere in winter with a positive phase associated with positive SST anomalies and less vigorous winter mixing in the northern European marginal seas [Cayan, 1992; Cullen et al., 2001]. In the Bay of Biscay*, Padin et al.* [2008] suggested that the meteorological conditions during the formation of winter MLD have a significant influence on the biogeochemical behavior. Changes in MLD and hydrographic structure and their effect on the marine ecosystem and biogeochemistry in the southern Bay of Biscay have been related to the atmospheric forcing [Cabrillo et al., 2011; Somavilla et al., 2009]. A reconstruction of MLD variability in the southern Bay of Biscay over the past 60 years suggested that decadal variability in MLD seems to follow the NAO, while the negative phase of EA may result in intense episodes of cooling and deep mixing [Cabrillo et al., 2011; Somavilla et al., 2009].

Table 5.3 The interannual differences in the Bay of Biscay from 2003 to 2010 including the years 2006/2007 and 2007/2008 with exceptionally warm winters

Year	Winter condition						Annual amplitude			Spring Bloom (Feb. - May.)	
	mean NAO	mean EA	min SST (°C)	max MLD (m)	max NO_x (µmol kg^{-1})	max DIC (µmol kg^{-1})	SST (°C)	NO_x (µmol kg^{-1})	DIC (µmol kg^{-1})	integrated $NCP_{MLD(DO)}$ (mol C m^{-2})	integrated CO_2 flux (mol C m^{-2})
2003/2004	0.31	0.15	12.34		5.30		9.07	5.27			
2004/2005	0.21	-0.99	12.25	348	7.25		8.90	7.27		13.83	
2005/2006	-0.24	-0.88	11.76	423	7.76	2133	9.29	7.73	70	16.94	-0.31
2006/2007	0.63	1.10	13.06	230	3.93	2109	7.64	3.91	47	13.36	-0.71
2007/2008	0.51	0.04	12.61	177			6.77			11.20	
2008/2009	0.09	-0.59	11.89	437	7.45	2137	8.36	7.41	81	15.83	-0.48
2009/2010	-1.48	0.95	11.81	496	7.22	2134	8.86	7.13	62	14.40	-0.39

As shown in Table 5.3, this study examined the link between the wintertime indices of NAO and EA (averaged throughout December to March) and the biogeochemical variability in the Bay of Biscay. The interannual variability of winter mixing is likely to be more affected by the NAO: the winter maximum MLD shows a negative correlation with the winter mean NAO index ($R^2 = 0.77$, $p = 0.02$), but its correlation with winter mean EA index is not significant ($R^2 = 0.01$, $p = 0.84$). Positive wintertime NAO index tends to coincide with shallower winter MLDs in the Bay of Biscay. This is similar to that at BATS [Bates, 2001, 2007; Gruber et al., 2002], but is opposite to that in the subpolar gyre [Carton et al., 2008; Henson et al., 2009]. As shown in Table 5.2 and Figure 5.11, the warm winters and shallow winter MLDs corresponded to lower winter concentrations and seasonal amplitudes of DIC and NO_x, as well as reduced Chl-a concentrations and NCP_{MLD} in the following spring bloom. In contrast, higher seasonal ranges of DIC and NO_x were observed in cold years with deep winter mixing, which appear to be associated with the negative winter NAO indices.

It is predicted that shallower winter MLDs in the future, under global warming, would result in a consequent reduction in primary production and oceanic CO_2 uptake in low and mid-latitudinal oceans [Bopp et al., 2001; Sarmiento et al., 1998] as well as in the North Atlantic [Gruber et al., 2002]. However, the study in the Bay of Biscay has shown that a reduction in NCP associated with a shallow winter MLD does not necessarily result in a decrease in CO_2 uptake by the ocean. Following the reduced winter convection in 2006/2007, the NCP_{MLD} did indeed decrease during the bloom period, but the integrated CO_2 sink was nevertheless stronger than those in other years (Table 5.2). As discussed by *Dumousseaud et al.* [2010], this is mainly explained by a smaller amount of seasonal warming from winter to summer which resulted in a smaller pCO_2 rise, together with higher wind speeds which facilitated gas exchange.

5.10 Conclusions

In the mid-latitude Northeast Atlantic (Bay of Biscay), the seasonality of DIC is shaped by the winter increase due to deep convection followed by the spring biological drawdown. The stoichiometry of carbon and nutrient utilization did not show ‘carbon overconsumption’ during the bloom period when nutrients were not

limiting, but non-Redfield uptake was observed in the post-bloom summer with nutrient stress. Determined by the balance of the competing effect of temperature and non-thermal processes on pCO_2, the annual cycle of pCO_2 in the Bay of Biscay was characterized by a double-peak distribution. The temperature-dominated summer pCO_2 peak is similar to that in the North Atlantic subtropical gyre, while the winter pCO_2 peak following the DIC changes is similar to the observations in subpolar North Atlantic. Similar to results at BATS in the western North Atlantic subtropical gyre, the interannual DIC variations in the Bay of Biscay were mainly modulated by the changes in the strength of winter mixing. The seasonal amplitudes of DIC and NO_x were higher in years with cold winters and deep MLDs, apparently in response to the negative phases of the NAO. The Bay of Biscay was overall an atmospheric CO_2 sink because of greater CO_2 uptake in autumn and spring compared to the states of equilibrium or slight CO_2 oversaturation in winter and summer. An increase in annual mean seawater pCO_2 was observed from 2002-2004 to 2008-2010 (340 and 336 μatm to 359 and 369 μatm) associated with decreased rates of oceanic CO_2 uptake (-1.47 and -1.68 mol m^{-2} yr^{-1} to -0.97 and -0.75 mol m^{-2} yr^{-1}).

Chapter 6: Discussion and Implications

This chapter discusses the implications of the major findings of this PhD project, as well as the pending questions and the recommendations for future research.

The surface ocean plays an important role in the global carbon cycle, linking the atmosphere and the deep ocean as well as being a substantial reservoir in its own right. Through air-sea gas exchange, the carbonate system in the surface ocean has a significant impact on pCO_2 in the atmosphere (Chapter 1.3). The main aim of this PhD project has been to examine the variability and control of the surface ocean carbonate system (Chapter 1.7). In this study, the use of SOOs (Chapter 2) and an automatic pCO_2 sensor (Chapter 3) is promoted to enhance the surface ocean observing capacity in a cost-effective way. Based on the observations from two SOOs, this study investigated the spatial variability of TA and the TA-salinity relationships in different marine environments (Chapter 4), as well as the seasonal to interannual variations of DIC, pCO_2, air-sea CO_2 flux in the Northeast Atlantic (Chapter 5). The main findings have been summarized at the end of each chapter, and their implications for future studies are highlighted as follows.

6.1 Towards a better strategy for understanding the ocean carbon cycle

In addition to the SOO-based observation considered in this dissertation, there are various other methods to study the ocean carbon cycle, each of which has its advantages and shortcomings (Table 6.1).

Laboratory study: The high-precision measurements under stable laboratory conditions are able to provide the most accurate analysis results, and the well-controlled laboratory experiments can be designed to study specific processes by minimizing any irrelevant influences. However, it is difficult to reproduce the complex natural environmental settings in the laboratory, especially for large-scale phenomenon.

Scientific survey: Most of the historical observational data in the ocean came from dedicated oceanographic surveys carried out by research vessels. The traditional shipboard survey is capable of sampling the full water column and is suitable for detailed in-situ process studies. However, this kind of survey only provides a snapshot of the ocean and is too expensive to be operated with high frequency.

Time series observation: Time series stations are often carefully chosen to be representative of oceanic settings in different biogeochemical provinces of the world's ocean. Continuous records can be obtained from observations at stations repeatedly visited by cruise surveys or from in-situ measurements by automatic sensors at fixed positions. Time series observation is the most powerful approach to investigate the temporal evolution in a certain region. However, lots of resources are needed to maintain the repeated surveys, while the success of continuous in-situ measurements relies heavily on the application of mature sensor technologies.

Remote sensing: By measuring the characteristics of light or radiance that are emitted or reflected from the Earth's surface, remote sensing from aircraft or satellite provides large-scale observations of the ocean. Algorithms have been developed to use the remotely sensed satellite signals to derive various properties in the surface ocean. However, the resources needed for launching the satellites are huge, and the measurements from space are affected by cloud cover and the complex optical environment of coastal waters. In order to develop reliable satellite algorithms, in-situ observations are required to find consistent relationships between the radiances and the surface variable and then to test ('ground-truth') the resulting algorithms in different types of water.

Numerical modeling: Numerical modeling is a powerful tool for simulating the oceanic processes over various time and space scales. Conceptual models can be used to test hypotheses by comparing model predictions with observations, and established models can be used to extrapolate data to larger scales and to predict the future changes of the ocean. However, the development of a successful model needs to be based on a sound understanding of the controlling processes of the system. Moreover, observational data are required to force most models and to validate their results.

In order to achieve a better strategy for observing and understanding the ocean carbon cycle, the strengths of individual research methods should be integrated. Laboratory experiments and field expeditions should be carried out to investigate the mechanisms regulating the carbon dynamics on molecular to regional levels. In addition to research surveys, the time resolution and spatial coverage of in-situ observations can be improved by the use of automatic sensors on various observing

platforms such as SOOs, Argo floats, moorings, and gliders. In this study, the successes of the SNOMS and POB projects demonstrated the excellent collaboration between the science community and the shipping industry which should be promoted in the future. Furthermore, satellite data should be used to extrapolate and upscale in-situ observations to larger space scales. Based on the knowledge gain from laboratory studies and observations, sophisticated numerical models can be developed to examine the complex processes in the ocean carbon cycle and to predict its potential future changes. Ultimately the combination of complementary in-depth process studies, in-situ and remotely observations and modeling efforts will lead to advanced understanding of the global carbon cycle.

Table 6.1 Advantage and shortcomings of different research methods for ocean carbon study

	Lab study	**Research survey**	**Time-series**	**SOO**	**Satellite**	**Modelling**
Temporal resolution	depends	poor	√	depends	depends	√
Spatial coverage	poor	poor	poor	depends	√	√
Resources needed	relatively less	large	maintenance	cost efficient	huge	depends
In-depth process study	√	√	√	poor	poor	√
Precision, accuracy	√	√	√ (discrete sample) depends (sensor)	√ (discrete sample) depends (sensor)	poor	depends
Full water column	--	√	depends	surface	surface	depends
Measurable parameters	√	√	depends	depends	limited	--
Prediction capacity	poor	poor	poor	poor	poor	√

6.2 Towards a more accurate thermodynamic calculation of the carbonate system

The thermodynamic calculation (Chapter 2.5) was used in this study to calculate pCO_2 from the observed DIC and TA in Chapter 3 and 5. This kind of calculation is widely used to characterize the marine carbonate system in ocean biogeochemical models and CO_2 perturbations experiences in ocean acidification studies. There are currently several parameterizations of the dissociation constants of carbonic acid while different parameterizations produce different results in the carbonate calculation [Hydes et al., 2010; Lee et al., 2000]. This makes it difficult to estimate the accuracy of the calculated results. It has been recommended that the 'Mehrbach et al. [1973] as refit by Dickson and Millero [1987]' constants yield the best agreement with the measurements when calculating pCO_2 from DIC and TA [Lee et al., 2000; Wanninkhof et al., 1999]. However, this does not necessarily imply that these constants yield the best results when other carbonate variables are used as input parameters [Wanninkhof et al., 1999]. Moreover, previous studies have identified varying degree of discrepancies between the calculated variables and the direct measurements [Hoppe et al., 2012; Lee et al., 1996, 2000; Lueker et al., 2000; Millero et al., 2002; Sejr et al., 2011; Wanninkhof et al., 1999], while some studies showed significant mismatches that cannot be explained by uncertainties of dissociation constants and relevant measurements. In the laboratory test (Chapter 3), abnormal changes in TA were observed which cannot be explained by changes in the carbonate chemistry. This TA anomaly resulted in a 7-90 μatm underestimation of the calculated pCO_2 (from DIC and TA) when compared to the measured pCO_2.

There is evidence that the discrepancy in the carbonate calculation is likely to arise from problems in alkalinity measurement resulting from chemically reactive carbonate particles [Sejr et al., 2011], organic particles (i.e. phytoplankton and bacterial cells) [Kim et al., 2006], and dissolved organic matter [Kim and Lee, 2009]. Errors in calculation can also be caused by the fact that alkalinity is not fully represented in the carbonate thermodynamic model used for the carbonate calculation. For example, many studies have proved the existent of organic alkalinity in both laboratory cultures and natural coastal environments [Cai et al., 1998; Hernandez-Ayon et al., 2007; Kim and Lee, 2009; Muller and Bleie, 2008]. However,

organic alkalinity is not considered in the current thermodynamic model for the carbonate calculation. When TA is used as an input variable for carbonate calculation, organic contribution of alkalinity thus would result in errors in the calculated results.

In the future, more accurate measurements of relevant dissociation constants are clearly needed. When possible, the CO_2 system should be over-determined by measuring more than two carbonate variables. Because of the potential bias in the carbonate calculation as discussed above, care must be taken when applying this calculation in waters with high concentrations of organic matter or chemically reactive particles. Otherwise, the bias in calculated pCO_2 would result in inappropriate interpretations of observation results or inaccurate air-sea CO_2 flux estimation. When studying the organic matter-rich waters, alkalinity is recommended to be measured by the method proposed by Cai et al. [1998] or Hernández-Ayón et al. [1999]. It was shown that the calculated pCO_2 is less sensitive to the changes in either DIC and TA when pH is used as one of the input parameters for calculation [Hydes et al., 2010]. As high accuracy and precision pH measurement is available by using a spectrophotometric method [Dickson et al., 2007], pH should be considered as a preferred input parameter for pCO_2 calculation. Note that the pH scale should be taken into account as huge differences may arise if different pH scales are used for calculation [Zeebe and Wolf-Gladrow, 2001]. For the ocean acidification research community, Hoppe et al. [2012] recommended the use of a certain pair of pH and TA for pCO_2 calculation to make the results of different studies to be comparable. Given the uncertainties just described for TA measurements as found in this research and elsewhere, perhaps the preferred pair should instead be pH and DIC.

6.3 Towards a more reliable air-sea CO_2 flux estimation

In this study, it is argued that observations with appropriate temporal resolution and spatial coverage are needed to address the variability of the carbonate system. This is important to get representative values of $pCO_{2,sea}$ for air-sea CO_2 flux estimation ($F = k * \alpha * (pCO_{2,sea} - pCO_{2,air})$, Equation 1.20). However, this is just one step to a robust estimation of air-sea CO_2 flux as the flux calculation is also significantly affected by the parameterization of the gas transfer velocity ($pCO_{2,air}$ and α can be relatively well constrained). Currently, there are a number of algorithms developed to determine gas transfer velocity from wind speed [Ho et al., 2006; Liss and Merlivat, 1986; McGillis

et al., 2001; Nightingale et al., 2000; Sweeney et al., 2007b; Wanninkhof, 1992; Wanninkhof et al., 2009]. Using different algorithms and different wind speed data would possibly result in significantly different flux estimates. How to apply the gas exchange-wind relationships correctly over temporal and spatial scales with varying winds is another issue that needs to be considered [Wanninkhof et al., 2009]. It has been demonstrated that small differences at intermediate winds has an appreciable effect on the global CO_2 flux calculation [Wanninkhof et al., 2002]. A growing amount of evidence also suggests that the wind-only polynomial equations do not capture the full range of parameters that affect gas transfer, which include friction velocity, bubbles, buoyancy fluxes, energy dissipation, fetch, surface slicks, rain, and chemical enhancement [Wanninkhof et al., 2009]. Towards a more accurate estimate of air-sea CO_2 flux, future efforts need to be made to better constrain the value fields of pCO_2 and to improve the theories and techniques quantifying gas transfer velocity.

6.4 What do TA-salinity relationships tell us?

Salinity is a fundamental variable for marine science as it indicates the mixing ratio of seawater and fresher water. The relationships between biogeochemical variables and salinity thus contains important information revealing physical and biogeochemical interactions. As shown in Equation 4.2, the alkalinity of a particular water parcel can be considered as a mixing product (salinity-related TA_{mix}) with additional biogeochemical alterations (salinity-independent ΔTA_{bgc}). If the mixing scheme is well defined, the difference between observation and the TA_{mix} predicted from conservative mixing indicates the changes induced by biogeochemical processes (i.e. ΔTA_{bgc}).

6.4.1 Predicting TA from salinity and SST

In this data, as in other datasets, the TA in the surface waters of the (sub)tropical open ocean are mainly controlled by simple mixing between the open ocean water and zero-alkalinity freshwater (precipitation and evaporation). Therefore, the concentrations of TA in these regions can be well predicted from salinity and SST using empirical algorithms [Lee et al., 2006]. However, this approach should be applied with caution in coastal environments due to the potentially large uncertainties

resulting from the complex physical and biogeochemical interactions. In coastal regions, the locally observed TA-S relationship is recommended to be used to estimate TA at salinity that is not directly measured.

6.4.2 The intercept of TA-S regression (TA_{S0}) and salinity normalization

In Chapter 4, the influences of different bio-physical processes on the TA-S relationship were discussed, particularly the TA_{S0} (see Figure 4.2 and Table 4.1). In contrast to the zero TA_{S0} resulting from simple dilution or concentration (SDC) processes, the non-SDC changes in alkalinity at different salinities generate either positive or negative TA_{S0}. This study suggests that the concentration of the river end member can be reliably estimated from TA_{S0} only in river-dominated regions. It follows that estimating the river end member in this way can lead to errors (even negative values of TA_{S0}) in coastal regions where other processes (e.g. evaporation, upwelling, shelf current, biological activity) are more influential.

Normalization to a constant salinity is often used to compare the measurements of conservative variables at different salinities. To avoid any overcorrection or artificial variance in the normalization, the non-zero freshwater end member of TA_{S0} should be considered as suggested by Friis et al. [2003]. It should be noted that this TA_{S0} can vary from region to region, depending on the geology of the river catchment (e.g. prevalence of limestone rocks), as well as other processes such as coastal upwelling, advection and biological activity.

It is proposed that NTA can be used as an indicator of the non-SDC addition or removal of TA in the surface water. As shown in Table 4.1, this can be done by comparing NTA with that of the open ocean end member (NTA_{ocean}). Moreover, the vertical changes in NTA can be used to examine the TA addition from the dissolution of $CaCO_3$ in the deep. However, Ca^{2+} may be a better indicator to study the cycling of $CaCO_3$ as TA is affected by many controlling factors (Chapter 1.3) [Brewer et al., 1975; Cao and Dai, 2011]. The high precision titration of Ca^{2+} should be promoted to better examine $CaCO_3$ cycling, and together with the carbonate system to study the production and decomposition of both organic and inorganic carbon.

6.5 What can be learned from the time-series observations in the Northeast Atlantic?

In this study, temporal variability of the surface ocean carbonate system in the Northeast Atlantic was examined on seasonal to inter-annual time scales (Chapter 5). The deep winter convection and the spring biological production were proved to be the main controlling factors on the seasonality of DIC and nutrients. The comparison with other observations in the Atlantic showed a transition in pCO_2 seasonality from the temperature-dominated oligotrophic subtropical gyre to DIC-dominated high latitude regions. The competing effects of changes in DIC and temperature determine the double-peak seasonal variability of pCO_2 in the mid-latitude Northeast Atlantic that was observed in this study. It is expected that this kind of double-peak seasonality of pCO_2 will be observed in other mid-latitude transition regions. On the inter-annual scale, this study demonstrated the impact of the large-scale climate variations such as NAO on the year-to-year changes in the surface ocean carbonate system in different regions in the Atlantic (Chapter 5.8 and 5.9). Overall, investigation of long-term trends in the ocean needs to carefully consider the natural temporal variability on multiple different time scales.

Our observations also provided direct evidence appearing to show the nutrient dependence of the surface ocean ‘carbon overconsumption’ (Chapter 5.6). C:N ratios close to Redfield stoichiometry were observed during the spring bloom when nutrients were not limiting, while non-Redfield consumption of carbon versus nitrogen was observed in the ‘post-bloom’ period with nutrient stress.

Appendices

Manufacturer's Response by the Pro-Oceanus Instruments

We at Pro-Oceanus Systems Inc. (PSI) are very pleased to have been involved in the studies described in Jiang, et. al. The importance to us as a company lies in the range of deployment platforms and the feedback from the researchers that has allowed us to improve our products. We very much thank all involved, as it has been a pleasure working with you. We also acknowledge the advantages of the SNOMS type tank for underway measurements and suggest that those planning SOO systems consider the many advantages of this approach.

We at PSI expend a large portion of our time and resources in research and development (R&D), and thus, some improvements to our products were implemented during the period of the studies. For example, the PAP and ACT deployments, especially, used sensors that were not fitted with our advanced optical cell temperature control. While the results showing the correction for cell temperature offsets are very important, all CO_2-Pro sensors are now equipped with this advanced temperature control feature.

The apparent errors in the data are as described in Jiang, et. al. as being due to:'…a number of factors including the sensor error, the uncertainties in the reference and the comparison process, how well the sensor was set up, contamination issues, etc.' Apportioning the error to each of these causes is difficult, but one systematic error that is described for the ACT and Dalhousie results is very likely due to a small error in calibration. We have addressed this at PSI by changing our calibration gases to include only NOAA and NOAA traceable standards. Calibrations are then performed to typically ± 1 ppm. This change is proving to greatly reduce calibration offset errors.

Recent recalibrations of CO_2-Pro instruments at Pro-Oceanus have shown remarkably stable span results, with some instruments showing less than 1 ppm drift over a one year deployment. However, for use on shipboard or in the laboratory, if more certain span calibration is desired, we offer our CO_2-Pro Atmosphere instrument that has a built in gas port that allows introduction of a standard gas at fixed intervals. While the gas port is normally used on this instrument to sample the

atmosphere alternately with CO_2 in surface ocean water, the instrument can be configured to accept standard gas or with some additional modifications, both, standard gases and atmospheric gas.

All CO_2-Pro instruments make measurements at 4.26 μm and use a humidity cell measurement to correct both for the water vapour contribution to the signal and the cross-sensitivity of water vapour with CO_2. We have had good success with this approach, but have recently begun a study to determine if our algorithms and/or our calibration routine that uses these algorithms can be improved.

While the PSI CO_2 instruments used in the SNOMS tank, as described in Jiang et al., are the CO_2-Pro with exposed tubular interface, the CO_2-Pro with unexposed interface is more commonly used. With the unexposed version the tubular interface resides in an enclosed channel machined into the endcap. Copper wire wound around the interface provides protection from biofouling, and also provides a standoff from the channel wall. Water pumped through the channel not only reduces the thickness of the mass transfer boundary layer, but also produces shear that discourages biofilm formation. This interface configuration is offered on the CO_2-Pro and CO_2-Pro Atmosphere. We have recently introduced the CO_2-Pro CV, a more compact version of the CO_2-Pro with flat Advanced Matrix Interface. This instrument offers the same detector features in a lower cost more compact instrument.

Accurate measurement of pCO_2 in the oceans is extremely important but also very demanding as shown by Jiang, et. al., and results from studies involving other submersible sensors, e.g., as reported in the ACT study. We at Pro-Oceanus applaud the work done as described in Jiang, et. al., in which deployment of sensors on a range of platforms offers independent assessments of instrument performance. Through this work and through ongoing feedback from our instrument users we are realizing our goal of offering sensors that meet the highest standards of researchers at prices that make them broadly affordable. Again, we offer our thanks to all of the researchers involved in this study.

Bruce D. Johnson, BEng, PhD

President, Pro-Oceanus Systems Inc.

List of References

Abril, G., H. Etcheber, B. Delille, M. Frankignoulle, and A. V. Borges (2003), Carbonate dissolution in the turbid and eutrophic Loire estuary, *Mar. Ecol. Prog. Ser., 259*, 129-138, doi: 10.3354/meps259129.

ACT (2009a), *Performance demonstration statement Pro-Oceanus Systems Inc. PSI CO_2-Pro^{TM}*. Alliance for Coastal Technologies, Ref.No.TD10-03.

ACT (2009b), *Protocols for demonstrating the performance of in situ pCO_2 analyzers*. 11 pp, Alliance for Coastal Technologies, Ref.No. ACT PD09-01.

Aguilar, R. (2007), *The corals of the Mediterranean*. 83 pp, Oceana, Fondazione Zegna, Biella, Italia.

Ainsworth, C. (2008), FerryBoxes begin to make waves, *Science, 322*(5908), 1627-1629, doi: 10.1126/science.322.5908.1627.

Al-Fukaha, F. (1994), A textural and geochemical study on reefal sediments of the Gulf of Aqaba, and the input of airborne dust to the area, M.S. thesis, Yarmouk University, Irbid, Jordan.

Al-Rousan, S. (1998), Sediment role in nutrient cycle within coral reefs of the Gulf of Aqaba, Red Sea., M.S. thesis, Yarmouk University, Irbid, Jordan.

Anderson, L., and D. Dyrssen (1994), Alkalinity and total carbonate in the Arabian Sea. Carbonate depletion in the Red Sea and Persian Gulf, *Mar. Chem., 47*(3–4), 195-202, doi: 10.1016/0304-4203(94)90019-1.

Anderson, L. A. (1995), On the hydrogen and oxygen-content of marine-phytoplankton, *Deep Sea Res., Part I*, *42*(9), 1675-1680.

Anderson, L. A., and J. L. Sarmiento (1994), Redfield ratios of remineralization determined by nutrient data-analysis, *Global Biogeochem. Cycles*, *8*(1), 65-80.

Andersson, A. J., and D. Gledhill (2013), Ocean acidification and coral reefs: effects on breakdown, dissolution, and net ecosystem calcification, *Annu. Rev. Mar. Sci.*, *5*(1), 321-348.

Bargeron, C. P., D. J. Hydes, D. K. Woolf, B. A. Kelly-Gerreyn, and M. A. Qurban (2006), A regional analysis of new production on the northwest European shelf using oxygen fluxes and a ship-of-opportunity, *Estuar. Coast. Shelf Sci., 69*(3-4), 478-490, doi: 10.1016/j.ecss.2006.05.015.

Bates, N. R. (2001), Interannual variability of oceanic CO_2 and biogeochemical properties in the Western North Atlantic subtropical gyre, *Deep Sea Res., Part II, 48*(8-9), 1507-1528, doi: 10.1016/S0967-0645(00)00151-X.

Bates, N. R. (2002), Seasonal variability of the effect of coral reefs on seawater CO_2 and air-sea CO_2 exchange, *Limnol. Oceanogr.*, *47*(1), 43-52.

List of References

Bates, N. R. (2007), Interannual variability of the oceanic CO_2 sink in the subtropical gyre of the North Atlantic Ocean over the last 2 decades, *J. Geophys. Res., 112*(C9), C09013, doi: 10.1029/2006jc003759.

Bates, N. R., A. F. Michaels, and A. H. Knap (1996), Seasonal and interannual variability of oceanic carbon dioxide species at the US JGOFS Bermuda Atlantic Time-series Study (BATS) site, *Deep Sea Res., Part II, 43*(2-3), 347-383, doi: 10.1016/0967-0645(95)00093-3.

Bates, N. R., A. F. Michaels, and A. H. Knap (1996), Alkalinity changes in the Sargasso Sea: geochemical evidence of calcification?, *Mar. Chem.*, *51*(4), 347-358.

Bates, N. R., T. Takahashi, D. W. Chipman, and A. H. Knap (1998), Variability of pCO_2 on diel to seasonal timescales in the Sargasso Sea near Bermuda, *J. Geophys. Res.*, *103*(C8), 15567-15585.

Batteen, M. L., C. A. Collins, C. R. Gunderson, and C. S. Nelson (1995), The effect of salinity on density in the California Current system, *J. Geophys. Res.*, *100*(C5), 8733-8749.

Beggs, H. M., R. Verein, G. Paltoglou, H. Kippo, and M. Underwood (2012), Enhancing ship of opportunity sea surface temperature observations in the Australian region, *J. Oper. Oceanogr.*, *5*(1), 59-73.

Bender, M. L., D. T. Ho, M. B. Hendricks, R. Mika, M. O. Battle, P. P. Tans, T. J. Conway, B. Sturtevant, and N. Cassar (2005), Atmospheric O_2/N_2 changes, 1993-2002: Implications for the partitioning of fossil fuel CO_2 sequestration, *Global Biogeochem. Cycles, 19*(4), GB4017, doi: 10.1029/2004gb002410.

Benson, B. B., and D. Krause (1984), The concentration and isotopic fractionation of oxygen dissolved in fresh-water and seawater in equilibrium with the atmosphere, *Limnol. Oceanogr., 29*(3), 620-632, doi: 10.4319/lo.1984.29.3.0620.

Bopp, L., P. Monfray, O. Aumont, J. L. Dufresne, H. Le Treut, G. Madec, L. Terray, and J. C. Orr (2001), Potential impact of climate change on marine export production, *Global Biogeochem. Cycles, 15*(1), 81-99, doi: 10.1029/1999GB001256.

Borges, A. V., and M. Frankignoulle (1999), Daily and seasonal variations of the partial pressure of CO_2 in surface seawater along Belgian and southern Dutch coastal areas, *J. Mar. Syst.*, *19*(4), 251-266.

Borges, A. V., B. Delille, and M. Frankignoulle (2005), Budgeting sinks and sources of CO_2 in the coastal ocean: Diversity of ecosystems counts, *Geophys. Res. Lett., 32*(14), L14601, doi: 10.1029/2005gl023053.

Bosworth, W., P. Huchon, and K. McClay (2005), The Red Sea and Gulf of Aden basins, *J. Afr. Earth Sci.*, *43*(1-3), 334-378.

Bozec, Y., H. Thomas, L. S. Schiettecatte, A. V. Borges, K. Elkalay, and H. J. W. de Baar (2006), Assessment of the processes controlling seasonal variations of dissolved inorganic carbon in the North Sea, *Limnol. Oceanogr., 51*(6), 2746-2762, doi: 10.4319/lo.2006.51.6.2746.

Brewer, P. G., and J. C. Goldman (1976), Alkalinity changes generated by phytoplankton growth, *Limnol. Oceanogr.*, *21*(1), 108-117.

Brewer, P. G., G. T. F. Wong, M. P. Bacon, and D. W. Spencer (1975), An oceanic calcium problem?, *Earth. Planet. Sci. Lett.*, *26*(1), 81-87.

Cabrillo, R. S., C. Gonzalez-Pola, M. Ruiz-Villarreal, and A. L. Montero (2011), Mixed layer depth (MLD) variability in the southern Bay of Biscay. Deepening of winter MLDs concurrent with generalized upper water warming trends?, *Ocean Dynam., 61*(9), 1215-1235, doi: 10.1007/s10236-011-0407-6.

Cai, W. J., Y. C. Wang, and R. E. Hodson (1998), Acid-base properties of dissolved organic matter in the estuarine waters of Georgia, USA, *Geochim. Cosmochim. Acta, 62*(3), 473-483, doi: 10.1016/s0016-7037(97)00363-3.

Cai, W. J., Z. H. A. Wang, and Y. C. Wang (2003), The role of marsh-dominated heterotrophic continental margins in transport of CO_2 between the atmosphere, the land-sea interface and the ocean, *Geophys. Res. Lett., 30*(16), 1849, doi: 10.1029/2003GL017633.

Cai, W. J., M. H. Dai, and Y. C. Wang (2006), Air-sea exchange of carbon dioxide in ocean margins: A province-based synthesis, *Geophys. Res. Lett., 33*(12), L12603, doi: 10.1029/2006GL026219.

Cai, W. J., X. P. Hu, W. J. Huang, L. Q. Jiang, Y. C. Wang, T. H. Peng, and X. Zhang (2010), Alkalinity distribution in the western North Atlantic Ocean margins, *J. Geophys. Res., 115*, C08014, doi: 10.1029/2009jc005482.

Cao, Z. M., and M. H. Dai (2011), Shallow-depth $CaCO_3$ dissolution: Evidence from excess calcium in the South China Sea and its export to the Pacific Ocean, *Global Biogeochem. Cycles, 25*, GB2019, doi: 10.1029/2009gb003690.

Cao, Z. M., M. H. Dai, N. Zheng, D. L. Wang, Q. Li, W. D. Zhai, F. F. Meng, and J. P. Gan (2011), Dynamics of the carbonate system in a large continental shelf system under the influence of both a river plume and coastal upwelling, *J. Geophys. Res., 116*, G02010, doi: 10.1029/2010jg001596.

Carton, J. A., S. A. Grodsky, and H. Liu (2008), Variability of the oceanic mixed layer, 1960-2004, *J. Clim., 21*(5), 1029-1047, doi: 10.1175/2007jcli1798.1.

Cayan, D. R. (1992), Latent and sensible heat-flux anomalies over the Northern Oceans - driving the sea-surface temperature, *J. Phys. Oceanogr., 22*(8), 859-881.

Chelton, D. B. (2001), *Report of the high-eesolution ocean topography science working group meeting: Executive summary*. 19 pp, Oregon State University, Corvallis, Oregon.

Chen, C.-T. A. (2002), Shelf-vs. dissolution-generated alkalinity above the chemical lysocline, *Deep Sea Res., Part II, 49*(24–25), 5365-5375, doi: 10.1016/S0967-0645(02)00196-0.

Chen, C.-T. A., and A. V. Borges (2009), Reconciling opposing views on carbon cycling in the coastal ocean: Continental shelves as sinks and near-shore ecosystems as sources of atmospheric CO_2, *Deep Sea Res., Part II*, *56*(8-10), 578-590.

Chen, C.-T. A., T.-H. Huang, Y.-H. Fu, Y. Bai, and X. He (2012), Strong sources of CO_2 in upper estuaries become sinks of CO_2 in large river plumes, *Curr. Opin. Environ. Sustainability*, *4*(2), 179-185.

Chen, C. T. A. (2004), Exchange of carbon in the coastal seas. In: Field, C.B., Raupach, M.R. (Eds.), The Global Carbon Cycle: Integrating Human, Climate and the Natural World. SCOPE, Washington, DC, pp. 341-351. .

Chen, C. T. A., and D. P. Swaney (2012), Terrestrial-ocean transfers of carbon and nutrient across the coastal boundary: Editorial overview, *Curr. Opin. Environ. Sustainability*, *4*(2), 159-161.

Chen, C. T. A., K. K. Liu, and R. MacDonald (2003), Continental margin exchanges, in *Ocean Biogeochemistry: A JGOFS Synthesis*, edited by M. J. R. Fasham, pp. 53-97, Springer, Berlin.

Chou, W.-C., Y.-L. L. Chen, D. D. Sheu, Y.-Y. Shih, C.-A. Han, C. L. Cho, C.-M. Tseng, and Y.-J. Yang (2006), Estimated net community production during the summertime at the SEATS time-series study site, northern South China Sea: Implications for nitrogen fixation, *Geophys. Res. Lett., 33*(22), L22610, doi: 10.1029/2005gl025365.

Copin-Montégut, C. (1993), Alkalinity and carbon budgets in the Mediterranean Sea, *Global Biogeochem. Cycles, 7*(4), 915-925, doi: 10.1029/93gb01826.

Copin-Montégut, C., and M. Bégovic (2002), Distributions of carbonate properties and oxygen along the water column (0-2000m) in the central part of the NW Mediterranean Sea (Dyfamed site): influence of winter vertical mixing on air-sea CO_2 and O_2 exchanges, *Deep Sea Res., Part II, 49*(11), 2049-2066, doi: 10.1016/S0967-0645(02)00027-9.

Corbiere, A., N. Metzl, G. Reverdin, C. Brunet, and A. Takahashi (2007), Interannual and decadal variability of the oceanic carbon sink in the North Atlantic subpolar gyre, *Tellus, Ser. B, 59*(2), 168-178, doi: 10.1111/j.1600-0889.2006.00232.x.

Cullen, H. M., R. D. D'Arrigo, E. R. Cook, and M. E. Mann (2001), Multiproxy reconstructions of the North Atlantic Oscillation, *Paleoceanography, 16*(1), 27-39, doi: 10.1029/1999PA000434.

Dai, M., Z. Yin, F. Meng, Q. Liu, and W.-J. Cai (2012), Spatial distribution of riverine DOC inputs to the ocean: an updated global synthesis, *Curr. Opin. Environ. Sustainability*, *4*(2), 170-178.

Dai, M., Z. Cao, X. Guo, W. Zhai, Z. Liu, Z. Yin, Y. Xu, J. Gan, J. Hu, and C. Du (2013), Why are some marginal seas sources of atmospheric CO_2?, *Geophys. Res. Lett.*, *40*(10), 2154-2158.

Dai, M. H., Z. M. Lu, W. D. Zhai, B. S. Chen, Z. M. Cao, K. B. Zhou, W. J. Cai, and C. T. A. Chen (2009), Diurnal variations of surface seawater pCO_2 in contrasting coastal environments, *Limnol. Oceanogr.*, *54*(3), 735-745.

de la Paz, M., A. Gomez-Parra, and J. Forja (2008a), Tidal-to-seasonal variability in the parameters of the carbonate system in a shallow tidal creek influenced by anthropogenic inputs, Rio San Pedro (SW Iberian Peninsula), *Cont. Shelf Res., 28*(10-11), 1394-1404, doi: 10.1016/j.csr.2008.04.002.

de la Paz, M., A. Gomez-Parra, and J. Forja (2008b), Variability of the partial pressure of CO_2 on a daily-to-seasonal time scale in a shallow coastal system affected by intensive aquaculture activities (Bay of Cadiz, SW Iberian Peninsula), *Mar. Chem.*, *110*(3-4), 195-204.

de la Paz, M., X. A. Padin, A. F. Rios, and F. F. Perez (2010), Surface fCO_2 variability in the Loire plume and adjacent shelf waters: High spatio-temporal resolution study using ships of opportunity, *Mar. Chem.*, *118*(3-4), 108-118.

DeGrandpre, M. D. (1993), Measurement of seawater pCO_2 using a renewable-reagent fiber optic sensor with colorimetric detection, *Anal. Chem.*, *65*, 331-337.

DeGrandpre, M. D., T. R. Hammar, and C. D. Wirick (1998), Short-term pCO_2 and O_2 dynamics in California coastal waters, *Deep Sea Res., Part II*, *45*(8-9), 1557-1575.

DeGrandpre, M. D., M. M. Baehr, and T. R. Hammar (1999), Calibration-free optical chemical sensors, *Anal. Chem.*, *71*(6), 1152-1159.

DeGrandpre, M. D., T. R. Hammar, S. P. Smith, and F. L. Sayles (1995), In situ measurements of seawater pCO_2, *Limnol. Oceanogr.*, *40*(5), 969-975.

DeGrandpre, M. D., T. R. Hammar, D. W. R. Wallace, and C. D. Wirick (1997), Simultaneous mooring-based measurements of seawater CO_2 and O_2 off Cape Hatteras, North Carolina, *Limnol. Oceanogr.*, *42*(1), 21-28.

DeGrandpre, M. D., R. Wanninkhof, W. R. McGillis, and P. G. Strutton (2004), A Lagrangian study of surface pCO_2 dynamics in the eastern equatorial Pacific Ocean, *J. Geophys. Res., 109*(C8), C08S07, doi: 10.1029/2003JC002089.

List of References

Dickson, A. G. (1981), An exact definition of total alkalinity and a procedure for the estimation of alkalinity and total inorganic carbon from titration data, *Deep Sea Res., Part I, 28*(6), 609-623, doi: 10.1016/0198-0149(81)90121-7.

Dickson, A. G. (1990), Standard potential of the ($AgCl(s)+½ H_2(g) = Ag(s) + HCl(aq)$) cell and the dissociation constant of bisulfate ion in synthetic sea water from 273.15 to 318.15 K, *J. Chem. Thermodyn., 22*, 113-127, doi: 10.1016/0021-9614(90)90074-Z.

Dickson, A. G. (1992), The development of the alkalinity concept in marine chemistry, *Mar. Chem.*, *40*(1–2), 49-63.

Dickson, A. G., C. L. Sabine, and J. R. Christian (2007), *Guide to best practices for ocean CO_2 measurements*, 191 pp., North Pacific Marine Science Organization (PICES), Sidney, British Columbia.

Doney, S. (2009), *The consequences of human-driven ocean acidification for marine life*. 36 pp, F1000 Biol Rep, Department of Marine Chemistry and Geochemistry, Woods Hole Oceanographic Institution, MA, USA.

Doney, S. C., V. J. Fabry, R. A. Feely, and J. A. Kleypas (2009a), Ocean acidification: the other CO_2 problem, *Annu. Rev. Mar. Sci.*, *1*, 169-192.

Doney, S. C., B. Tilbrook, S. Roy, N. Metzl, C. Le Quere, M. Hood, R. A. Feely, and D. Bakker (2009b), Surface-ocean CO_2 variability and vulnerability, *Deep Sea Res., Part II*, *56*(8-10), 504-511.

Donlon, C., I. S. Robinson, W. Wimmer, G. Fisher, M. Reynolds, R. Edwards, and T. J. Nightingale (2008), An Infrared Sea Surface Temperature Autonomous Radiometer (ISAR) for Deployment aboard Volunteer Observing Ships (VOS), *J. Atmos. Oceanic Technol.*, *25*(1), 93-113.

Dumousseaud, C., E. P. Achterberg, T. Tyrrell, A. Charalampopoulou, U. Schuster, M. Hartman, and D. J. Hydes (2010), Contrasting effects of temperature and winter mixing on the seasonal and inter-annual variability of the carbonate system in the Northeast Atlantic Ocean, *Biogeosciences, 7*(5), 1481-1492, doi: 10.5194/bg-7-1481-2010.

Elageed, S. (2010), Factors controlling the total alkalinity in the Arabian Sea and Red Sea, M. S. thesis, University of Bergen, Bergen, Norway.

Ellis, J. P., and J. D. Milliman (1985), Calcium-Carbonate Suspended in Arabian Gulf and Red-Sea Waters - Biogenic and Detrital, Not Chemogenic, *J. Sediment. Petrol.*, *55*(6), 805-808.

Emerson, S., and J. Hedges (2008), *Chemical Oceanography and the Marine Carbon Cycle*, 462 pp., Cambridge University Press, Cambridge

Fabry, V. J., B. A. Seibel, R. A. Feely, and J. C. Orr (2008), Impacts of ocean acidification on marine fauna and ecosystem processes, *ICES J. Mar. Sci.*, *65*, 414-432.

Falkowski, P. G., R. T. Barber, and V. Smetacek (1998), Biogeochemical controls and feedbacks on ocean primary production, *Science, 281*, 200-206, doi: 10.1126/science.281.5374.200.

Feely, R., and C. Sabine (2011), *Carbon dioxide and hydrographic measurements during the 2007 NACP West Coast Cruise.* http://cdiac.ornl.gov/ftp/oceans/NACP_West_Coast_Cruise_2007/. Carbon Dioxide Information Analysis Center, Oak Ridge National Laboratory, US Department of Energy, Oak Ridge, Tennessee. doi: 10.3334/CDIAC/otg.CLIVAR_NACP_West_Coast_Cruise_2007.

Feely, R. A., S. C. Doney, and S. R. Cooley (2009), Ocean acidification: present conditions and future changes in a high-CO_2 world, *Oceanography*, *22*(4), 36-47.

Feely, R. A., C. L. Sabine, J. M. Hernandez-Ayon, D. Ianson, and B. Hales (2008), Evidence for upwelling of corrosive "acidified" water onto the continental shelf, *Science, 320*(5882), 1490-1492, doi: 10.1126/science.1155676.

Feely, R. A., C. L. Sabine, K. Lee, W. Berelson, J. Kleypas, V. J. Fabry, and F. J. Millero (2004), Impact of anthropogenic CO_2 on the $CaCO_3$ system in the oceans, *Science, 305*(5682), 362-366, doi: 10.1126/science.1097329.

Fiedler, B., P. Fietzek, N. Vieira, P. Silva, H. C. Bittig, and A. Körtzinger (2012), In situ CO_2 and O_2 measurements on a profiling float, *J. Atmos. Oceanic Technol.*, *30*(1), 112-126.

Field, C. B., and M. R. Raupach (Eds.) (2004), *The global carbon cycle: integrating humans, climate, and the natural world*, Island Press, Washington, DC.

Findlay, H. S., T. Tyrrell, R. G. J. Bellerby, A. Merico, and I. Skjelvan (2008), Carbon and nutrient mixed layer dynamics in the Norwegian Sea, *Biogeosciences, 5*(5), 1395-1410, doi: 10.5194/bg-5-1395-2008.

Fletcher, S. E. M., N. Gruber, A. R. Jacobson, S. C. Doney, S. Dutkiewicz, M. Gerber, M. Follows, F. Joos, K. Lindsay, D. Menemenlis, A. Mouchet, S. A. Muller, and J. L. Sarmiento (2006), Inverse estimates of anthropogenic CO_2 uptake, transport, and storage by the ocean, *Global Biogeochem. Cycles, 20*(2), GB2002, doi: 10.1029/2005GB002530.

Fofonoff, N. P., and R. C. Millard (1983), Algorithms for computation of fundamental properties of seawater, *NESCO Tech. Pap. Mar. Sci.*, *44*, 53.

Friis, K., A. Kortzinger, and D. W. R. Wallace (2003), The salinity normalization of marine inorganic carbon chemistry data, *Geophys. Res. Lett., 30*(2), 1085, doi: 10.1029/2002gl015898.

Fung, I. Y., S. C. Doney, K. Lindsay, and J. John (2005), Evolution of carbon sinks in a changing climate, *Proc. Natl. Acad. Sci. U. S. A., 102*(32), 11201-11206, doi: 10.1073/pnas.0504949102.

Gattuso, J.-P., and L. Hansson (Eds.) (2011), *Ocean Acidification*, 352 pp., Oxford University Press, Oxford.

Gattuso, J.-P., M. Frankignoulle, and R. Wollast (1998), Carbon and carbonate metabolism in coastal aquatic ecosystems, *Annu. Rev. Ecol. Evol. Syst.*, *29*, 405-434.

Gevirtz, J. L., and G. M. Friedman (1966), Deep-Sea Carbonate Sediments of the Red Sea and their Implications on Marine Lithification, *J. Sediment. Petrol.*, *36*(1), 143-151.

Gloor, M., N. Gruber, J. Sarmiento, C. L. Sabine, R. A. Feely, and C. Rodenbeck (2003), A first estimate of present and preindustrial air-sea CO_2 flux patterns based on ocean interior carbon measurements and models, *Geophys. Res. Lett., 30*(1), 1010, doi: 10.1029/2002gl015594.

Goni, G. (2010), The ship of opportunity program, in *ESA Publication WPP-306*, edited by Hall J, H. DE and S. D, Proceedings of OceanObs' 09: sustained ocean observations and information for society (vol. 2), Venice, Italy.

González-Dávila, M., J. M. Santana-Casiano, and E. F. González-Dávila (2007a), Interannual variability of the upper ocean carbon cycle in the northeast Atlantic Ocean, *Geophys. Res. Lett., 34*(7), L07608, doi: 10.1029/2006gl028145.

González-Dávila, M., J. M. Santana-Casiano, and E. F. González-Dávila (2007b), Interannual variability of the upper ocean carbon cycle in the northeast Atlantic Ocean, *Geophys. Res. Lett.*, *34*(7), L07608.

González-Dávila, M., J. M. Santana-Casiano, M. J. Rueda, O. Llinas, and E. F. Gonzalez-Davila (2003), Seasonal and interannual variability of sea-surface carbon dioxide species at the European Station for Time Series in the Ocean at the Canary Islands (ESTOC) between 1996 and 2000, *Global Biogeochem. Cycles, 17*(3), 1076, doi: 10.1029/2002gb001993.

González-Pola, C., J. M. Fernández-Díaz, and A. Lavín (2007), Vertical structure of the upper ocean from profiles fitted to physically consistent functional forms, *Deep Sea Res., Part I, 54*(11), 1985-2004, doi: 10.1016/j.dsr.2007.08.007.

Goyet, C., and E. T. Peltzer (1997), Variation of CO_2 partial pressure in surface seawater in the equatorial Pacific Ocean, *Deep Sea Res., Part I*, *44*(9-10), 1611-1625.

Goyet, C., D. R. Walt, and P. G. Brewer (1992), Development of a fiber optic sensor for measurement of pCO_2 in sea water: design criteria and sea trials, *Deep Sea Res., Part I*, *39*(6), 1015-1026.

Gruber, N., C. D. Keeling, and N. R. Bates (2002), Interannual variability in the North Atlantic Ocean carbon sink, *Science, 298*(5602), 2374-2378, doi: 10.1126/science.1077077.

Gruber, N., P. Friedlingstein, C. B. Field, R. Valentini, M. Heimann, J. E. Richey, R. L. P., E.-D. Schulze, and C.-T. A. Chen (2004), The vulnerability of the carbon cycle in the 21st century: an assessment of carbon-climate-human interactions., in *The global carbon cycle. Integrating humans, climate and the natural world*, edited by C. B. Field and M. R. Raupauch, pp. 45-76, Island Press, Washington, DC.

Harlay, J., L. Chou, C. De Bodt, N. Van Oostende, J. Piontek, K. Suykens, A. Engel, K. Sabbe, S. Groom, B. Delille, and A. V. Borges (2011), Biogeochemistry and carbon mass balance of a coccolithophore bloom in the northern Bay of Biscay (June 2006), *Deep Sea Res., Part I*, *58*(2), 111-127.

Harlay, J., A. V. Borges, C. V. D. Zee, B. Delille, R. H. M. Godoi, L.-S. Schiettecatte, N. Roevros, K. Aerts, P.-E. Lapernat, L. Rebreanu, S. Groom, M.-H. Daro, R. V. Grieken, and L. Chou (2010), Biogeochemical study of a coccolithophore bloom in the northern Bay of Biscay (NE Atlantic Ocean) in June 2004, *Prog. Oceanogr.*, *86*, 317-336.

Hartman, S. E., R. S. Lampitt, K. E. Larkin, M. Pagnani, J. Campbell, T. Gkritzalis, Z. P. Jiang, C. A. Pebody, H. A. Ruhl, A. J. Gooday, B. J. Bett, D. S. M. Billett, P. Provost, R. McLachlan, J. D. Turton, and S. Lankester (2012), The Porcupine Abyssal Plain fixed-point sustained observatory (PAP-SO): variations and trends from the Northeast Atlantic fixed-point time-series, *ICES J. Mar. Sci.*, *69*(5), 776-783.

Hedges, J. I., J. A. Baldock, Y. Gelinas, C. Lee, M. L. Peterson, and S. G. Wakeham (2002), The biochemical and elemental compositions of marine plankton: A NMR perspective, *Mar. Chem.*, *78*(1), 47-63.

Hansen, H. P., and F. Koroleff (2007), Determination of nutrients, in *Methods of Seawater Analysis*, edited by K. Grasshoff, M. Ehrhardt and K. Kremling, pp. 159-228, Wiley-VCH Verlag GmbH, Weinheim, Germany.

Henson, S. A., J. P. Dunne, and J. L. Sarmiento (2009), Decadal variability in North Atlantic phytoplankton blooms, *J. Geophys. Res., 114*, C04013, doi: 10.1029/2008jc005139.

Hernandez-Ayon, J. M., A. Zirino, A. G. Dickson, T. Camiro-Vargas, and E. Valenzuela-Espinoza (2007), Estimating the contribution of organic bases from microalgae to the titration alkalinity in coastal seawaters, *Limnol. Oceanogr. Methods*, *5*, 225-232.

Hernández-Ayón, J. M. n., S. L. Belli, and A. Zirino (1999), pH, alkalinity and total CO_2 in coastal seawater by potentiometric titration with a difference derivative readout, *Anal. Chim. Acta*, *394*(1), 101-108.

Ho, D. T., C. S. Law, M. J. Smith, P. Schlosser, M. Harvey, and P. Hill (2006), Measurements of air-sea gas exchange at high wind speeds in the Southern Ocean: Implications for global parameterizations, *Geophys. Res. Lett.*, *33*(16).

Hoffman, R. N. (2011), Neutral stability height correction for ocean winds, *arXiv:1107.1416v1 [physics.ao-ph]*.

Hopkinson, C. S. (1988), Patterns of organic carbon exchange between coastal ecosystems: the mass balance approach in slat marsh ecosystems, in *Coastal-Offshore Ecosystem Interactions*, edited by B.-O. Jansson, pp. 122-154, Springer, Berlin/Heidelberg.

Hopkinson, C. S., W. J. Cai, and X. P. Hu (2012), Carbon sequestration in wetland dominated coastal systems - a global sink of rapidly diminishing magnitude, *Curr. Opin. Environ. Sustainability*, *4*(2), 186-194.

Hoppe, C. J. M., G. Langer, S. D. Rokitta, D. A. Wolf-Gladrow, and B. Rost (2012), Implications of observed inconsistencies in carbonate chemistry measurements for ocean acidification studies, *Biogeosciences*, *9*(7), 2401-2405.

Hydes, D., S. Loucaides, and T. Tyrrell (2010), *Report on a desk study to identify likely sources of error in the measurements of carbonate system parameters and related calculations, particularly with respect to coastal waters and ocean acidification experiments*. Supplement to DEFRA contract ME4133 "DEFRApH monitoring project". Southampton, UK, National Oceanography Centre Southampton, 53pp. (National Oceanography Centre Southampton Research and Consultancy Report, 83).

Hydes, D. J., and J. M. Campbell (2007), *SNOMS: Diary of the system development and installation on the MV Pacific Celebes in 2006 and 2007*. National Oceanography Centre, Southampton, Internal Document No. 10.

Hydes, D. J., M. C. Hartman, J. Kaiser, and J. M. Campbell (2009), Measurement of dissolved oxygen using optodes in a FerryBox system, *Estuar. Coast. Shelf Sci., 83*(4), 485-490, doi: 10.1016/j.ecss.2009.04.014.

Hydes, D. J., M. C. Hartman, C. P. Bargeron, J. M. Campbell, M. S. Cure, and D. K. Woolf (2008), A study of gas exchange during the transition from deep winter mixing to spring bloom in the Bay of Biscay measured by continuous observation from a ship of opportunity, *J. Oper. Oceanogr.*, *1*(2), 41-50.

Hydes, D. J., M. C. Hartman, J. M. Campbell, Z.-P. Jiang, S. E. Hartman, M. Pagnani, B. A. Kelly-Gerreyn, and J. Donahoe (2013), *Report of the SNOMS Project 2006 to 2012, SNOMS: SWIRE NOCS Ocean Monitoring System. Part 1: Narrative description.*, National Oceanography Centre Research and Consultancy Report, 33, Southampton, UK.

Hydes, D. J., A. Yool, J. M. Campbell, N. A. Crisp, J. Dodgson, B. Dupee, M. Edwards, S. E. Hartman, B. A. Kelly-Gerreyn, A. M. Lavin, C. M. González-Pola, and P. Miller (2003), Use of a Ferry-Box system to look at shelf sea and ocean margin processes, in *Elsevier Oceanography Series*, edited by H. Dahlin, N. C. Flemming, K. Nittis and S. E. Petersson, pp. 297-303, Elsevier, Athens, Greece.

IPCC (2007), *Climate Change 2007: Synthesis Report.* . Contribution of Working Groups I, II and III to the Fourth Assessment Report of the Intergovernmental Panel on Climate Change [Core Writing Team, Pachauri, R.K and Reisinger, A. (eds.)]. IPCC, Geneva, Switzerland, 104 pp.

IPCC (2013), *Summary for Policymakers. In: Climate Change 2013: The Physical Science Basis.*, Contribution of Working Group I to the Fifth Assessment Report of the Intergovernmental Panel on Climate Change [Stocker, T.F., D. Qin, G.-K. Plattner, M. Tignor, S. K. Allen, J. Boschung, A. Nauels, Y. Xia, V. Bex and P.M. Midgley (eds.)]. Cambridge University Press, Cambridge, United Kingdom and New York, NY, USA.

Jacobson, A. R., S. E. M. Fletcher, N. Gruber, J. L. Sarmiento, and M. Gloor (2007a), A joint atmosphere-ocean inversion for surface fluxes of carbon dioxide: 2. Regional results, *Global Biogeochem. Cycles, 21*(1), GB1020, doi: 10.1029/2006gb002703.

Jacobson, A. R., S. E. M. Fletcher, N. Gruber, J. L. Sarmiento, and M. Gloor (2007b), A joint atmosphere-ocean inversion for surface fluxes of carbon dioxide: 1. Methods and global-scale fluxes, *Global Biogeochem. Cycles, 21*(1), GB1019, doi: 10.1029/2005gb002556.

Jiang, L. Q., W. J. Cai, R. Wanninkhof, Y. C. Wang, and H. Luger (2008), Air-sea CO_2 fluxes on the US South Atlantic Bight: Spatial and seasonal variability, *J. Geophys. Res., 113*(C7), C07019, doi: 10.1029/2007jc004366.

Jiang, Z.-P., J. C. Huang, M. H. Dai, S. J. Kao, D. J. Hydes, W. C. Chou, and S. Jan (2011), Short-term dynamics of oxygen and carbon in productive nearshore shallow seawater systems off Taiwan: Observations and modeling, *Limnol. Oceanogr.*, *56*(5), 1832-1849.

Jiang, Z.-P., D. J. Hydes, T. Tyrrell, S. E. Hartman, M. C. Hartman, C. Dumousseaud, X. A. Padin, I. Skjelvan, and C. González-Pola (2013), Key controls on the seasonal and interannual variations of the carbonate system and air-sea CO_2 flux in the Northeast Atlantic (Bay of Biscay), *J. Geophys. Res.*, *118*, 1-16.

Johnson, K. S., S. C. Riser, and D. M. Karl (2010), Nitrate supply from deep to near-surface waters of the North Pacific subtropical gyre, *Nature, 465*(7301), 1062-1065, doi: 10.1038/Nature09170.

Kaluza, P., A. Kolzsch, M. T. Gastner, and B. Blasius (2010), The complex network of global cargo ship movements, *J. R. Soc., Interface*, *7*(48), 1093-1103.

Keeling, C. D., H. Brix, and N. Gruber (2004), Seasonal and long-term dynamics of the upper ocean carbon cycle at Station ALOHA near Hawaii, *Global Biogeochem. Cycles, 18*(4), GB4006, doi: 10.1029/2004gb002227.

Kelly-Gerreyn, B. A., D. J. Hydes, M. C. Hartman, J. Siddorn, P. Hyder, and M. W. Holt (2007), The phosphoric acid leak from the wreck of the MV Ece in the English Channel in 2006: Assessment with a ship of opportunity, an operational ecosystem model and historical data, *Mar. Pollut. Bull.*, *54*(7), 850-862.

Kelly-Gerreyn, B. A., D. J. Hydes, A. M. Jégou, P. Lazure, L. J. Fernand, I. Puillat, and C. Garcia-Soto (2006), Low salinity intrusions in the western English Channel, *Cont. Shelf Res., 26*(11), 1241-1257, doi: 10.1016/j.csr.2006.03.007.

Key, R. M., A. Kozyr, C. L. Sabine, K. Lee, R. Wanninkhof, J. L. Bullister, R. A. Feely, F. J. Millero, C. Mordy, and T. H. Peng (2004), A global ocean carbon climatology: Results from Global Data Analysis Project (GLODAP), *Global Biogeochem. Cycles, 18*(4), GB4031, doi: 10.1029/2004gb002247.

Kim, H.-C., and K. Lee (2009), Significant contribution of dissolved organic matter to seawater alkalinity, *Geophys. Res. Lett.*, *36*(20).

Kim, H. C., K. Lee, and W. Y. Choi (2006), Contribution of phytoplankton and bacterial cells to the measured alkalinity of seawater, *Limnol. Oceanogr.*, *51*(1), 331-338.

Klausmeier, C. A., E. Litchman, T. Daufresne, and S. A. Levin (2004), Optimal nitrogen-to-phosphorus stoichiometry of phytoplankton, *Nature, 429*(6988), 171-174, doi: 10.1038/Nature02454.

Koczy, F. F. (1956), The specific alkalinity, *Deep Sea Research*, *3*(4), 279-288.

Koeve, W. (2004), Spring bloom carbon to nitrogen ratio of net community production in the temperate N. Atlantic, *Deep Sea Res., Part I, 51*(11), 1579-1600, doi: 10.1016/j.dsr.2004.07.002.

Koeve, W. (2006), C : N stoichiometry of the biological pump in the North Atlantic: Constraints from climatological data, *Global Biogeochem. Cycles, 20*(3), GB3018, doi: 10.1029/2004gb002407.

Körtzinger, A., J. Schimanski, and U. Send (2005), High quality oxygen measurements from profiling floats: A promising new technique, *J. Atmos. Oceanic Technol.*, *22*(3), 302-308.

Körtzinger, A., W. Koeve, P. Kahler, and L. Mintrop (2001), C : N ratios in the mixed layer during the productive season in the northeast Atlantic Ocean, *Deep Sea Res., Part I, 48*(3), 661-688, doi: 10.1016/S0967-0637(00)00051-0.

Körtzinger, A., H. Thomas, B. Schneider, N. Gronau, L. Mintrop, and J. C. Duinker (1996), At-sea intercomparison of two newly designed underway pCO_2 systems - encouraging results, *Mar. Chem.*, *52*(2), 133-145.

Körtzinger, A., U. Send, R. S. Lampitt, S. Hartman, D. W. R. Wallace, J. Karstensen, M. G. Villagarcia, O. Llinás, and M. D. DeGrandpre (2008), The seasonal pCO_2 cycle at 49°N/16.5°W in the northeastern Atlantic Ocean and what it tells us about biological productivity, *J. Geophys. Res., 113*(C4), C04020, doi: 10.1029/2007jc004347.

Lascaratos, A., W. Roether, K. Nittis, and B. Klein (1999), Recent changes in deep water formation and spreading in the eastern Mediterranean Sea: a review, *Prog. Oceanogr., 44*(1–3), 5-36, doi: 10.1016/S0079-6611(99)00019-1.

Lavín, A., L. Valdés, F. Sanchez, P. Abaunza, A. Forest, B. Boucher, P. Lazure, and A. M. Jegou (2006), The Bay of Biscay: the encountering of the ocean and the shelf, in *The Sea* edited by A. R. Robinson and K. H. Brink, pp. 933-1001, Harvard University Press, Harvard.

Le Quere, C., M. R. Raupach, J. G. Canadell, G. Marland, L. Bopp, P. Ciais, T. J. Conway, S. C. Doney, R. A. Feely, P. Foster, P. Friedlingstein, K. Gurney, R. A. Houghton, J. I. House, C. Huntingford, P. E. Levy, M. R. Lomas, J. Majkut, N. Metzl, J. P. Ometto, G. P. Peters, I. C. Prentice, J. T. Randerson, S. W. Running, J. L. Sarmiento, U. Schuster, S. Sitch, T. Takahashi, N. Viovy, G. R. van der Werf, and F. I. Woodward (2009), Trends in the sources and sinks of carbon dioxide, *Nature Geoscience, 2*(12), 831-836, doi: 10.1038/Ngeo689.

Le Quéré, C., T. Takahashi, E. T. Buitenhuis, C. Rödenbeck, and S. C. Sutherland (2010), Impact of climate change and variability on the global oceanic sink of CO_2, *Global Biogeochem. Cycles*, *24*(4), GB4007.

Lee, K., F. J. Millero, and D. M. Campbell (1996), The reliability of the thermodynamic constants for the dissociation of carbonic acid in seawater, *Mar. Chem.*, *55*(3), 233-245.

Lee, K., F. J. Millero, R. H. Byrne, R. A. Feely, and R. Wanninkhof (2000), The recommended dissociation constants for carbonic acid in seawater, *Geophys. Res. Lett.*, *27*(2), 229-232.

Lee, K., L. T. Tong, F. J. Millero, C. L. Sabine, A. G. Dickson, C. Goyet, G. H. Park, R. Wanninkhof, R. A. Feely, and R. M. Key (2006), Global relationships of total alkalinity with salinity and temperature in surface waters of the world's oceans, *Geophys. Res. Lett., 33*(19), L19605, doi: 10.1029/2006gl027207.

Lee, S. S., C. Park, P. Fenter, N. C. Sturchio, and K. L. Nagy (2010), Competitive adsorption of strontium and fulvic acid at the muscovite–solution interface observed with

resonant anomalous X-ray reflectivity, *Geochim. Cosmochim. Acta*, *74*(6), 1762-1776.

Lefevre, N., A. J. Watson, A. Olsen, A. F. Rios, F. F. Perez, and T. Johannessen (2004), A decrease in the sink for atmospheric CO_2 in the North Atlantic, *Geophys. Res. Lett., 31*(7), L07306, doi: 10.1029/2003gl018957.

Lefévre, N., J. P. Ciabrini, G. Michard, B. Brient, M. Duchaffaut, and L. Merlivat (1993), A new optical sensor for pCO_2 measurement, *Mar. Chem.*(42), 189-198.

Liss, P. S., and L. Merlivat (1986), Air-sea gas exchange rates: Introduction and synthesis, in *The Role of Air-Sea Exchange in Geochemical Cycling*, edited by P. Buat-Menard, D. Reidel, Hingham, Mass.

Liu, Q., M. Dai, W. Chen, C. A. Huh, G. Wang, Q. Li, and M. A. Charette (2012), How significant is submarine groundwater discharge and its associated dissolved inorganic carbon in a river-dominated shelf system?, *Biogeosciences, 9*(5), 1777-1795, doi: 10.5194/bg-9-1777-2012.

Lu, Z., M. Dai, K. Xu, J. Chen, and Y. Liao (2008), A high precision, fast response, and low power consumption in situ optical fiber chemical pCO_2 sensor, *Talanta*, *76*, 353-359. doi: 310.1016/j.talanta.2008.1003.1005.

Lu, Z. M., J. P. Gan, and M. H. Dai (2012), Modeling seasonal and diurnal pCO_2 variations in the northern South China Sea, *J. Mar. Syst.*, *92*(1), 30-41.

Lueker, T. J., A. G. Dickson, and C. D. Keeling (2000), Ocean pCO_2 calculated from dissolved inorganic carbon, alkalinity, and equations for K_1 and K_2: validation based on laboratory measurements of CO_2 in gas and seawater at equilibrium, *Mar. Chem.*, *70*(1–3), 105-119.

Luger, H., R. Wanninkhof, D. W. R. Wallace, and A. Kortzinger (2006), CO_2 fluxes in the subtropical and subarctic North Atlantic based on measurements from a volunteer observing ship, *J. Geophys. Res., 111*(C6), doi: 10.1029/2005JC003101.

Luterbacher, J., M. A. Liniger, A. Menzel, N. Estrella, P. M. Della-Marta, C. Pfister, T. Rutishauser, and E. Xoplaki (2007), Exceptional European warmth of autumn 2006 and winter 2007: Historical context, the underlying dynamics, and its phenological impacts, *Geophys. Res. Lett., 34*(12), L12704, doi: 10.1029/2007gl029951.

Mackenzie, F. T., L. M. Ver, and A. Lerman (2000), Coastal-zone biogeochemical dynamics under global warming, *Inter. Geol. Rev.*, *42*(3), 193-206.

Marshall, J., H. Johnson, and J. Goodman (2001), A study of the interaction of the North Atlantic oscillation with ocean circulation, *J. Clim., 14*(7), 1399-1421, doi: 10.1175/1520-0442(2001)014<1399:ASOTIO>2.0.CO;2.

McGillis, W. R., J. B. Edson, J. D. Ware, J. W. H. Dacey, J. E. Hare, C. W. Fairall, and R. Wanninkhof (2001), Carbon dioxide flux techniques performed during GasEx-98, *Mar. Chem., 75*(4), 267-280, doi: 10.1016/S0304-4203(01)00042-1.

McKinley, G. A., A. R. Fay, T. Takahashi, and N. Metzl (2011), Convergence of atmospheric and North Atlantic carbon dioxide trends on multidecadal timescales, *Nat. Geosci., 4*(9), 606-610, doi: 10.1038/Ngeo1193.

Mehrbach, C., C. H. Culberson, J. E. Hawley, and R. M. Pytkowicz (1973), Measurement of the apparent dissociation constants of carbonic acid in seawater at atmospheric pressure, *Limnol. Oceanogr., 18*, 897-907, doi: 10.4319/lo.1973.18.6.0897.

Millero, F. J., K. Lee, and M. Roche (1998), Distribution of alkalinity in the surface waters of the major oceans, *Mar. Chem.*, *60*(1-2), 111-130.

Millero, F. J., T. B. Graham, F. Huang, H. Bustos-Serrano, and D. Pierrot (2006), Dissociation constants of carbonic acid in seawater as a function of salinity and temperature, *Mar. Chem.*, *100*(1-2), 80-94.

Millero, F. J., D. Pierrot, K. Lee, R. Wanninkhof, R. Feely, C. L. Sabine, R. M. Key, and T. Takahashi (2002), Dissociation constants for carbonic acid determined from field measurements, *Deep Sea Res., Part I*, *49*(10), 1705-1723.

Mojica Prieto, F. J., and F. J. Millero (2002), The values of $pK_1 + pK_2$ for the dissociation of carbonic acid in seawater, *Geochim. Cosmochim. Acta*, *66*(14), 2529-2540.

Muller-Karger, F. E., R. Varela, R. Thunell, R. Luerssen, C. M. Hu, and J. J. Walsh (2005), The importance of continental margins in the global carbon cycle, *Geophys. Res. Lett., 32*(1), L01602, doi: 10.1029/2004gl021346.

Muller, F. L. L., and B. Bleie (2008), Estimating the organic acid contribution to coastal seawater alkalinity by potentiometric titrations in a closed cell, *Anal. Chim. Acta, 619*(2), 183-191, doi: 10.1016/j.aca.2008.05.018.

Nakano, Y., H. Kimoto, S. Watanabe, K. Harada, and Y. W. Watanabe (2006), Simultaneous vertical measurements of in situ pH and CO_2 in the sea using spectrophotometric profilers, *J. Oceanogr.*, *62*(1), 71-81.

Nemoto, K., T. Midorikawa, A. Wada, K. Ogawa, S. Takatani, H. Kimoto, M. Ishii, and H. Y. Inoue (2009), Continuous observations of atmospheric and oceanic CO_2 using a moored buoy in the East China Sea: Variations during the passage of typhoons, *Deep Sea Res., Part II*, *56*(8-10), 542-553.

Nightingale, P. D., G. Malin, C. S. Law, A. J. Watson, P. S. Liss, M. I. Liddicoat, J. Boutin, and R. C. Upstill-Goddard (2000), In situ evaluation of air-sea gas exchange parameterizations using novel conservative and volatile tracers, *Global Biogeochem. Cycles, 14*(1), 373-387, doi: 10.1029/1999GB900091.

Olsen, A., K. R. Brown, M. Chierici, T. Johannessen, and C. Neill (2008), Sea-surface CO_2 fugacity in the subpolar North Atlantic, *Biogeosciences, 5*(2), 535-547, doi: 10.5194/bg-5-535-2008.

Orr, J. C., V. J. Fabry, O. Aumont, L. Bopp, S. C. Doney, R. A. Feely, A. Gnanadesikan, N. Gruber, A. Ishida, F. Joos, R. M. Key, K. Lindsay, E. Maier-Reimer, R. Matear, P. Monfray, A. Mouchet, R. G. Najjar, G. K. Plattner, K. B. Rodgers, C. L. Sabine, J. L. Sarmiento, R. Schlitzer, R. D. Slater, I. J. Totterdell, M. F. Weirig, Y. Yamanaka, and A. Yool (2005), Anthropogenic ocean acidification over the twenty-first century and its impact on calcifying organisms, *Nature, 437*(7059), 681-686, doi: 10.1038/Nature04095.

Padin, X. A., C. G. Castro, A. F. Rios, and F. F. Perez (2008), fCO_2^{SW} variability in the Bay of Biscay during ECO cruises, *Cont. Shelf Res., 28*(7), 904-914, doi: 10.1016/j.csr.2008.01.004.

Padin, X. A., G. Navarro, M. Gilcoto, A. F. Rios, and F. F. Perez (2009), Estimation of air-sea CO_2 fluxes in the Bay of Biscay based on empirical relationships and remotely sensed observations, *J. Mar. Syst., 75*(1-2), 280-289, doi: 10.1016/j.jmarsys.2008.10.008.

Park, P. K. (1968), Alkalinity and pH off the coast of Oregon, *Deep Sea Res.*, *15*(2), 171-183.

Park, P. K. (1966), Columbia River plume identification by specific alkalinity, *Limnol. Oceanogr.*, *11*, 118-120.

Park, P. K., G. R. Webster, and R. Yamamoto (1970), *Alkalinity budget of the Columbia River*, Department of Oceanography, Oregon State University, Oregon, US.

PERSGA (2000), *Coral reefs in the Red Sea and Gulf of Aden surveys 1990 to 2000 summary and recommendations*. PERSGA Technical Series No. 7, The Regional Organization for the Conservation of the Environment of the Red Sea and Gulf of Aden, Jeddah, Saudi Arabia.

PERSGA (2010), *The Status of Coral Reefs in the Red Sea and Gulf of Aden: 2009*. PERSGA Technical Series No. 16, The Regional Organization for the Conservation of the Environment of the Red Sea and Gulf of Aden, Jeddah, Saudi Arabia.

Petersen, W., F. Schroeder, and F. D. Bockelmann (2011), FerryBox - Application of continuous water quality observations along transects in the North Sea, *Ocean Dynam.*, *61*(10), 1541-1554.

Pierrot, D., E. Lewis, and D. W. R. Wallace (2006), MS Excel program developed for CO_2 system Calculations, *ORNL/CDIAC-105a. Carbon Dioxide Information Analysis Center, Oak Ridge National Laboratory, US Department of Energy, Oak Ridge, TN*.

Pierrot, D., C. Neill, K. Sullivan, R. Castle, R. Wanninkhof, H. Luger, T. Johannessen, A. Olsen, R. A. Feely, and C. E. Cosca (2009), Recommendations for autonomous

underway pCO_2 measuring systems and data-reduction routines, *Deep Sea Res., Part II*, *56*(8-10), 512-522.

Pollard, R. T., M. J. Griffiths, S. A. Cunningham, J. F. Read, F. F. Perez, and A. F. Rios (1996), Vivaldi 1991-A study of the formation, circulation and ventilation of Eastern North Atlantic Central Water, *Prog. Oceanogr., 37*(2), 167-192, doi: 10.1016/S0079-6611(96)00008-0.

Quigg, A., Z. V. Finkel, A. J. Irwin, Y. Rosenthal, T. Y. Ho, J. R. Reinfelder, O. Schofield, F. M. M. Morel, and P. G. Falkowski (2003), The evolutionary inheritance of elemental stoichiometry in marine phytoplankton, *Nature, 425*(6955), 291-294, doi: 10.1038/Nature01953.

Redfield, A. C., B. H. Ketchum, and F. A. Richards (1934), On the proportions of organic derivatives in sea water and their relation to the composition of plankton in *James Johnstone Memorial Volume*, edited by R. J. Daniel, pp. 176-192, University Press of Liverpool, Liverpool.

Redfield, A. C., B. H. Ketchum, and F. A. Richards (1963), The influence of organisms on the composition of sea-water, in *The sea*, edited by M. N. Hill, pp. p.-26-77, Interscience, London.

Rees, A. P., J. A. Gilbert, and B. A. Kelly-Gerreyn (2009), Nitrogen fixation in the western English Channel (NE Atlantic Ocean), *Mar. Ecol.: Prog. Ser., 374*, 7-12, doi: 10.3354/meps07771.

Reid, P. C., M. Edwards, H. G. Hunt, and A. J. Warner (1998), Phytoplankton change in the North Atlantic, *Nature*, *391*(6667), 546-546.

Rossby, T., G. Siedler, and W. Zenk (1995), The Volunteer Observing Ship and Future Ocean Monitoring, *Bull. Amer. Meteor. Soc.*, *76*(1), 5-11.

Sabine, C. L., R. A. Feely, N. Gruber, R. M. Key, K. Lee, J. L. Bullister, R. Wanninkhof, C. S. Wong, D. W. R. Wallace, B. Tilbrook, F. J. Millero, T. H. Peng, A. Kozyr, T. Ono, and A. F. Rios (2004), The oceanic sink for anthropogenic CO_2, *Science, 305*(5682), 367-371, doi: 10.1126/science.1097403.

Saderne, V., P. Fietzek, and P. M. J. Herman (2013), Extreme variations of pCO_2 and pH in a macrophyte meadow of the Baltic Sea in summer: Evidence of the effect of photosynthesis and local upwelling, *PLoS ONE*, *8*(4), e62689.

Sambrotto, R. N., G. Savidge, C. Robinson, P. Boyd, T. Takahashi, D. M. Karl, C. Langdon, D. Chipman, J. Marra, and L. Codispoti (1993), Elevated consumption of carbon relative to nitrogen in the surface ocean, *Nature, 363*(6426), 248-250, doi: 10.1038/363248a0.

Santana-Casiano, J. M., M. Gonzalez-Davila, M. J. Rueda, O. Llinas, and E. F. Gonzalez-Davila (2007), The interannual variability of oceanic CO_2 parameters in the

northeast Atlantic subtropical gyre at the ESTOC site, *Global Biogeochem. Cycles, 21*(1), C09013, doi: 10.1029/2006gb002788.

Sarmiento, J. L., and N. Gruber (2006), Ocean Biogeochemical Dynamics, edited, p. 528, Princeton University Press, Princeton, NJ.

Sarmiento, J. L., T. M. C. Hughes, R. J. Stouffer, and S. Manabe (1998), Simulated response of the ocean carbon cycle to anthropogenic climate warming, *Nature, 393*(6682), 245-249, doi: 10.1038/30455.

Sarmiento, J. L., P. Monfray, E. Maier-Reimer, O. Aumont, R. J. Murnane, and J. C. Orr (2000), Sea-air CO_2 fluxes and carbon transport: A comparison of three ocean general circulation models, *Global Biogeochem. Cycles, 14*(4), 1267-1281, doi: 10.1029/1999GB900062.

Sarmiento, J. L., J. Dunne, A. Gnanadesikan, R. M. Key, K. Matsumoto, and R. Slater (2002), A new estimate of the $CaCO_3$ to organic carbon export ratio, *Global Biogeochem. Cycles, 16*(4), doi: 10.1029/2002GB001919.

Schlitzer, R. (2011), Ocean Data View, http://odv.awi.de.

Schneider, A., D. W. R. Wallace, and A. Kortzinger (2007), Alkalinity of the Mediterranean Sea, *Geophys. Res. Lett., 34*(15), doi: 10.1029/2006GL028842.

Schneider, B., and W. Roether. (2007), *Meteor 06MT20011018 cruise data from the 2001 cruises, CARINA Data Set. http://cdiac.ornl.gov/ftp/oceans/CARINA/Meteor/06MT512/*. Carbon Dioxide Information Analysis Center, Oak Ridge National Laboratory, US Department of Energy, Oak Ridge, Tennessee. doi: 10.3334/CDIAC/otg.CARINA_06MT20011018.

Schneider, B., S. Kaitala, and P. Maunula (2006), Identification and quantification of plankton bloom events in the Baltic Sea by continuous pCO_2 and chlorophyll a measurements on a cargo ship, *J. Mar. Syst.*, *59*(3–4), 238-248.

Schneider, N., E. Di Lorenzo, and P. P. Niiler (2005), Salinity Variations in the Southern California Current, *J. Phys. Oceanogr.*, *35*(8), 1421-1436.

Schuster, U., A. J. Watson, N. R. Bates, A. Corbiere, M. Gonzalez-Davila, N. Metzl, D. Pierrot, and M. Santana-Casiano (2009), Trends in North Atlantic sea-surface fCO_2 from 1990 to 2006, *Deep Sea Res., Part II*, *56*(8-10), 620-629.

SCOR/IAPSO (2011), *OceanScope: A proposed partnership between the maritime industries and the ocean observing community to monitor the global ocean water column*. 86 pp, Report of SCOR/IAPSO Working Group 133.

Sejr, M. K., D. Krause-Jensen, S. Rysgaard, L. L. Sorensen, P. B. Christensen, and R. N. Glud (2011), Air-sea flux of CO_2 in arctic coastal waters influenced by glacial melt water and sea ice, *Tellus, Ser. B*, *63*(5), 815-822.

Seppälä, J., P. Ylöstalo, S. Kaitala, S. Hällfors, M. Raateoja, and P. Maunula (2007), Ship-of-opportunity based phycocyanin fluorescence monitoring of the filamentous cyanobacteria bloom dynamics in the Baltic Sea, *Estuar. Coast. Shelf Sci.*, *73*(3–4), 489-500.

Skjelvan, I., E. Falck, F. Rey, and S. B. Kringstad (2008), Inorganic carbon time series at Ocean Weather Station M in the Norwegian Sea, *Biogeosciences, 5*(2), 549-560, doi: 10.5194/bg-5-549-2008.

Smith, H. E. K., T. Tyrrell, A. Charalampopoulou, C. Dumousseaud, O. J. Legge, S. Birchenough, L. R. Pettit, R. Garley, S. E. Hartman, M. C. Hartman, N. Sagoo, C. J. Daniels, E. P. Achterberg, and D. J. Hydes (2012), Predominance of heavily calcified coccolithophores at low $CaCO_3$ saturation during winter in the Bay of Biscay, *Proc. Natl. Acad. Sci. U. S. A., 109*(23), 8845-8849, doi: 10.1073/pnas.1117508109.

Smith, S. V., and F. T. Mackenzie (1987), The ocean as a net heterotrophic system: Implications From the carbon biogeochemical cycle, *Global Biogeochem. Cycles*, *1*(3), 187-198.

Smith, S. V., and J. T. Hollibaugh (1993), Coastal Metabolism and the Oceanic Organic-Carbon Balance, *Rev. Geophys.*, *31*(1), 75-89.

Royal Society. (2005), *Ocean acidification due to increasing atmospheric carbon dioxide*. London: The Royal Society, 57 pp.

Somavilla, R., C. Gonzalez-Pola, C. Rodriguez, S. A. Josey, R. F. Sanchez, and A. Lavin (2009), Large changes in the hydrographic structure of the Bay of Biscay after the extreme mixing of winter 2005, *J. Geophys. Res., 114*(C1), C01001, doi: 10.1029/2008jc004974.

Steinacher, M., F. Joos, T. L. Frolicher, G. K. Plattner, and S. C. Doney (2009), Imminent ocean acidification in the Arctic projected with the NCAR global coupled carbon cycle-climate model, *Biogeosciences*, *6*(4), 515-533.

Suzuki, T., M. Ishii, M. Aoyama, J. R. Christian, K. Enyo, T. Kawano, R. M. Key, N. Kosugi, A. Kozyr, L. A. Miller, A. Murata, T. Nakano, T. Ono, T. Saino, K. Sasaki, D. Sasano, Y. Takatani, M. Wakita, and C. Sabine. (2013), *PACIFICA Data Synthesis Project*. ORNL/CDIAC-159, NDP-092, Carbon Dioxide Information Analysis Center, Oak Ridge National Laboratory, U.S. Department of Energy, Oak Ridge, Tennessee. doi:10.3334/CDIAC/OTG.PACIFICA_NDP092.

Sweeney, C., E. Gloor, A. R. Jacobson, R. M. Key, G. McKinley, J. L. Sarmiento, and R. Wanninkhof (2007a), Constraining global air-sea gas exchange for CO_2 with recent bomb ^{14}C measurements, *Global Biogeochem. Cycles, 21*(2), GB2015, doi: 10.1029/2006gb002784.

Sweeney, C., E. Gloor, A. R. Jacobson, R. M. Key, G. McKinley, J. L. Sarmiento, and R. Wanninkhof (2007b), Constraining global air-sea gas exchange for CO_2 with recent bomb C-14 measurements, *Global Biogeochem. Cycles*, *21*(2), GB2015, doi:2010.1029/2006GB002784.

Takahashi, T., S. C. Sutherland, R. A. Feely, and R. Wanninkhof (2006), Decadal change of the surface water pCO_2 in the North Pacific: A synthesis of 35 years of observations, *J. Geophys. Res., 111*(C7), C07s05, doi: 10.1029/2005jc003074.

Takahashi, T., J. Olafsson, J. G. Goddard, D. W. Chipman, and S. C. Sutherland (1993), Seasonal variation of CO_2 and nutrients in the high-latitude surface ocean: a comparative study, *Global Biogeochem. Cycles, 7*, 843-878, doi: 10.1029/93GB02263.

Takahashi, T., R. A. Feely, R. F. Weiss, R. H. Wanninkhof, D. W. Chipman, S. C. Sutherland, and T. T. Takahashi (1997), Global air-sea flux of CO_2: An estimate based on measurements of sea-air pCO_2 difference, *Proc. Natl. Acad. Sci. U. S. A.*, *94*(16), 8292-8299.

Takahashi, T., S. C. Sutherland, C. Sweeney, A. Poisson, N. Metzl, B. Tilbrook, N. Bates, R. Wanninkhof, R. A. Feely, C. Sabine, J. Olafsson, and Y. Nojiri (2002), Global sea-air CO_2 flux based on climatological surface ocean pCO_2, and seasonal biological and temperature effects, *Deep Sea Res., Part II*, *49*(9-10), 1601-1622.

Takahashi, T., S. C. Sutherland, R. Wanninkhof, C. Sweeney, R. A. Feely, D. W. Chipman, B. Hales, G. Friederich, F. Chavez, C. Sabine, A. Watson, D. C. E. Bakker, U. Schuster, N. Metzl, H. Yoshikawa-Inoue, M. Ishii, T. Midorikawa, Y. Nojiri, A. Kortzinger, T. Steinhoff, M. Hoppema, J. Olafsson, T. S. Arnarson, B. Tilbrook, T. Johannessen, A. Olsen, R. Bellerby, C. S. Wong, B. Delille, N. R. Bates, and H. J. W. de Baar (2009), Climatological mean and decadal change in surface ocean pCO_2, and net sea-air CO_2 flux over the global oceans, *Deep-Sea Res., Pt II, 56*(8-10), 554-577, doi: 10.1016/j.dsr2.2008.12.009.

Tanhua, T., M. Alvarez, and L.Mintrop. (2012), *Carbon Dioxide, Hydrographic, and Chemical Data Obtained During the R/V Meteor MT84_3 Mediterranean Sea Cruise (April 5. - April 28, 2011).* http://cdiac.ornl.gov/ftp/oceans/CLIVAR/Met_84_3_Med_Sea/. Carbon Dioxide Information Analysis Center, Oak Ridge National Laboratory, US Department of Energy, Oak Ridge, Tennessee. doi: 10.3334/CDIAC/OTG.CLIVAR_06MT20110405.

Tanhua, T., A. Olsen, M. Hoppema, S. Jutterström, C. Schirnick, S. v. Heuven, A. Velo, X. Lin, A. Kozyr, M. Alvarez, D. C. E. Bakker, P. Brown, E. Falck, E. Jeansson, C. L. Monaco, J. Olafsson, F. F. Perez, D. Pierrot, A. F. Rios, C. L. Sabine, U. Schuster,

R. Steinfeldt, I. Stendardo, L. G. Anderson, N. R. Bates, R. G. J. Bellerby, J. Blindheim, J. L. Bullister, N. Gruber, M. Ishii, T. Johannessen, E. P. Jones, J. Köhler, A. Körtzinger, N. Metzl, A. Murata, S. Musielewicz, A. M. Omar, K. A. Olsson, M. d. l. Paz, B. Pfeil, F. Rey, M. Rhein, I. Skjelvan, B. Tilbrook, R. Wanninkhof, L. Mintrop, D. W. R. Wallace, and R. M. Key (2008), *CARINA Data Synthesis Project*. ORNL/CDIAC-157, NDP-091, Carbon Dioxide Information Analysis Center, Oak Ridge National Laboratory, U.S. Department of Energy, Oak Ridge, Tennessee. doi:10.3334/CDIAC/otg.ndp091.

Taylor, J. R. (1982), *An introduction to error analysis: The study of uncertainties in physical measurements*, 327 pp., University Science Books, Sausalito, Calif.

Tengberg, A., J. Hovdenes, H. J. Andersson, O. Brocandel, R. Diaz, D. Hebert, T. Arnerich, C. Huber, A. Kortzinger, A. Khripounoff, F. Rey, C. Ronning, J. Schimanski, S. Sommer, and A. Stangelmayer (2006), Evaluation of a lifetime-based optode to measure oxygen in aquatic systems, *Limnology and Oceanography-Methods*, *4*, 7-17.

Toggweiler, J. R. (1993), Carbon overconsumption, *Nature, 363*(6426), 210-211, doi: 10.1038/363210a0.

Turk, D., J. W. Book, and W. R. McGillis (2013), pCO_2 and CO_2 exchange during high bora winds in the Northern Adriatic, *J. Mar. Syst.*, *117–118*(0), 65-71.

Turk, D., V. Malačič, M. D. DeGrandpre, and W. R. McGillis (2010), Carbon dioxide variability and air-sea fluxes in the northern Adriatic Sea, *J. Geophys. Res., 115*(C10), C10043, doi: 10.1029/2009jc006034.

Tyrrell, T. (2011), Anthropogenic modification of the oceans, *Philos. Trans. R. Soc., A, 369*(1938), 887-908, doi: 10.1098/rsta.2010.0334.

Ver, L. M. B., F. T. Mackenzie, and A. Lerman (1999a), Carbon cycle in the coastal zone: effects of global perturbations and change in the past three centuries, *Chem. Geol.*, *159*(1-4), 283-304.

Ver, L. M. B., F. T. Mackenzie, and A. Lerman (1999b), Biogeochemical responses of the carbon cycle to natural and human perturbations: Past, present, and future, *Am. J. Sci.*, *299*(7-9), 762-801.

Visbeck, M., E. P. Chassignet, R. G. Curry, T. L. Delworth, R. R. Dickson, and G. Krahmann (2003), The ocean's response to North Atlantic Oscillation variability, in *The North Atlantic Oscillation: Climatic Significance and Environmental Impact*, edited by J. W. Hurrell, Y. Kushnir, G. Ottersen and M. Visbeck, pp. 113-145, AGU, Washington, DC.

Wang, Z. A., W. J. Cai, Y. C. Wang, and B. L. Upchurch (2003), A long pathlength liquid-core waveguide sensor for real-time pCO_2 measurements at sea, *Mar. Chem.*, *84*(1-2), 73-84.

Wang, Z. H., Y. H. Wang, W. J. Cai, and S. Y. Liu (2002), A long pathlength spectrophotometric pCO_2 sensor using a gas-permeable liquid-core waveguide, *Talanta*, *57*(1), 69-80.

Wang, Z. H. A., and W. J. Cai (2004), Carbon dioxide degassing and inorganic carbon export from a marsh-dominated estuary (the Duplin River): A marsh CO_2 pump, *Limnol. Oceanogr.*, *49*(2), 341-354.

Wanninkhof, R. (1992), Relationship between Wind-Speed and Gas-Exchange over the Ocean, *J. Geophys. Res., 97*(C5), 7373-7382, doi: 10.1029/92JC00188.

Wanninkhof, R., E. Lewis, R. A. Feely, and F. J. Millero (1999), The optimal carbonate dissociation constants for determining surface water pCO_2 from alkalinity and total inorganic carbon, *Mar. Chem.*, *65*(3-4), 291-301.

Wanninkhof, R., S. C. Doney, T. Takahashi, and W. R. McGillis (2002), The effect of using time-averaged winds on regional air-sea CO_2 fluxes, in *Gas Transfer at Water Surfaces*, edited, pp. 351-356, AGU, Washington, DC.

Wanninkhof, R., W. E. Asher, D. T. Ho, C. Sweeney, and W. R. McGillis (2009), Advances in quantifying air-sea gas exchange and environmental forcing, *Annu. Rev. Mar. Sci.*, *1*(1), 213-244.

Wanninkhof, R., J.-Z. Zhang, M. Baringer, C. Langdon, W.-J. Cai, J. Salisbury, and R. Byrne (2011), *Carbon dioxide and hydrographic measurements during the 2007 NACP East Coast Cruise.* http://cdiac.ornl.gov/ftp/oceans/NACP_East_Coast_Cruise/. Carbon Dioxide Information Analysis Center, Oak Ridge National Laboratory, US Department of Energy, Oak Ridge, Tennessee. doi: 10.3334/CDIAC/otg.CLIVAR_NACP_East_Coast_Cruise_2007.

Ware, J. R., S. V. Smith, and M. L. Reaka-Kudla (1992), Coral reefs: sources or sinks of atmospheric CO_2?, *Coral Reefs*, *11*, 127-130.

Watson, A. J., N. Metzl, and U. Schuster (2011), Monitoring and interpreting the ocean uptake of atmospheric CO_2, *Phil. Trans. R. Soc. A 369*, 1997-2008.

Watson, A. J., U. Schuster, D. C. E. Bakker, N. R. Bates, A. Corbiere, M. Gonzalez-Davila, T. Friedrich, J. Hauck, C. Heinze, T. Johannessen, A. Kortzinger, N. Metzl, J. Olafsson, A. Olsen, A. Oschlies, X. A. Padin, B. Pfeil, J. M. Santana-Casiano, T. Steinhoff, M. Telszewski, A. F. Rios, D. W. R. Wallace, and R. Wanninkhof (2009), Tracking the variable North Atlantic sink for atmospheric CO_2, *Science*, *326*(5958), 1391-1393.

Weiss, R. F. (1974a), Carbon dioxide in water and seawater: the solubility of a non-ideal gas, *Mar. Chem.*, *2*, 203-215.

Weiss, R. F. (1974b), Carbon dioxide in water and seawater: the solubility of a non-ideal gas, *Mar. Chem., 2*, 203-215, doi: 10.1016/0304-4203(74)90015-2.

Whitledge, T. E., S. C. Malloy, C. J. Patton, and C. O. Wirick (1981), *Automated nutrient analysis in seawater*. Brookhaven National Lab Report 51398: 216, Brookhaven, NY.

Willcox, S., C. Meinig, C. L. Sabine, N. Lawrence-Slavas, T. Richardson, R. Hine, and J. Manley (2009), An autonomous mobile platform for underway surface carbon measurements in open-ocean and coastal waters, paper presented at OCEANS 2009, MTS/IEEE Biloxi - Marine Technology for Our Future: Global and Local Challenges, 26-29 Oct. 2009.

Wolf-Gladrow, D. A., R. E. Zeebe, C. Klaas, A. Kortzinger, and A. G. Dickson (2007), Total alkalinity: The explicit conservative expression and its application to biogeochemical processes, *Mar. Chem., 106*(1-2), 287-300, doi: 10.1016/j.marchem.2007.01.006.

Yates, K. K., C. Dufore, N. Smiley, C. Jackson, and R. B. Halley (2007), Diurnal variation of oxygen and carbonate system parameters in Tampa Bay and Florida Bay, *Mar. Chem.*, *104*(1-2), 110-124.

Zeebe, R. E. (2012), History of seawater carbonate chemistry, atmospheric CO_2, and ocean acidification, *Annu. Rev. Earth Planet. Sci.*, *40*(1).

Zeebe, R. E., and D. Wolf-Gladrow (2001), *CO_2 in seawater: Equilibrium, kinetics, isotopes.*, Elsevier, Amsterdam.